A13

MAX-PLANCK-INSTITUT FÜR PHYSIK

WERNER-HEISENBERG-INSTITUT

MPI-PhE/97-19
September 1997

Inclusive single-particle distributions and transverse momenta of forward produced charged hadrons in μp scattering at 470 GeV

THE FERMILAB E665 COLLABORATION

(to be published in Zeitschrift für Physik C)

80805 München · Föhringer Ring 6

Inclusive single-particle distributions and transverse momenta of forward produced charged hadrons in μp scattering at 470 GeV

THE FERMILAB E665 COLLABORATION

(to be published in Zeitschrift für Physik C)

Inclusive single-particle distributions and transverse momenta of forward produced charged hadrons in μp scattering at 470 GeV.

E665 Collaboration

M.R. Adams[6], M. Aderholz[12], S. Aïd[10,a], P.L. Anthony[9,b], D.A. Averill[6], M.D. Baker[11], B.R. Baller[4], A. Banerjee[15,c], A.A. Bhatti[16,d], U. Bratzler[16,e], H.M. Braun[17], T.J. Carroll[12,f], H.L. Clark[14,g], J.M. Conrad[5,h], R. Davisson[16], I. Derado[12], F.S. Dietrich[9], W. Dougherty[16], T. Dreyer[1], V. Eckardt[12], U. Ecker[17,i], M. Erdmann[1,j], G.Y. Fang[5,k], J. Figiel[8], R.W. Finlay[14], H.J. Gebauer[12], D.F. Geesaman[2], K.A. Griffioen[15,l], R.S. Guo[6,m], J. Haas[1], C. Halliwell[6], D. Hantke[12,n], K.H. Hicks[14], H.E. Jackson[2], D.E. Jaffe[6,o], G. Jancso[7], D.M. Jansen[16,p], Z. Jin[16], S. Kaufmann[2], R.D. Kennedy[3,q], E.R. Kinney[2,r], H.G.E. Kobrak[3], A.V. Kotwal[5,h], S. Kunori[10], J.J. Lord[16], H.J. Lubatti[16], D. McLeod[6], P. Madden[3,s], S. Magill[6,t], A. Manz[12], H. Melanson[4], D.G. Michael[5,u], H.E. Montgomery[4], J.G. Morfin[4], R.B. Nickerson[5,v], J. Novak[13,w], K. Olkiewicz[8], L. Osborne[11], R. Otten[17], V. Papavassiliou[2,x], B. Pawlik[8], F.M. Pipkin[5,*], D.H. Potterveld[2], A. Röser[17,y], J.J. Ryan[11,z], C.W. Salgado[4,aa], H. Schellman[13], M. Schmitt[5,bb], N. Schmitz[12], K.P. Schüler[18,z], J. Seyerlein[12], G. Siegert[1,cc], A. Skuja[10], G.A. Snow[10], S. Söldner-Rembold[12,dd], P. Spentzouris[13,h], P. Stopa[8], R.A. Swanson[3], H. Venkataramania[13], M. Wilhelm[1,ee], Richard Wilson[5], W. Wittek[12], S.A. Wolbers[4], A. Zghiche[2], and T. Zhao[16]

[1] Albert-Ludwigs-Universität Freiburg i. Br., Germany
[2] Argonne National Laboratory , Argonne, Illinois 60439
[3] University of California, San Diego, California 92093
[4] Fermi National Accelerator Laboratory, Batavia, Illinois 60510
[5] Harvard University, Cambridge, Massachusetts 02138
[6] University of Illinois, Chicago, Illinois 60680
[7] KFKI Research Institute for Particle and Nuclear Physics, H-1525 Budapest, Hungary
[8] Institute for Nuclear Physics, Krakow, Poland
[9] Lawrence Livermore National Laboratory, Livermore, California 94551
[10] University of Maryland, College Park, Maryland 20742
[11] Massachusetts Institute of Technology, Cambridge, Massachusetts 02139
[12] Max-Planck-Institut für Physik, Munich, Germany
[13] Northwestern University, Evanston, Illinois 60208
[14] Ohio University, Athens, Ohio 45701
[15] University of Pennsylvania, Philadelphia, Pennsylvania 19104
[16] University of Washington, Seattle, Washington 98195
[17] University of Wuppertal, Wuppertal, Germany
[18] Yale University, New Haven, Connecticut 06511

Received: August 1997/ Accepted:

Present addresses:
[*] deceased
[a] University of Hamburg, D-22603 Hamburg, Germany.
[b] SLAC, Stanford, CA 94309, USA.
[c] Fidelity Investments Corp., Boston, MA, USA.
[d] The Rockefeller University, New York NY 10021, USA.
[e] Max-Planck-Institut für Physik, D-80805 München, Germany.
[f] University of Wisconsin Hospital, Madison, WI 53792, USA.
[g] Texas A&M University, College Station, TX 77843, USA.
[h] Columbia University, New York, NY 10027, USA.
[i] Jenfelderstr. 147, D-22045 Hamburg, Germany.
[j] Heidelberg University, D-69120, Heidelberg Germany.
[k] Dept. of Medical Physics, University of Wisconsin, Madison, WI 53706, USA.
[l] College of William and Mary, Williamsburg, VA 23187, USA.
[m] Department of Physics, National Kaohsiung Normal University, Kaohsiung, Taiwan.
[n] GSF - Forschungszentrum für Umwelt und Gesundheit GmbH, D-85764 Oberschleißheim, Germany.
[o] SCRI, Florida State University, Tallahassee, FL 32606, USA.
[p] LANL, Los Alamos, NM 87545, USA.
[q] Fermi National Accelerator Laboratory, Batavia, IL 60510, USA.
[r] University of Colorado, Boulder, CO 80309, USA.
[s] Linear Technology Inc., Milpitas, CA 95395, USA.
[t] Argonne National Laboratory, Argonne, IL 60439, USA.
[u] California Institute of Technology, Pasadena, CA 91125, USA.
[v] Oxford University, Oxford OX1 3RH, UK.
[w] Yale University, New Haven, CT 06511, USA.
[x] New Mexico State University, Las Cruces, NM 88003, USA.
[y] Klinikum Barmen, Abt. Radiologie, D-42283 Wuppertal, Germany.
[z] DESY, D-22603 Hamburg, Germany.
[aa] Thomas Jefferson National Accelerator Facility, Newport News, VA 23606, USA.
[bb] CERN, CH-1211 Geneva 23, Switzerland.
[cc] University of Wuppertal, D-42119 Wuppertal, Germany.
[dd] Albert-Ludwigs-Universität Freiburg, D-79104 Freiburg, Germany.
[ee] Hoffmann-LaRoche, CH-4002 Basel, Switzerland.

Abstract. Using data from the Fermilab fixed target experiment E665, general properties of forward produced charged hadrons in μp interactions at a primary muon energy of 470 GeV are investigated. The normalized inclusive single-particle distributions for Feynman-x $D(x_F)$ and for the transverse momentum $D(p_t^2, x_F)$ are measured as a function of W and Q^2. The dependence of the average transverse momentum squared $\langle p_t^2 \rangle$ on x_F, W and Q^2 is studied. The increasing contribution from diffractive production as Q^2 decreases leads to a reduction of the average charged hadron multiplicities at low (positive) x_F and an enhancement at large x_F, for $Q^2 \lesssim 10$ GeV^2. It also reduces $\langle p_t^2 \rangle$ for $Q^2 \lesssim 5$ GeV^2 and $0.4 \lesssim x_F < 1.0$.

1 Introduction

Hadron production in lepton nucleon scattering has been widely studied during the past 20 years in experiments using electron, muon [1–19] and neutrino [20–29] beams. Comprehensive reviews of the main observations are given in [30, 31]. Those experiments cover the region $W \leq 30$ GeV, $Q^2 \leq 40$ GeV^2 and $x_{Bj} \geq 10^{-2}$. More recently, measurements from the experiments at the *ep* collider HERA have become available [32–38]. They extend the W range up to 220 GeV, the Q^2 range up to 1000 GeV^2, and the x_{Bj} range down to 10^{-5}.

In those experiments, the main objectives of analyses on the hadronic system are: quark fragmentation, resonance production, strange particle and charmed particle production, correlations between hadrons, diffractive production, perturbative QCD effects and measurements of the QCD coupling constant α_s.

The experiment discussed here covers the kinematic region $7.5 < W < 30$ GeV, $0.15 < Q^2 < 20$ GeV^2 and $1.5 \cdot 10^{-4} < x_{Bj} < 0.6$. This is an intermediate region between the range of very low Q^2 ($Q^2 \ll 1$ GeV^2), where non-perturbative effects are expected to dominate, and the region of larger Q^2 ($Q^2 \gg 1$ GeV^2), which is characterized by hard QCD processes. The E665 kinematic range also has a considerable overlap with the x_{Bj}-region $< 10^{-2}$, where diffractive processes occur preferentially.

It is of particular theoretical interest to know at which Q^2 the hard QCD processes actually set in, and how the diffractive processes affect the properties of the hadronic system.

In this analysis charged hadrons produced in μp interactions at a primary muon energy of 470 GeV, and emitted into the forward region (current fragmentation hemisphere) of the overall hadronic center-of-mass system are investigated. Normalized inclusive single-particle distributions and their dependence on W^2 and Q^2 are measured for the variables x_F (Feynman-x) and p_t (transverse momentum relative to the virtual-photon direction). The average $\langle p_t^2 \rangle$ is determined as a function of x_F, W^2 and Q^2.

The paper is organized as follows: Section 2 describes the experimental procedure. This includes the definition of the kinematical variables, the data taking and reconstruction, the event selections, the Monte Carlo simulations and the corrections applied to the experimental data. The results are presented in Section 3, and a summary is given in Section 4.

2 Experimental procedure

2.1 Definition of kinematic variables

In the kinematic region of the present experiment the μp interaction proceeds to a very good approximation via the exchange of a single virtual photon. Therefore, the reaction actually studied is the interaction of the single virtual photon with the proton. The definition of the relevant kinematic variables is given in Table 1.

The overall hadronic center-of-mass system (cms) is the system formed by the virtual photon and the proton. The forward region in the cms is defined as the hemisphere for which the virtual-photon direction defines the pole.

It should be noted that for the kinematics of this experiment the numerical values of z_{had} and x_F differ by less than 0.01, for hadrons with $x_F > 0.1$.

The main part of the paper deals with normalized inclusive single-particle distributions. They are defined as:

$$D(v) = \frac{1}{N_\mu} \cdot \frac{dN}{dv} \qquad v = (p_{lab}, x_F, p_t^2) \quad (1)$$

where dN is the number of hadrons in the interval $(v, v + dv)$ and N_μ is the number of events considered. The integrated quantity $\int D(v)dv$ is the average hadron multiplicity. Therefore $D(v)$ is also denoted as the "differential multiplicity". The average multiplicity of hadrons travelling into the forward hemisphere is denoted as $\langle n_F \rangle$:

$$\langle n_F \rangle = \int_0^1 D(x_F)dx_F \quad (2)$$

In Sect. 3.2 also the double-differential distribution

$$D(p_t^2, x_F) = \frac{1}{N_\mu} \cdot \frac{dN}{dp_t^2 dx_F} \quad (3)$$

will be considered.

2.2 Data taking, event reconstruction and selection

In this analysis data from the 1991 run of E665 are used. The E665 detector is described in [39]. Details of data taking, the trigger and the event reconstruction are given in [40].

The momenta of the positively charged beam muons had a mean of 470 GeV and a root mean squared deviation of 56 GeV. The target was liquid hydrogen (H_2).

The E665 forward spectrometer has acceptance for charged hadrons in the region $1 < p_{lab} < 450$ GeV of the laboratory momentum. This corresponds approximately to the forward region ($x_F > 0$) in the cms. The analysis is therefore restricted to forward produced hadrons. All charged hadrons are assigned the pion mass.

Photons are detected in the electromagnetic calorimeter. However, information from this part of the detector is only used to reduce the background due to radiative events and μe elastic scattering.

A small-angle trigger (SAT) accepted events with muon scattering angles $\Theta_\mu > 0.5$ mrad. Interactions of the primary muons with a target proton were selected by restricting the position of the reconstructed event vertex to the target region. Further cuts were applied in order to ensure good muon identification, good track and vertex reconstruction, good resolution in the determination of the kinematic quantities and low background from radiative events and from elastic μe scattering. In order to be accepted in the analysis the events had to fulfill the following criteria:

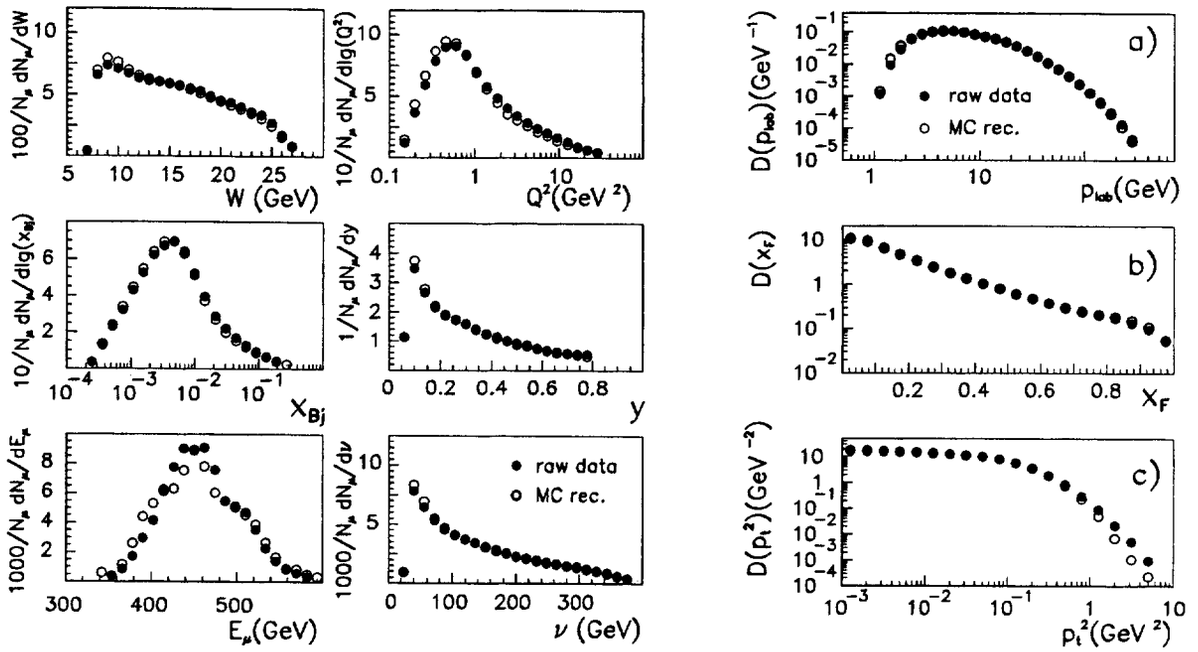

Fig. 1. Comparison of raw experimental data and reconstructed MC for distributions of event variables (left) and hadron variables (right).

$$
\begin{aligned}
&320 < E_\mu < 650 \text{ GeV} \\
&0.15 < Q^2 < 100 \text{ GeV}^2 \\
&30 < \nu < 600 \text{ GeV} \\
&0.00015 < x_{Bj} < 0.6 \\
&y < 0.8
\end{aligned}
\tag{4}
$$

$$
\begin{aligned}
&\Delta Q^2/Q^2 < 0.2 \\
&\Delta\nu/\nu < 0.2 \\
&E_{cl}/\nu < 0.35
\end{aligned}
\tag{5}
$$

$$
\textit{no. of ``accepted'' hadrons} \geq 1 \tag{6}
$$

ΔQ^2 and $\Delta\nu$ are the experimental measurement errors of Q^2 and ν respectively. E_{cl} is the energy of the most energetic cluster in the electromagnetic calorimeter within an event. The cut on E_{cl}/ν removes events in which high–energetic bremsstrahlung photons are emitted, and it reduces the background from elastic μe scattering considerably.

Only those charged hadrons were "accepted" in the analysis which, according to the geometrical vertex fit, originated at the interaction vertex, defined by the trajectories of the incident and outgoing muon. In addition, they had to pass the cuts:

$$
\begin{aligned}
&p_{lab} > 1.0 \text{ GeV} \quad \text{and} \\
&\Delta p_{lab}/p_{lab} < 0.3,
\end{aligned}
\tag{7}
$$

where Δp_{lab} is the experimental measurement error of p_{lab}.

In order to further suppress elastic μe interactions, events were removed which fulfilled all of the following criteria:

there is only one accepted negative hadron
(the hypothetical electron) in the event
$x_{Bj} < m_e/M + 2\Delta x_{Bj}$ (8)
$\{x_F$ *of the negative hadron is* > 0.4 or
E_{cl} *is* > 40 GeV$\}$

where Δx_{Bj} is the experimental measurement error of x_{Bj} and m_e is the electron mass. The numbers of reconstructed events after all cuts, and the average values of W, Q^2 and x_{Bj} are compiled in Table 2 for the different intervals in W and Q^2. One notices the strong correlation between x_{Bj} and Q^2, the moderate correlation between x_{Bj} and W, and the very weak correlation between W and Q^2 in the data sample.

2.3 Monte Carlo simulation

In order to study experimental losses and biases and for determining the corrections to the data, artificial events were generated using a Monte Carlo (MC) program. The program simulates the primary μp interaction and tracks the particles produced at the interaction vertex through the E665 detector, simulating decays, photon conversions, reinteractions, multiple scattering and energy loss in the target and the detector material [41]. The event sample and the set of kinematic quantities for the particles (including the decay products of short-lived particles) at the primary μp interaction vertex at this stage of the simulation is called "MC true". Finally, the detector response to the passage of all produced particles and the triggers are simulated, taking into account the chamber efficiencies and resolutions. The Monte Carlo generated events are then subjected to the same reconstruction and analysis as the experimental data. The resulting event sample along with the set of reconstructed kinematic quantities is called "MC reconstructed".

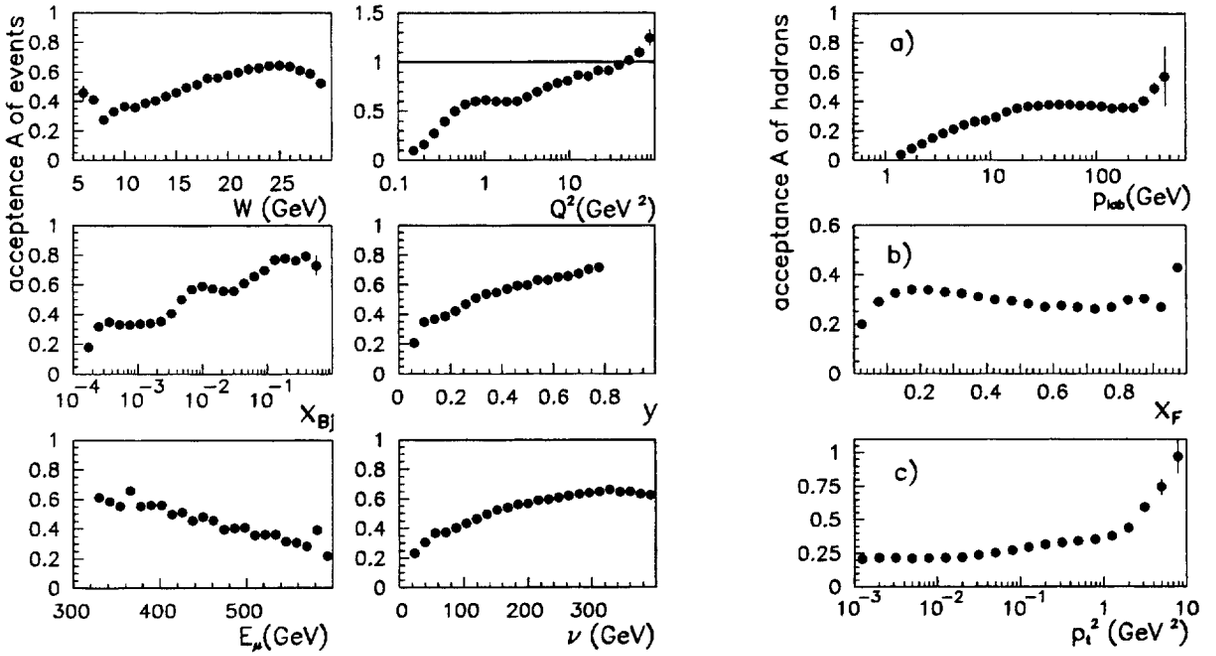

Fig. 2. The acceptance of events as a function of event variables (left) and the acceptance of hadrons as a function of hadron variables (right).

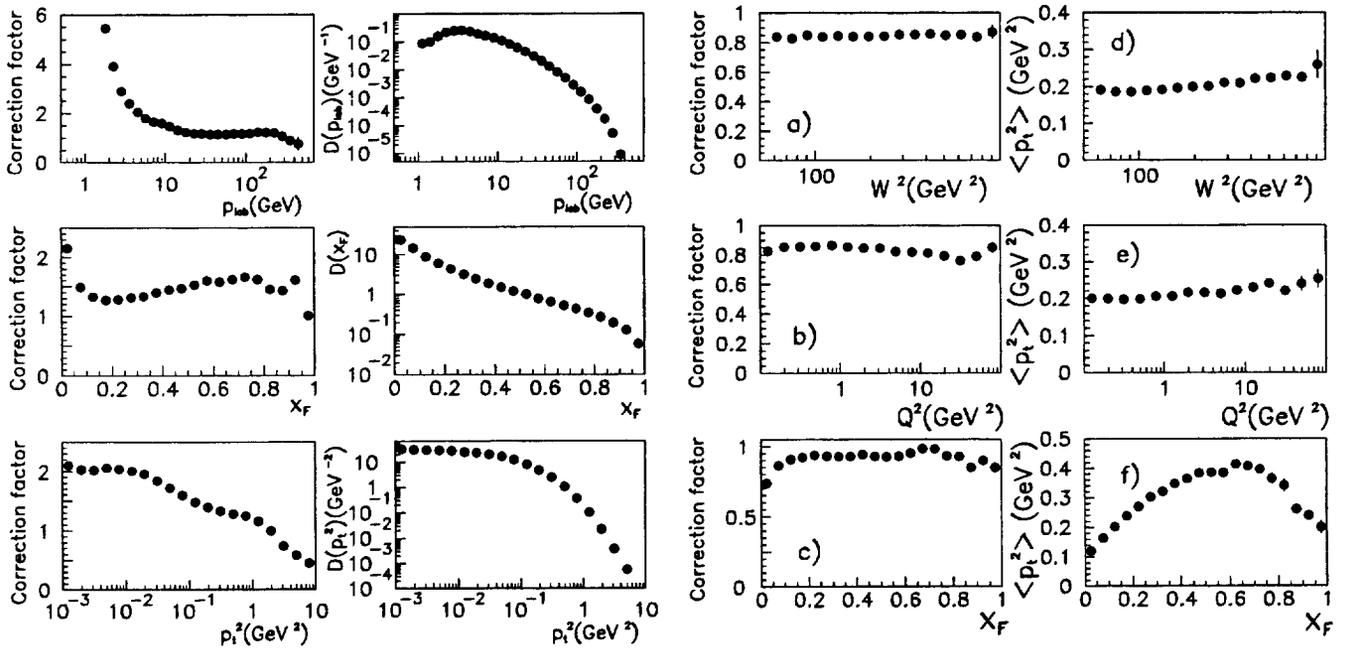

Fig. 3. Correction factors $c_D(v)$ for the normalized inclusive single-particle distributons $D(v)$, and the global corrected distributions $D(v)$, for $v = p_{lab}$, x_F and p_t^2 (left). Correction factor $c_{p_t^2}$ and the corrected $\langle p_t^2 \rangle$ as a function of W^2, Q^2 and x_F (right).

In the primary μp interaction both non-diffractive and diffractive production is considered. This is done by calling a standard LUND generator (LEPTO 5.2, JETSET 6.3 [42]) for non-diffractive and the E665 generator GENDIF for diffractive production. The relative normalization of diffractive and all (= diffractive + non-diffractive) events is given by absolute differential cross sections for diffractive and inelastic μp interactions, which are based on experimental measurements. In the simulation the parton distribution functions by Donnachie and Landshoff [43] were used, which provide a very good description of the F_2^p measurements by the E665 experiment [40]. As they do not contain a gluon distribution, the photon-gluon fusion process is not simulated. Hard gluon radiation from quarks according to first order QCD calculations is included in the LUND program. Radiative effects are taken into account by the GAMRAD program [44], which is based on the formulae

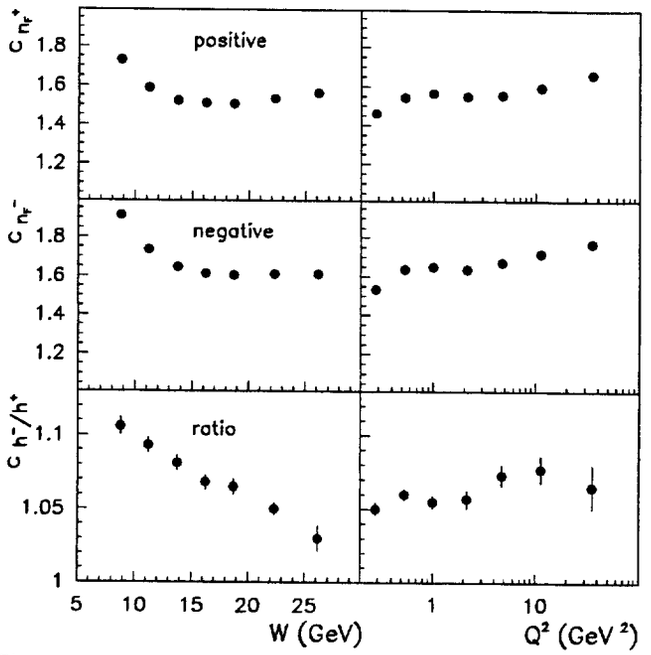

Fig. 4. Correction factors c_{n_F} for average multiplicities $\langle n_F \rangle$ of positive and negative hadrons and the correction factor c_{h^-/h^+} for the ratio $\langle n_F^- \rangle / \langle n_F^+ \rangle$ as a function of W and Q^2.

given in [45, 46]. Further details of the Monte Carlo program, in particular about the generator GENDIF, are given in [19].

In total 1,253,322 events were generated. The number of reconstructed MC events is 301,049.

Comparisons of the raw (uncorrected) experimental data with the reconstructed MC are shown in Fig. 1 for the differential distributions of the event variables W, Q^2,x_{Bj}, y, E_μ and ν. In each plot, the distributions of the experimental data and the reconstructed MC were normalized to the same area. In all cases the MC distributions describe the data distributions satisfactorily.

The corresponding comparison for the hadron variables p_{lab}, x_F and p_t^2 is made in Fig. 1 as well. The quantities plotted are the normalized inclusive single-particle distributions $D(p_{lab})$, $D(x_F)$ and $D(p_t^2)$ for all charged hadrons travelling into the forward hemisphere.

Except for the high-p_t^2 tail, there is good agreement between the (raw) experimental data and the reconstructed MC data. Similar agreement is found for the positive and negative hadrons separately.

At $p_t^2 \gtrsim 1$ GeV^2 the experimental data for $D(p_t^2)$ lie above the MC prediction. This is attributed to hard QCD effects which are only partly simulated in the Monte Carlo model. From a study of systematic effects (see Sect. 2.6) it is found that this difference has a negligible effect on the corrected results.

From Fig. 1 one can conclude that the simulation of the physical processes in the target and the detector is reasonable, and that the MC event samples are appropriate for calculating corrections to the experimental data (see Sect. 2.5).

In order to study the influence from diffractive production on the measured quantities, in some cases results are also given for non-diffractive production only. For this purpose "diffractive events" in the samples of the raw experimental data and of the reconstructed MC events were removed by rejecting events which fulfill all of the following criteria:

$$\begin{aligned} &\textit{net hadronic charge} = 0 \\ &\Sigma z_{had} > 0.85 \ , \ \textit{where} \\ &\quad \textit{the sum extends over all accepted hadrons} \\ &(t - t_{min}) < 1 \text{ GeV}^2 \ , \ \textit{where } t \textit{ is the} \\ &\quad \textit{negative four-momentum-transfer squared} \\ &\quad \textit{from the virtual photon to the target proton} \\ &\quad \textit{and } t_{min} \textit{ is its minimum value} \end{aligned} \tag{9}$$

These selections are suggested by the studies of diffractive production in the same experiment [19]. When performing the corrections, in the MC true sample only the non-diffractive events (13% of all generated events were diffractive) were retained. By the selection (9) in the samples of experimental data and reconstructed MC events $\sim 5\%$ of the events are rejected. The lower fraction is explained by the fact that by the selection (9) only the fully reconstructed diffractive events are rejected.

2.4 Acceptance

The acceptance of the detector can be estimated as the ratio of the distributions for the reconstructed MC events and the true MC events:

$$A(v) = \left(\frac{dN}{dv}\right)_{MC\ rec} \Big/ \left(\frac{dN}{dv}\right)_{MC\ true} , \tag{10}$$

where N is the number of events or hadrons and v is the variable of interest. The acceptance defined in this way includes the geometrical acceptance of the detector, the trigger and reconstruction efficiency, the losses due to the kinematic cuts and the migration effects because of the experimental resolution. The acceptance A of events is plotted in Fig. 2 (left) as a function of W, Q^2, x_{Bj}, y, E_μ, and ν. The drop of A with decreasing Q^2, which is also reflected in the dependence on x_{Bj}, is mainly due to the trigger [40]. At the highest Q^2, A exceeds 1 because of migration effects.

The decrease of A with decreasing ν, y and W is a consequence of the restricted reconstruction efficiency for charged hadrons which leads to a loss of events with low charged multiplicity. On average, A is $\sim 50\%$, implying that $\sim 50\%$ of the generated events, which pass the selections (4) for the true quantities, are reconstructed and pass the selections (4), (5) and (6) for the reconstructed quantities and are deselected by condition (8).

The acceptance A of hadrons is plotted in Fig. 2 (right) as a function of p_{lab}, x_F and p_t^2. On average, A is $\sim 30\%$, falling rapidly at $p_{lab} \lesssim 5$ GeV or $x_F \lesssim 0.05$.

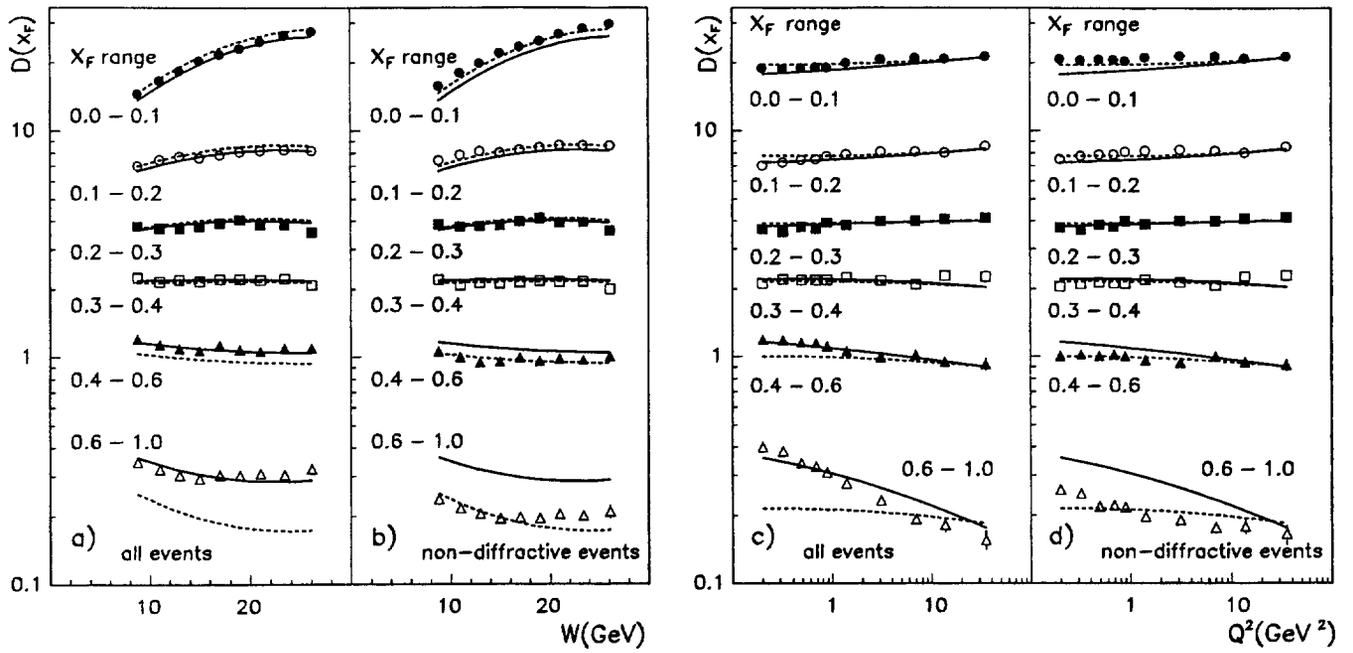

Fig. 5. W (a,b) and Q^2 (c,d) dependence of the differential multiplicity $D(x_F)$ for different intervals of x_F. The data points in a) and c) are for all events (diffractive + non-diffractive), those in b) and d) for non-diffractive events only. Numerical values of the data points in a) and c) are given in Table 5. The curves represent the prediction of the MC model described in Sect. 2.3, including (solid curves) and excluding (dashed curves) diffractive events.

2.5 Corrections of the experimental data

A raw measurement $R_{meas}(v)$, where v denotes one or more kinematic variables (W, Q^2, x_{Bj}, x_F, p_t^2), is corrected by applying a multiplicative correction factor $c(v)$

$$R_{corr}(v) = R_{meas.}(v) \cdot c(v) \ , \tag{11}$$

where $c(v)$ is the ratio of the quantities $R_{MCtrue}(v)$ and $R_{MCrec}(v)$ as determined from the sample of true and reconstructed MC events:

$$c(v) = \frac{R_{MCtrue}(v)}{R_{MCrec}(v)} \tag{12}$$

In the present analysis R may be a normalized inclusive single-particle distribution (differential multiplicity), the average forward multiplicity or $\langle p_t^2 \rangle$.

The correction (11),(12) allows for all effects which have been simulated in the MC program. Those include losses and biases due to the geometrical acceptance of the detector, trigger and reconstruction inefficiencies, radiative effects, particle misidentifications and measurement errors.

The correction factor $c_D(v)$ for $R(v) = D(v)$ and the corrected global normalized inclusive single-particle distributions are shown in Fig. 3 (left), for the variables p_{lab}, x_F and p_t^2. The inverse of $c_D(v)$ can be approximately understood as the hadron acceptance under the condition that the event vertex has been reconstructed with at least 1 accepted charged hadron (requirement (6)). Therefore $c_D(v)$ exhibits similar features as $1/A(v)$, where $A(v)$ is shown in Fig. 2 (right). The fact that $c_D(v)$ is below 1 in some cases is explained by the strong suppression of low multiplicity events in the experimental data and in the reconstructed MC due to the requirement (6).

The correction factor $c_{p_t^2}(v)$ for $R(v) = \langle p_t^2 \rangle$ and the corrected $\langle p_t^2 \rangle$ are given in Fig. 3 (right) for the variables $v = W^2$, Q^2 and x_F. On average $c_{p_t^2}(v)$ is approximately 0.85 with little dependence on W and Q^2. At $x_F \gtrsim 0.1$ $c_{p_t^2}$ is approximately 0.9. It is less than 1 due to the reduced acceptance of low-p_t particles (Fig. 2 c). $c_{p_t^2}$ drops as x_F approaches zero, because the fraction of low-p_t particles is particularly large in this x_F region due to the seagull effect (Fig. 3 f).

The correction factor $c_{n_F}(v)$ for $R(v) = \langle n_F \rangle$ for positive and negative hadrons, and the correction factor $c_{h^-/h^+}(v)$ for the ratio of average multiplicities of negative and positive hadrons travelling into the forward hemisphere $R(v) = h^-/h^+$ are plotted in Fig. 4 for the variables $v = W$ and Q^2.

2.6 Systematic errors

Systematic errors in the measured quantities arise from deficiencies of the Monte Carlo simulation with respect to the physics model for the μp interaction and the modeling of the detector, the trigger and the detector response. In order to estimate the systematic errors the analysis was therefore repeated with slight modifications. In particular the following changes were considered:

- weighting (in the MC event sample) hadrons with high transverse momentum ($p_t^2 > 1$ GeV) in order to compensate for the difference in $D(p_t^2)$ seen between experimental data and reconstructed MC in Fig. 1c,

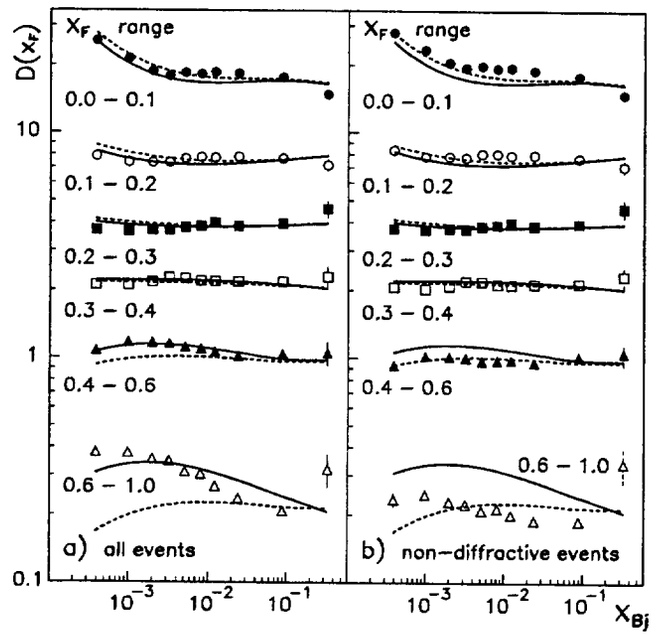

Fig. 6. x_{Bj} dependence of the differential multiplicity $D(x_F)$ for different intervals of x_F. The data points in a) are for all events (diffractive + non-diffractive), those in b) for non-diffractive events only. Numerical values of the data points in a) are given in Table 5. The curves represent the prediction of the MC model described in Sect. 2.3, including (solid curves) and excluding (dashed curves) diffractive events.

- changing in the MC event sample and / or in the experimental data sample the reconstruction efficiency for low momentum ($p_{lab} \lesssim 6.3$ GeV) charged hadrons by an amount suggested by studies of the reconstruction efficiency.
- rejecting randomly 10% of the reconstructed hadrons in the experimental data and in the reconstructed MC sample.

The results after these modifications were compared with each other. The first two modifications as compared to the last one showed only small effects. Therefore the root mean square of the differences between the results obtained after the last mentioned variation and the results from the standard analysis are taken as estimates of the systematic errors. They are compiled in Table 3.

In the fits to the experimental data discussed in Sect. 3, the systematic errors have been taken into account. The resulting errors of the fitted quantities thus include the systematic errors.

3 Results

In this section the corrected results are presented. Data points with a relative error (including the error of the correction factor) greater than 30% are not shown. Only statistical errors are drawn in the figures and listed in the tables.

3.1 The normalized inclusive single-particle distribution $D(x_F)$.

The normalized inclusive single-particle distribution or differential multiplicity $D(x_F)$ for charged hadrons is displayed as a function of W or Q^2 in Fig. 5, and as a function of x_{Bj} in Fig. 6. The data points in Figs. 5a, 5c and 6a refer to all (diffractive + non-diffractive) events, those in Figs. 5b, 5d and 6b to non-diffractive events only. The data points for the total event sample (diffractive + non-diffractive events) are discussed first:

For fixed x_F, there is in general only little dependence on W or Q^2, except in the following cases:

For $0 < x_F < 0.1$ $D(x_F)$ rises with increasing W. This behaviour can be attributed to the enhanced particle production with expanding longitudinal phase space. Note that the fixed bin $0 < x_F < 0.1$ corresponds to a rapidity interval whose size increases with W. For $0.6 < x_F < 1$, $D(x_F)$ decreases with increasing Q^2.

The solid curves in Figs. 5 and 6 represent the prediction of the MC model described in Sect. 2.3 . The model reproduces qualitatively the trends of $D(x_F)$ observed in the experimental data. As explained in Sect. 2.3 and in [19], the main ingredients of the MC model are the $F_2^p(x, Q^2)$ structure functions and corresponding parton distribution functions from [43], the quark parton model for the interaction of the virtual photon with the partons of the proton including first order QCD effects [LEPTO 5.2], the Lund string fragmentation model [JETSET 6.3] and a specific model of diffractive production [19]. The parametrization of F_2^p from [43] was used in the simulation, because it yields a very good description of the F_2^p measurements by E665 [40].

The influence from diffractive production can be seen by comparing the data points in Figs. 5a, 5c and 6a (all events) with those in Figs. 5b, 5d and 6b (non-diffractive events only) respectively: The presence of diffractive events leads to a reduction of multiplicities at low x_F and an enhancement of multiplicities at large x_F, for $Q^2 \lesssim 10$ GeV^2 and all W. The same trends are seen in the MC data, which are shown as solid (all events) and dashed (non-diffractive events only) curves in Figs. 5 and 6. These trends reflect characteristic features of diffractive production: the increase of the fraction of diffractive events as Q^2 decreases and the dominance in the sample of diffractive events of low multiplicity events, in which the hadrons carry a large fraction of the available energy [19]. The latter effect from diffractive production on $D(x_F)$ is also observed at much higher W ($\langle W \rangle = 120$ GeV) [35].

One can conclude that for $Q^2 \lesssim 5$ GeV^2 diffractive production has a strong effect on the multiplicities at low and high x_F. For $Q^2 \gtrsim 2$ GeV^2 and large x_F there may be small effects (reduction of multiplicities) due to QCD processes.

The W dependence of $D(x_F)$ at fixed Q^2, and the Q^2 dependence of $D(x_F)$ at fixed W are shown in Fig. 7. Qualitatively, Fig. 7 shows similar features to Fig. 5, except that for the highest-x_F bin a W dependence of $D(x_F)$ sets in at $Q^2 \gtrsim 2$ GeV^2.

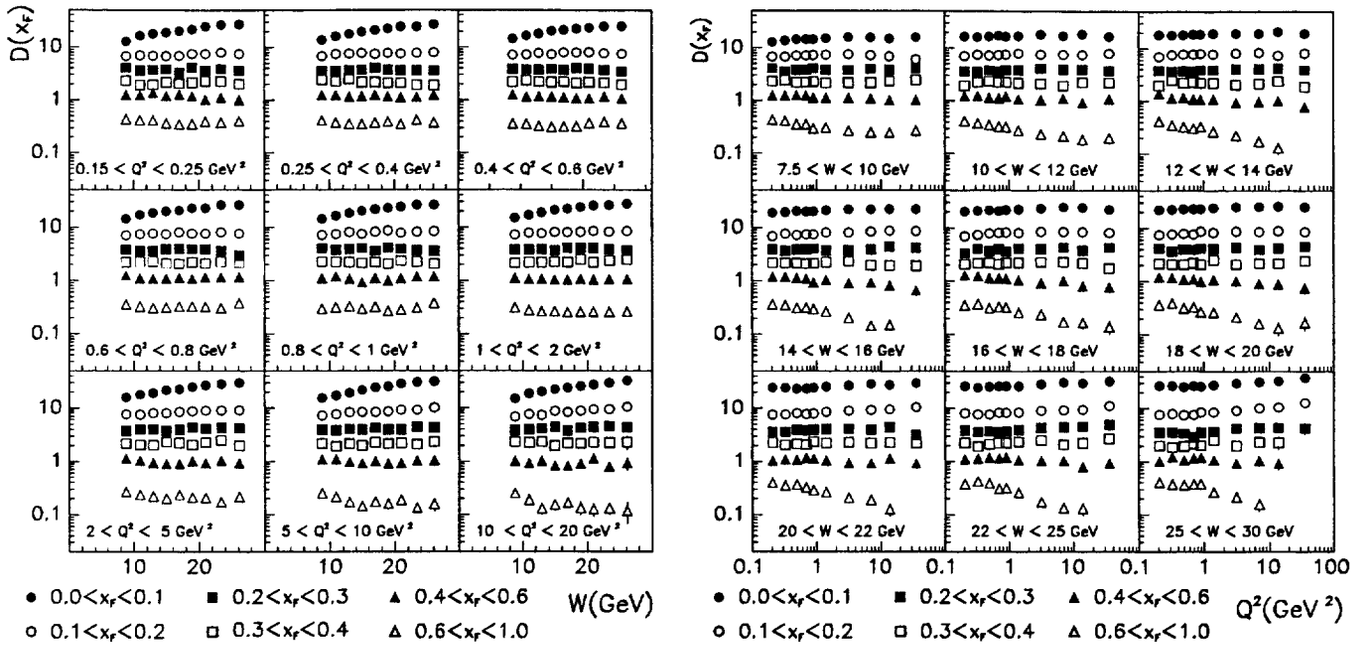

Fig. 7. Dependence of the differential multiplicity $D(x_F)$ in intervals of x_F on W for different regions of Q^2 (left), and on Q^2 for different regions of W (right). Numerical values are given in Table 6.

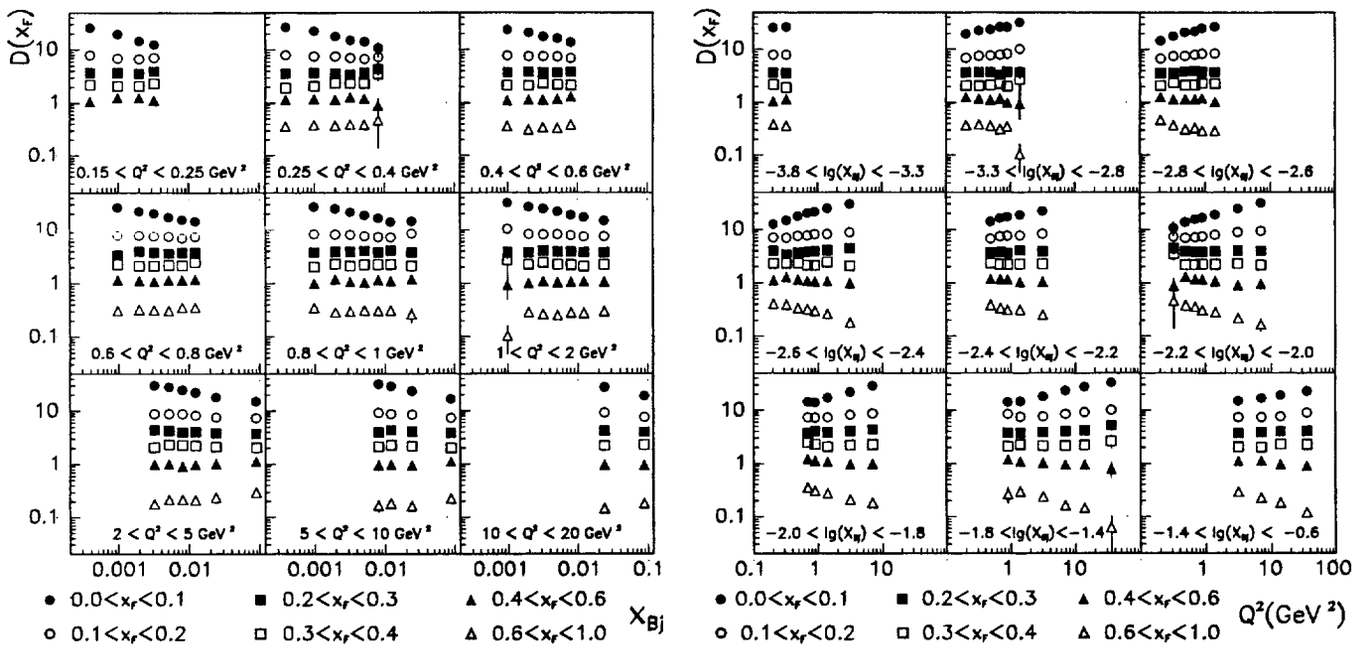

Fig. 8. Dependence of the differential multiplicity $D(x_F)$ in intervals of x_F on x_{Bj} for different regions of Q^2 (left), and on Q^2 for different regions of x_{Bj} (right).

Similar to Fig. 7, where the W and Q^2 dependence of $D(x_F)$ is investigated, in Fig. 8 the x_{Bj} and Q^2 dependence is studied. For the lowest-x_F bin one observes both a variation with Q^2 at fixed x_{Bj} and a variation with x_{Bj} at fixed Q^2. They can be understood as a reflection of the W dependence seen in Fig. 7. At high x_F, $D(x_F)$ does not depend on x_{Bj} if Q^2 is kept fixed, however it decreases with increasing Q^2 if x_{Bj} is kept fixed.

In order to quantify these observations, the data points for a fixed x_F interval in Fig. 7 were fitted by the expressions

$$ln(D(x_F)) = a_W + b_W \cdot ln(W^2) \qquad (13)$$

and

$$ln(D(x_F)) = a_Q + b_Q \cdot ln(Q^2)\ , \qquad (14)$$

with Q^2 and W^2 in GeV^2. The fit results for b_W and b_Q are compiled in Table 4. In the highest-x_F bin, b_Q is

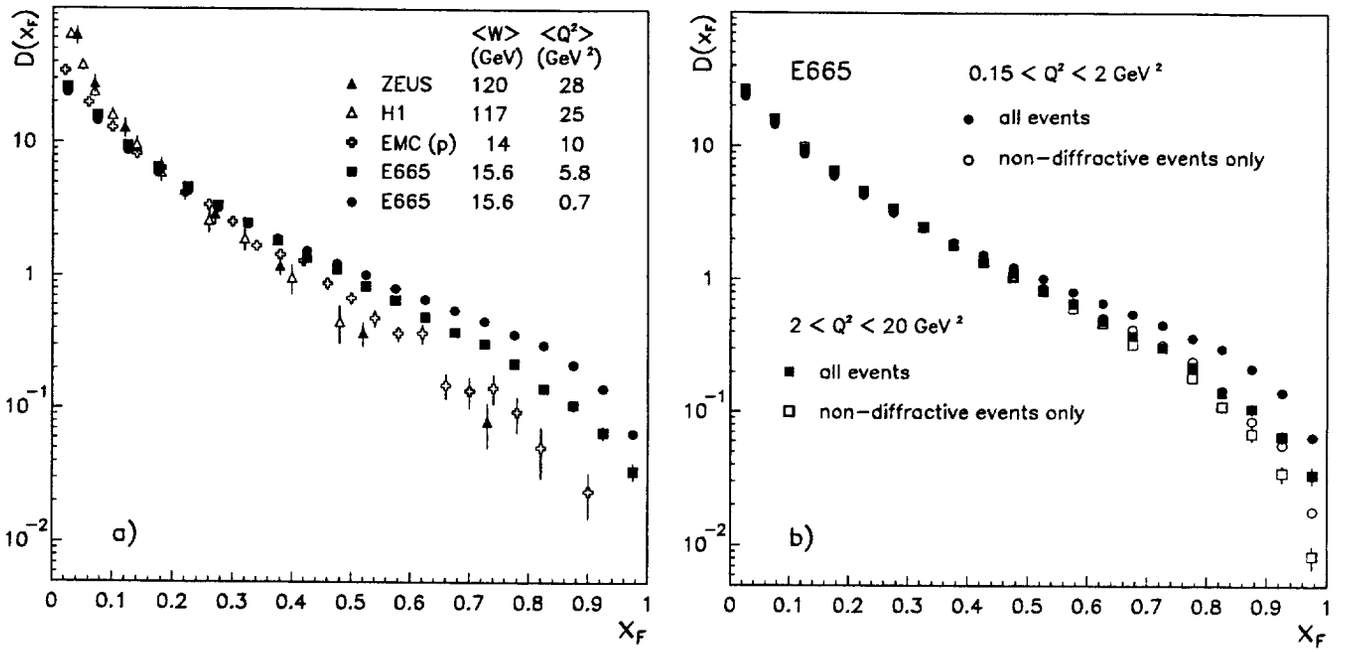

Fig. 9. The normalized inclusive single-particle distribution $D(x_F)$ for charged hadrons from different experiments: E665, EMC [9], H1 [32] and ZEUS [35]. For each data set the respective average values of W and Q^2 are given. The two E665 data sets correspond to $0.15 < Q^2 < 2.0$ GeV^2 and $2.0 < Q^2 < 20$ GeV^2. In Fig. b) the influence from diffractive production is shown for the E665 data.

in the order -0.2, rather independent of W. b_W on the other hand, is close to zero at $Q^2 \lesssim 2$ GeV^2 dropping to -0.25 at $Q^2 \approx 10$ GeV^2. In the lowest-x_F bin b_W is around 0.3, in all Q^2 regions.

Summarizing the behaviour of $D(x_F)$ observed in Figs. 7 and 8 one can conclude that at low x_F $D(x_F)$ is mainly a function of W, whereas at high x_F it is essentially a function of Q^2, with some additional W dependence for $Q^2 \gtrsim 2$ GeV^2.

The clear decrease of $D(x_F)$ with increasing Q^2 at high x_F was also observed in [13] and was qualitatively reproduced by the Lund string model (with or without first order QCD effects) or by the Lund parton shower model. The data from [13] are restricted to the region $Q^2 > 2$ GeV^2. The present results show that at high x_F the Q^2 dependence of $D(x_F)$ at fixed W persists down to lower Q^2, whereas the W dependence at fixed Q^2 diminishes or disappears as Q^2 drops below ~ 2 GeV^2.

As has been demonstrated in [35], hard QCD effects on $D(x_F)$ show up clearly at much higher W ($\langle W \rangle = 120$ GeV): hard gluon radiation leads to a softening of the $D(x_F)$ distribution as W increases. This is seen in Fig. 9a, in which the measurements at lower W (E665 and EMC) are compared with those at high W (H1 and ZEUS). The comparison of the EMC and E665 results, which refer to similar regions in W but different regions in Q^2, reveals a strong Q^2 dependence of $D(x_F)$ at large x_F. As can be seen from Fig. 9b, the contribution from diffractive events causes a hardening of $D(x_F)$. However, a weak Q^2 dependence at large x_F is also present in the sample of non-diffractive events alone.

3.2 The normalized inclusive single-particle distribution $D(p_t^2, x_F)$

The distributions $D(p_t^2, x_F)$ for charged hadrons are displayed in Fig. 10 for different regions of x_F and W (left), and for different regions of x_F and Q^2 (right). In the representation of Fig. 10, where $D(p_t^2, x_F)$ is shown as a function of $lg(p_t^2)$, the distributions exhibit a plateau in the region $p_t^2 \lesssim 0.1$ GeV^2 and a sharp drop around $p_t^2 \approx 1$ GeV^2. In the region $0.001 < p_t^2 < 1.5$ GeV^2 the distributions were fitted by the form:

$$D(p_t^2, x_F) = A_0 \cdot \left(1 + \frac{p_t^2}{m^2}\right)^{-\alpha} \qquad (15)$$

as suggested in [13]. The parameter α describes the shape of $D(p_t^2, x_F)$ at high p_t^2, whereas the parameter m is sensitive to the shape of $D(p_t^2, x_F)$ at low p_t^2.

It is found that for a given interval in x_F the distributions for the different bins in W or Q^2 can be fitted using the same value of m, without the quality of the fits deteriorating. The results of these fits are drawn as solid curves in Fig. 10. The fitted values of the parameters m and α are listed in Table 9 and displayed in Fig. 11. The parameters m and α are found to be strongly (positively) correlated.

The parameter m rises from 0.45 to 1.86 in the region $0 < x_F < 0.6$, dropping to a value of 0.78 in the region $0.6 < x_F < 1$ (Fig. 11, left). In a similar way, the exponent α at fixed W or Q^2 rises with x_F for $x_F < 0.6$, falling down to a low value at $x_F > 0.6$ (Fig. 11, right). At fixed x_F, the exponent α decreases as W increases. Since m is fixed for a given bin in x_F, the latter behaviour of α is equivalent to a reduction of the slope of $D(p_t^2, x_F)$ or a widening of the p_t^2 distribution with

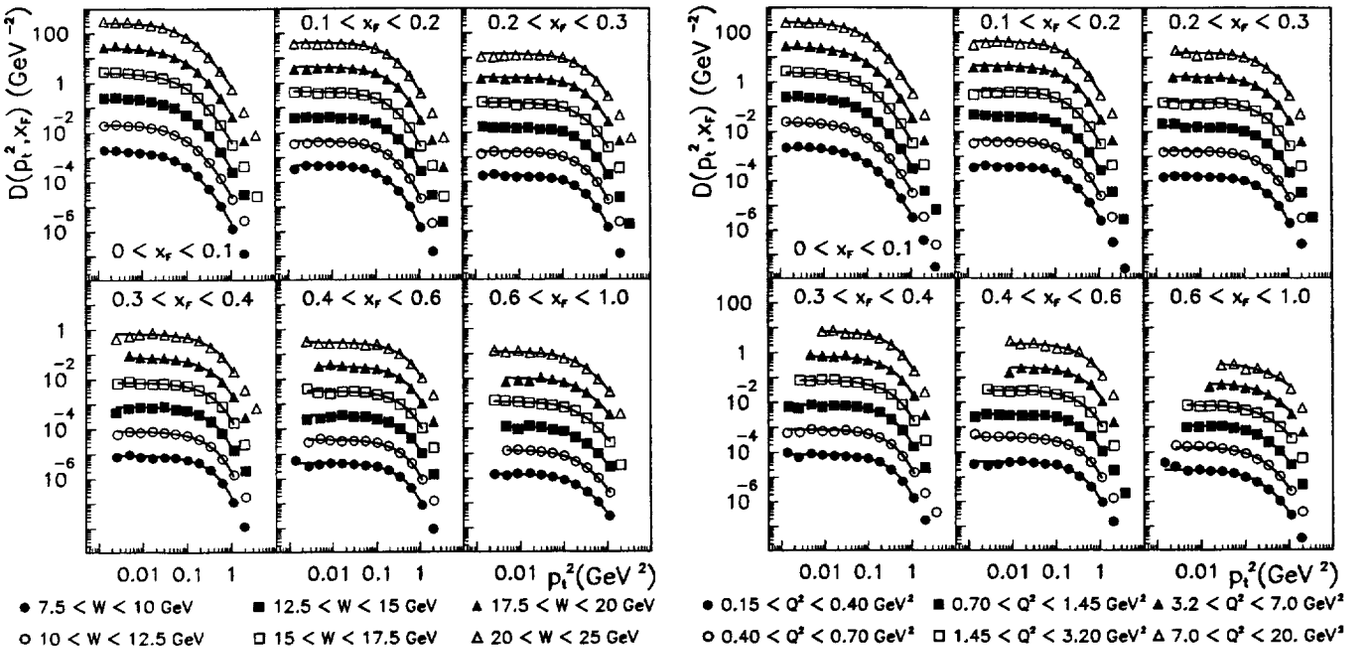

Fig. 10. Normalized inclusive single-particle distributions $D(p_t^2, x_F)$ in intervals of x_F, for different regions of W (left) and Q^2 (right). In each subfigure, starting from top, the distributions have been successively divided by increasing powers of 10 in order to avoid an overlap of the data points. Numerical values are given in Tables 7 and 8.

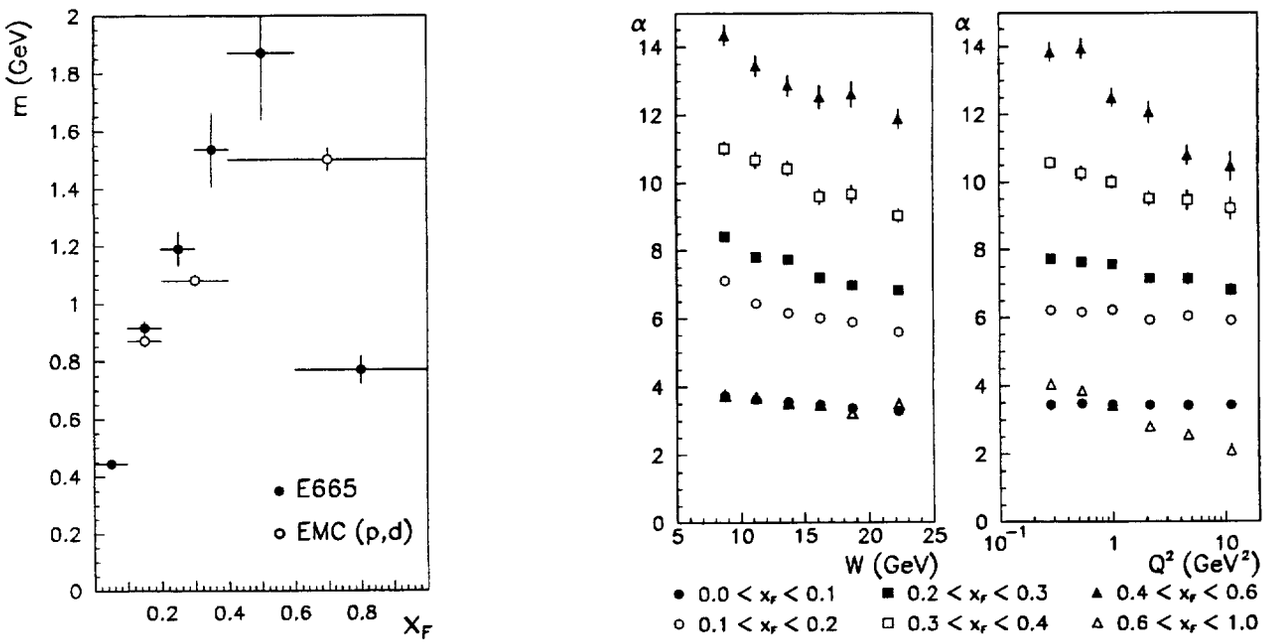

Fig. 11. The parameter m in the expression (15) as a function of x_F (left). The results were obtained by fitting (15) to $D(p_t^2, x_F)$ in the various bins of x_F (Fig. 10): E665 (full circles) and EMC [13] (open circles). Numerical values are given in Tables 9 and 10 for the E665 and EMC data respectively. The parameter α in the expression (15) as a function of W and Q^2 (right). The results were obtained by fitting (15) to $D(p_t^2, x_F)$ in the various bins of x_F (Fig. 10), assuming a common value of the parameter m for a given bin in x_F. Numerical values are given in Tables 9.

increasing W. There is also a variation of α with Q^2, however it is restricted to $x_F > 0.1$.

Performing fits of eq. (15) to the combined H_2 and D_2 data from [13] yields similar results for m (see Fig. 11, left) and the same trend of α with W (see Table 10). It should be noted that the EMC data refer to the Q^2 region 2 to ≈ 100 GeV^2 whereas the E665 data are for $0.15 \lesssim Q^2 \lesssim 20$ GeV^2. This may explain part of the differences between the E665 and EMC results. A more detailed comparison between the E665 and EMC results is made in Section 3.3 in terms of $\langle p_t^2 \rangle$.

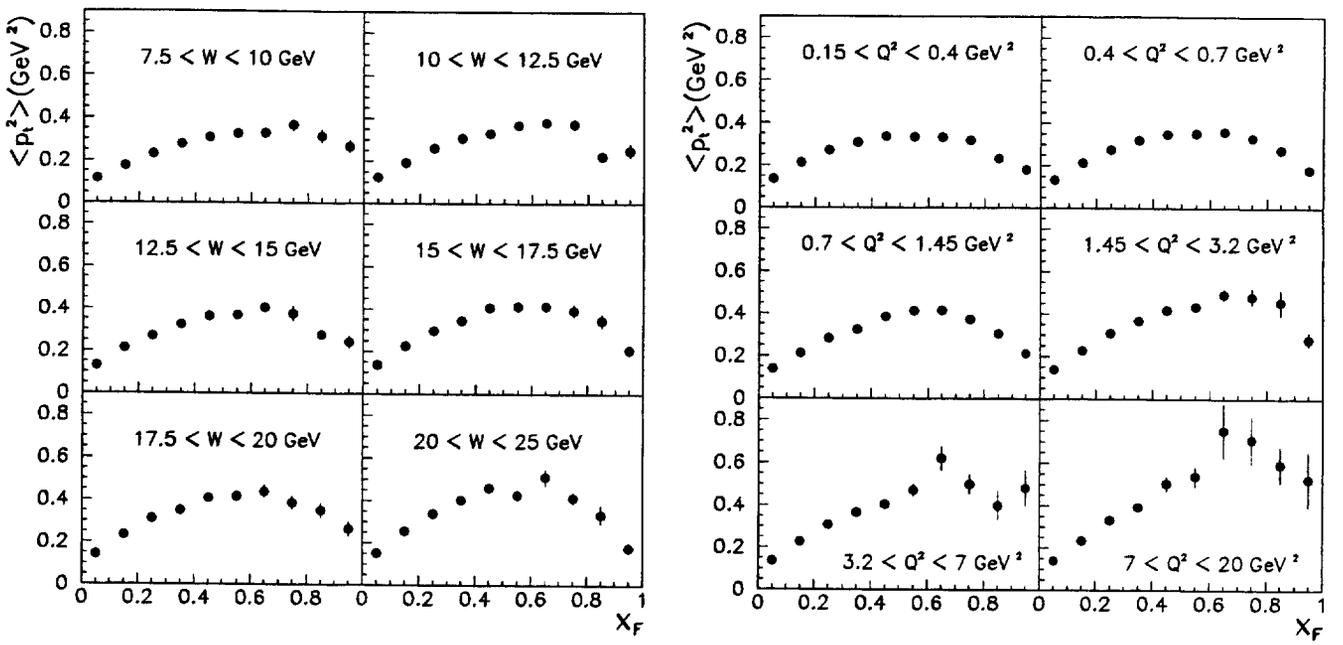

Fig. 12. Average p_t^2 as a function of x_F for different intervals of W (left) and for different intervals of Q^2 (right).

3.3 The dependence of $\langle p_t^2 \rangle$ on x_F, W and Q^2.

The average p_t^2 of charged hadrons is plotted in Fig. 12 as a function of x_F in different regions of W and in different regions of Q^2. For all W and Q^2 bins, the dependence on x_F is similar: a strong rise at low x_F (seagull effect), a maximum at x_F between 0.5 and 0.8, followed by a drop in the highest-x_F region. The latter effect is due to kinematics which requires $p_t \to 0$ in the limit $x_F \to 1$. With increasing W the position of the maximum of $\langle p_t^2 \rangle$ moves towards lower x_F, whereas it moves towards higher x_F as Q^2 increases.

The W and Q^2 dependence of $\langle p_t^2 \rangle$ for different regions of x_F is shown in Fig. 13. In all except the highest x_F bins, $\langle p_t^2 \rangle$ rises with increasing W. Except for the lowest-x_F bin, there is also a clear rise of $\langle p_t^2 \rangle$ as Q^2 increases. It follows that for a description of $\langle p_t^2 \rangle$ in the Q^2 region 0.15 to 20 GeV^2 all three variables x_F, W and Q^2 are relevant.

Fig. 14 displays for different x_F bins the W dependence of $\langle p_t^2 \rangle$ in different regions of Q^2 and similarly in different regions of W the Q^2 dependence of $\langle p_t^2 \rangle$.

Fits of the expressions

$$\langle p_t^2 \rangle = c_W + d_W \cdot ln(W^2) \tag{16}$$

and

$$\langle p_t^2 \rangle = c_Q + d_Q \cdot ln(Q^2) \ , \tag{17}$$

with W^2 and Q^2 in GeV^2, to the data points at fixed x_F in Figs. 14, yield the slope values d_W and d_Q plotted in Fig. 15 and listed in Table 13.

At all x_F below ≈ 0.8, there is a W dependence of $\langle p_t^2 \rangle$ at fixed Q^2, expressed by the slope parameter d_W (Fig. 15 right). The value of d_W is largest for x_F in the region $0.2 < x_F < 0.8$, where d_W increases with increasing Q^2. An appreciable Q^2 dependence at fixed

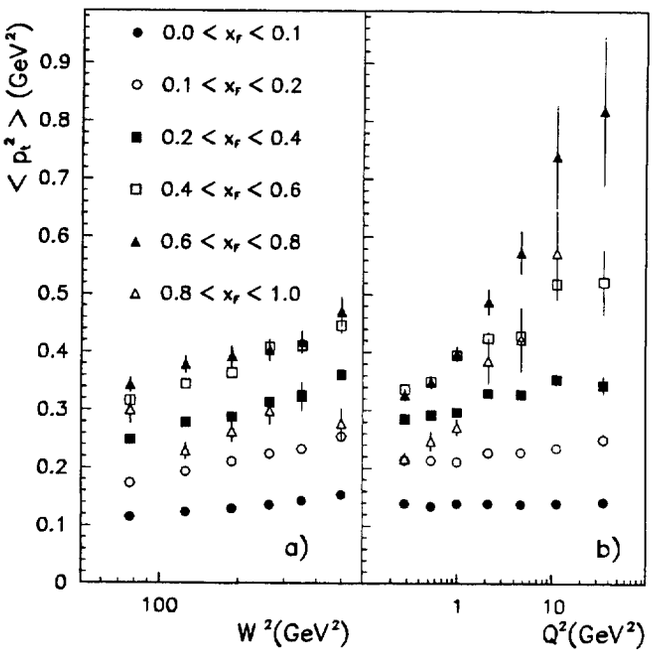

Fig. 13. Dependence of $\langle p_t^2 \rangle$ on W^2 and Q^2 for different intervals of x_F. Numerical values are given in Table 11.

W, expressed by the slope parameter d_Q, is observed for x_F above 0.2 (Fig. 15 left). The value of d_Q is largest for $0.6 < x_F < 0.8$, and increases as W increases.

In comparable regions of x_F and Q^2, the results on d_W are similar to those of [13], which are shown in Table 14 and plotted with open symbols in Fig. 15. Whereas d_Q from [13] is compatible with zero nearly at all x_F and W, d_Q from this analysis is clearly positive for $x_F > 0.2$ and all W. The difference is due to the different Q^2 re-

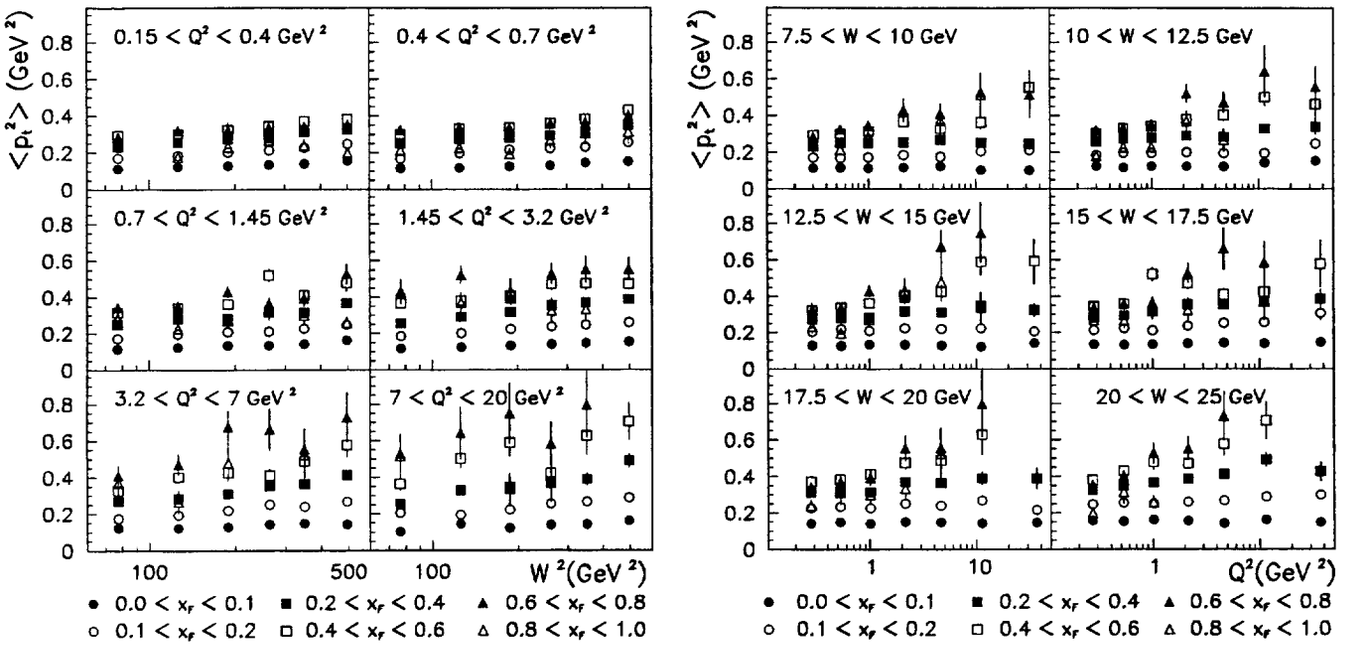

Fig. 14. Dependence of $\langle p_t^2 \rangle$ in different bins of x_F on W^2 for different regions of Q^2 (left) and on Q^2 for different regions of W (right). Numerical values are given in Table 12.

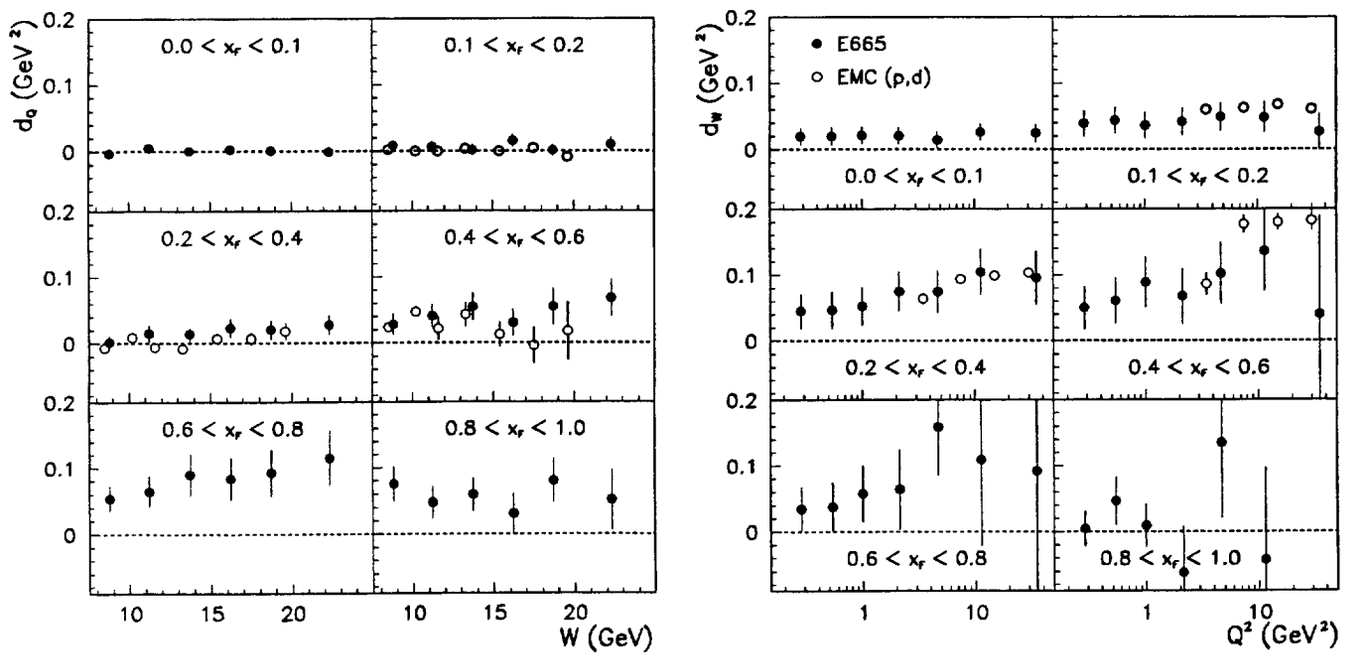

Fig. 15. Slopes d_Q as a function of W and slopes d_W as a function of Q^2, for different intervals of x_F. The slopes were obtained by fitting the expressions (16) and (17) to the experimental data on $\langle p_t^2 \rangle$ in Fig. 14. The slopes d_W and d_Q as obtained from fits to the data from EMC [13] are represented by open symbols. The EMC points drawn in the boxes labelled with $0.4 < x_F < 0.6$ actually are for $0.4 < z_{had} < 1.0$. Numerical values of the E665 data points are given in Table 13, of the EMC data points in Table 14.

gions covered by the two experiments: 0.15 to 20 GeV^2 in E665 and 2 to $\approx$ 100 GeV^2 in [13]. It implies a drop of $\langle p_t^2 \rangle$ when Q^2 passes from $Q^2 \gtrsim 5$ GeV^2 to $Q^2 \lesssim 5$ GeV^2 (see also Fig. 16b below).

The W and Q^2 dependence of $\langle p_t^2 \rangle$ in the x_F region 0.2 to 0.4 is displayed in Figs. 16 for the E665, EMC [13] and ZEUS [35] experiments. In Fig. 16a E665 results are given for two ranges in Q^2. In Fig. 16b the EMC and E665 data are for narrow W bins near 15 GeV. As can be seen from both figures, the E665 data exhibit a Q^2 dependence, approaching the EMC measurements at $Q^2 \gtrsim 3$ GeV^2. At comparable values of Q^2, the increase of $\langle p_t^2 \rangle$ with W is similar for E665 and EMC. A dramatic rise of $\langle p_t^2 \rangle$ with W, which is attributed to hard QCD radiation, is established by the ZEUS measurements in both figures.

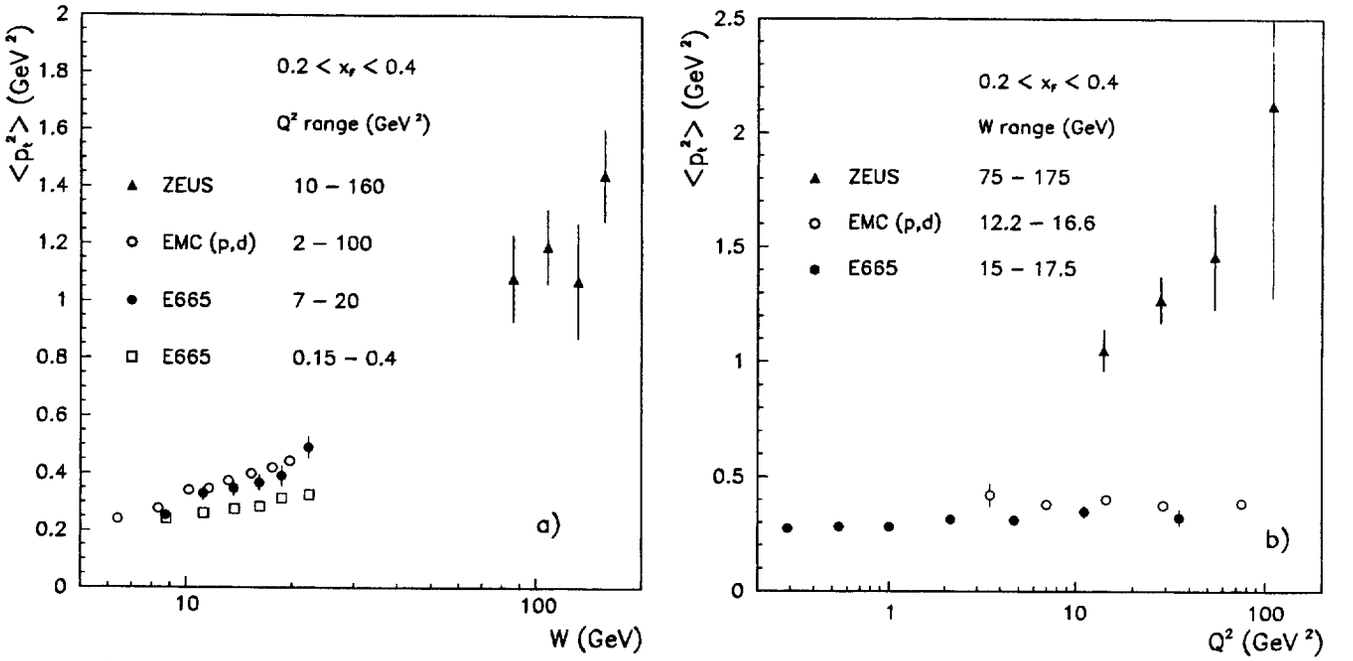

Fig. 16. $\langle p_t^2 \rangle$ for charged hadrons with $0.2 < x_F < 0.4$ as a function of W (left) and as a function of Q^2 (right) from different experiments: E665, EMC [13] and ZEUS [35]. For each data set the respective Q^2 or W range is given.

Predictions from models, which include soft and/or hard gluon effects were compared with experimental measurements of $\langle p_t^2 \rangle$ in [10, 13, 21]. Although completely satisfactory agreement between theory and data was not observed, those analyses suggest that the rise of $\langle p_t^2 \rangle$ with increasing W at $x_F > 0.2$ is due to soft and hard gluon effects. At higher energies, the $\langle p_t^2 \rangle$ data are well described by QCD models [32, 35, 38].

The influence from diffractive production on $\langle p_t^2 \rangle$ is investigated in Fig. 17. It shows $\langle p_t^2 \rangle$ as a function of Q^2 in different x_F bins, for a low-W and a high-W region. The data points for all events (diffractive + non-diffractive) are plotted with full circles, those for non-diffractive events with open circles. The effect from the presence of diffractive events is clearly seen: a reduction of $\langle p_t^2 \rangle$ for $x_F \gtrsim 0.4$, $Q^2 \lesssim 5$ GeV^2 and all W. The observed Q^2 dependence of $\langle p_t^2 \rangle$ in the Q^2 range 0.15 to 20 GeV^2 is thus at least partly due to diffractive production.

In the ZEUS analysis [35], covering the kinematic region $75 < W < 175$ GeV and $10 < Q^2 < 160$ GeV^2, the large-rapidity-gap events, which in good approximation can be identified with diffractive events, were also found to have a much lower $\langle p_t^2 \rangle$ than the events without a large rapidity gap.

3.4 Average forward multiplicities

Corrected average multiplicities $\langle n_F \rangle$ of charged hadrons travelling into the forward hemisphere in the cms were obtained using the standard correction procedure described in Sect. 2.5 . As a check they were also determined from a corrected multiplicity distribution $P_c(n_F)$. $P_c(n_F)$ was computed from the raw multiplicity distribution $P_m(n_F)$ by the unsmearing procedure proposed in [47], where the smearing matrix was determined by means of the MC data. The results obtained by the two methods differ by less then one standard deviation of the statistical errors. In the following only the results from the standard procedure are presented.

In Fig. 18 (left) $\langle n_F \rangle$, $\langle n_F^+ \rangle$ and $\langle n_F^- \rangle$ for charged, positive and negative hadrons respectively are plotted as functions of W^2, Q^2 and x_{Bj}. Straight line fits of the form

$$\langle n_F \rangle = e_W + f_W \cdot ln(W^2/W_0^2) \tag{18}$$

and

$$\langle n_F \rangle = e_Q + f_Q \cdot ln(Q^2/Q_0^2) \tag{19}$$

with W^2 and Q^2 in GeV^2, $W_0^2 = 196.$ GeV^2 and $Q_0^2 = 1.3$ GeV^2, yield the results listed in Table 16.

The forward multiplicities depend mainly on W, and only little on Q^2. Since W and Q^2 are practically uncorrelated in the present data sample (see Table 2), the Q^2 dependence seen in Fig. 18 is genuine and is not a reflection of a W dependence. The Q^2 dependence of $\langle n_F \rangle$, $\langle n_F^+ \rangle$ and $\langle n_F^- \rangle$ is also seen in individual bins of W (not shown). A Q^2 dependence at fixed W has previously been observed in $\mu^+ p$ and νp, $\bar{\nu} p$ interactions for the total average charged multiplicity [5, 7, 25], and separately for the average charged forward and backward multiplicities [25].

The strong variation of the average multiplicities with x_{Bj}, for $x_{Bj} \lesssim 0.0025$, is a reflection of the W dependence.

In Fig. 18 (left) also the ratio h^-/h^+, which is the ratio of average forward multiplicities of negative and positive hadrons, is displayed. It is less than 1 in the whole

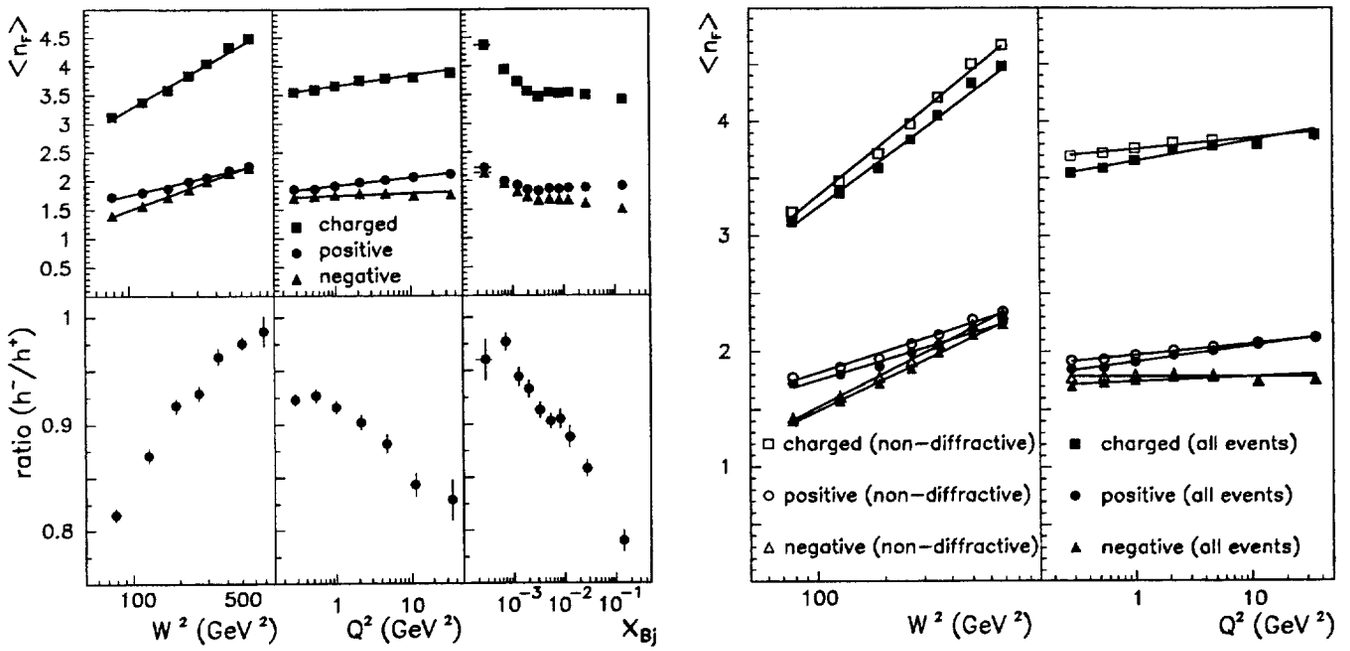

Fig. 18. Average forward multiplicities of positive, negative and charged hadrons, and the h^-/h^+ ratio as functions of W, Q^2 and x_{Bj} (left). Numerical values are given in Table 15. In the figure on the right the influence from diffractive production is shown: the data points for all events (diffractive + non-diffractive) are plotted with full symbols, those for non-diffractive events with open symbols. The solid lines represent the results of fits of straight lines to the data points.

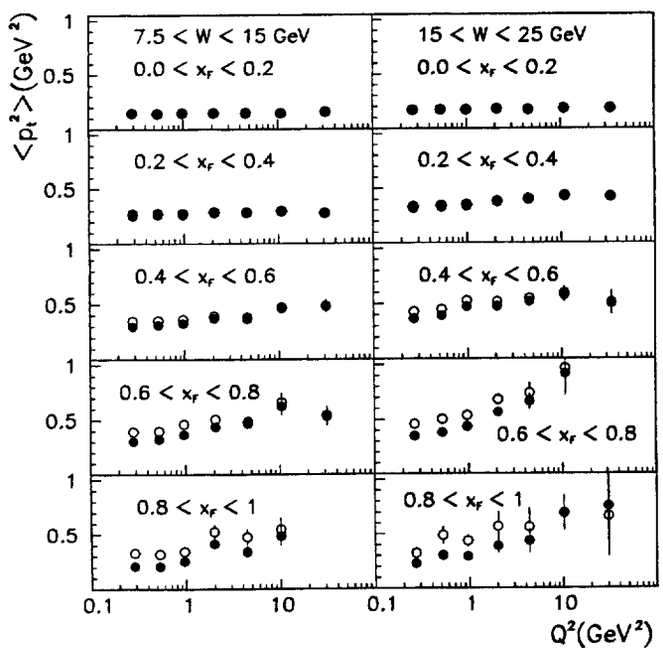

Fig. 17. Dependence of $\langle p_t^2 \rangle$ on Q^2 for different bins of x_F and two regions of W. The data points for all events (diffractive + non-diffractive) are shown as full circles, those for non-diffractive events by open circles.

W range, approaching 1 at the highest W, which corresponds to the lowest x_{Bj}. This behaviour reflects the predominance of the contribution from u quarks over that from d quarks in the proton at higher x_{Bj}, and the increasing contribution from scattering off sea quarks and gluons as x_{Bj} decreases. The same features are present in the Monte Carlo data.

From the comparison of the average forward multiplicities for all events (diffractive + non-diffractive) with those for the non-diffractive events (Fig. 18, right) it is seen that the main effect from the presence of diffractive events is a reduction of $\langle n_F \rangle$ for $Q^2 \lesssim 5$ GeV^2, both for positive and negative particles. The reduction becomes stronger as Q^2 decreases and it amounts to $\sim 4\%$ at the lowest Q^2.

In Fig. 19 $\langle n_F \rangle$ is compared with the results from other experiments as a function of W. The measurements from this analysis agree very well with those from previous neutrino [28] and muon [8] experiments. While the low-W data are still compatible with a linear increase with $ln(W^2)$, the high-W data from H1 [36] combined with the data at lower W suggest a much stronger rise for $W \gtrsim 30$ GeV. This behaviour, which is expected in perturbative QCD, is known from e^+e^- annihilations and hadron-hadron collisions. It should be noted that the data from the different experiments not only refer to different ranges in W but also to different regions in Q^2 and x_{Bj}. An apparent variation of $\langle n_F \rangle$ might therefore also be caused by the different production mechanisms contributing differently in the different kinematic regions.

The average forward multiplicities of charged hadrons were also measured for μd interactions using data taken with a streamer chamber and the E665 forward spectrometer [18]. Those multiplicities, which were determined for $Q^2 > 1$ GeV^2, are on average 15% higher than the ones measured for μp in this analysis, which has the kinematic limit $Q^2 > 0.15$ GeV^2. The systematic errors

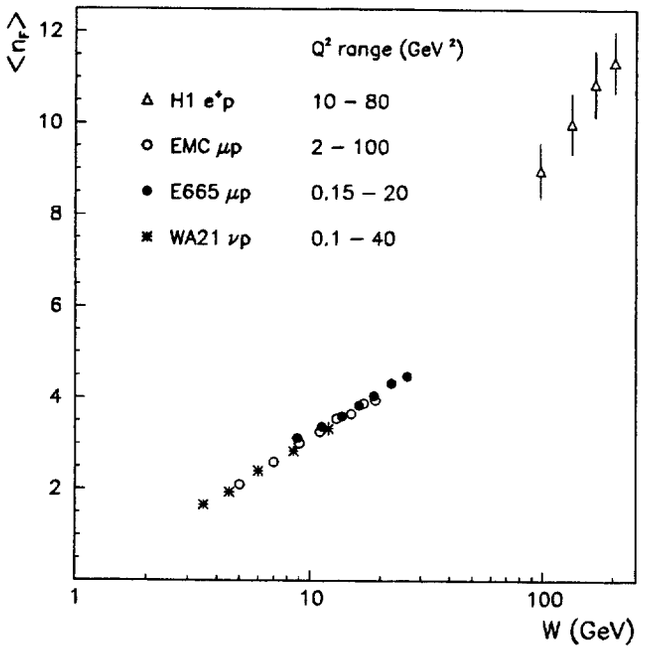

Fig. 19. Average forward multiplicities of charged hadrons from this analysis (full circles) and the WA21 [28], EMC [8] and H1 [36] experiments. For each data set the respective Q^2 range is given. The forward region is defined as the hemisphere in the overall hadronic cms for which the virtual-photon direction defines the pole.

of $\langle n_F \rangle$ are 5.5% and 1% from [18] and from this analysis respectively.

4 Conclusions

The differential multiplicities $D(x_F)$, $D(p_t^2, x_F)$, the mean squared transverse momentum $\langle p_t^2 \rangle$ and the total average multiplicities for charged particles, emitted into the forward (current fragmentation) hemisphere, were measured in the kinematic range $7.5 < W < 30$ GeV, $0.15 < Q^2 < 20$ GeV^2 and $1.5 \cdot 10^{-4} < x_{Bj} < 0.6$.

The main observations are:

- The differential multiplicity $D(x_F)$ is mainly a function of W at low x_F, and essentially a function of Q^2 at high x_F.
- For $Q^2 \lesssim 5$ GeV^2, the contribution from diffractive production leads to a reduction of $D(x_F)$ at low x_F and an enhancement at large x_F.
- There are only weak indications of QCD radiation effects on $D(x_F)$ at large x_F for $Q^2 \gtrsim 5$ GeV^2. Those effects show up more clearly in the comparison with high-W data from the HERA experiments.
- The mean squared transverse momentum $\langle p_t^2 \rangle$ depends on x_F, W and Q^2.
- The presence of diffractive events tends to reduce $\langle p_t^2 \rangle$ for $x_F \gtrsim 0.4$, $Q^2 \lesssim 5$ GeV^2 and all W. The variation of $\langle p_t^2 \rangle$ with Q^2 is partly due to diffractive production.
- The average forward multiplicities of charged hadrons continue to increase linearly with $ln(W^2)$, as seen by previous fixed target experiments, up to $W \approx 30$ GeV. A comparison with the results from the HERA experiments suggests a stronger than linear increase for $W > 30$ GeV.

Acknowledgement. This work was performed at the Fermi National Accelerator Laboratory, which is operated by Universities Research Association, Inc., under contract DE-AC02-76CHO3000 with the U.S. Department of Energy. The work of the University of California, San Diego was supported in part by the National Science Foundation, contract numbers PHY82-05900, PHY85-11584, and PHY88-10221; the University of Illinois at Chicago by NSF contract PHY88-11164; and the University of Washington by NSF contract numbers PHY83-13347 and PHY86-13003. The University of Washington was also supported by the U.S. Department of Energy. The work of Argonne National Laboratory was supported by the Department of Energy, Nuclear Physics Division, under Contract No. W-31-109-ENG-38. The Department of Energy, High Energy Physics Division, supported the work of Harvard University, the University of Maryland, the Massachussetts Institute of Technology under Contract No. DE-AC02-76ER03069, Northwestern University under Contract No. DE-FG02-91ER40684, and Yale University. Northwestern University also received support from the A.P. Sloan Foundation and an A.T.&T. Fellowship. The Albert-Ludwigs-Universität Freiburg and the University of Wuppertal were supported in part by the Bundesministerium für Forschung und Technologie. The work of the Institute for Nuclear Physics, Krakow, was supported in part by the Polish Committee for Scientific Research under grant No. 2P03B23008. The work of the KFKI, Institute for Particle and Nuclear Physics, Budapest, was supported by the Hungarian Science Foundation under grant No. OTKA T 16609 and T22503.
Useful discussions with N. Pavel and K. Hamacher are gratefully acknowledged.

References

1. J.J. Aubert et al. (EMC), Phys.Lett. 95B (1980) 306
2. J.J. Aubert et al. (EMC), Phys.Lett. 114B (1982) 373
3. M. Arneodo et al. (EMC, NA9), Phys.Lett. 149B (1984) 415
4. M. Arneodo et al. (EMC, NA9), Nucl.Phys. B258 (1985) 249
5. M. Arneodo et al. (EMC), Phys.Lett. 165B (1985) 222
6. J.J. Aubert et al. (EMC), Z.Phys. C30 (1986) 23
7. M. Arneodo et al. (EMC), Z.Phys. C31 (1986) 1
8. M. Arneodo et al. (EMC), Z.Phys. C35 (1987) 335
9. M. Arneodo et al. (EMC), Z.Phys. C35 (1987) 417
10. M. Arneodo et al. (EMC), Z.Phys. C36 (1987) 527
11. H. Schiemann (EMC, NA4), Thesis, Internal report, DESY F14-87-05
12. M.R. Adams et al. (E665), Phys.Lett. B272 (1991) 163
13. J. Ashman et al. (EMC), Z.Phys. C52 (1991) 361
14. J. Ashman et al. (EMC), Z.Phys. C52 (1991) 1
15. P. Amaudruz et al. (NMC), Z.Phys. C54 (1992) 239
16. M.R. Adams et al. (E665), Phys.Rev. D48 (1993) 5057
17. M.R Adams et al. (E665), Phys.Rev. D50 (1994) 1836
18. M.R Adams et al. (E665), Z.Phys. C61 (1994) 179
19. M.R. Adams et al. (E665), Z.Phys. C74 (1997) 237
20. D. Allassia et al. (WA25), Z.Phys. C24 (1984) 119
21. G.T. Jones et al. (WA21), Z.Phys. C25 (1984) 121
22. P.J. Fitch at al. (WA59), Z.Phys. C31 (1986) 51
23. W. Wittek et al. (WA59), Z.Phys. C40 (1988) 231
24. W. Wittek et al. (WA59), Z.Phys. C44 (1989) 175
25. G.T. Jones et al. (WA21), Z.Phys. C46 (1990) 25
26. P.C. Bosetti et al. (WA21,WA47), Z.Phys. C46 (1990) 377
27. G.T. Jones et al. (WA21), Z.Phys. C51 (1991) 11
28. G.T. Jones et al. (WA21), Z.Phys. C54 (1992) 45
29. G.T. Jones et al. (WA21), Z.Phys. C58 (1993) 375
30. N. Schmitz, Int. J. of Mod. Phys. A9 (1988) 1997

31. N. Schmitz, Int. J. of Mod. Phys. A8 (1993) 1993
32. I. Abt et al. (H1), Z.Phys. C63 (1994) 377
33. M. Derrick et al. (ZEUS), Z.Phys. C67 (1995) 93
34. N. Pavel, DESY report 95-147, July 1995
35. M. Derrick et al. (ZEUS), Z.Phys. C70 (1996) 1
36. S. Aid et al. (H1), Z.Phys. C72 (1996) 573
37. C. Adloff et al. (H1), DESY report 96-215, October 1996
38. T. Carli, DESY report 97-010, January 1997
39. M.R. Adams et al. (E665), Nucl.Inst.and Meth. A291 (1990) 533
40. M. Adams et al. (E665), Phys.Rev. D54 (1996) 3006
41. R. Brun et al., CERN report DD/78/2 (1978)
42. G. Ingelman, The Lund Monte Carlo for deep-inelastic lepton-nucleon scattering (1983);
T. Sjöstrand, Comp. Phys. Comm. **39**, 347 (1986)
43. A. Donnachie and P.V. Landshoff, Z.Phys. C61 (1994) 139
44. A. Arvidson and B. Badelek, The GAMRAD program, Int. report NMC/92/5 (1992)
45. L.W. Mo and Y.S. Tsai, Rev.Mod.Phys. 41 (1969) 205
46. Y.S. Tsai, SLAC-Pub 848 (1971)
47. M. Schmelling, Nucl.Inst.and Meth. A340 (1994) 400

Table 1. Definition of kinematic variables. With the exception of x_F, all quantities are defined in the laboratory system.

Variable	Description
Event variables:	
$k_\mu = (E_\mu, \mathbf{k}_\mu)$	Four-momentum of the incident μ
$k'_\mu = (E'_\mu, \mathbf{k}'_\mu)$	Four-momentum of the scattered μ
Θ_μ	μ scattering angle
$P = (M, 0)$	Four-momentum of the target proton
$q = k_\mu - k'_\mu = (\nu, \mathbf{q})$	Four-momentum transfer
$Q^2 = -q^2$	Negative invariant mass squared of the virtual photon
$\nu = P \cdot q/M = E_\mu - E'_\mu$	Energy of the virtual photon
$W^2 = M^2 + 2M\nu - Q^2$	Total hadronic center-of-mass energy squared
$x_{Bj} = Q^2/2M\nu$	Bjorken scaling variable
$y = \nu/E_\mu$	Fractional leptonic energy transfer
Hadron variables:	
$p_{lab} = (E_{had}, \mathbf{p}_{had})$	Four-momentum of a hadron
$p_t = \lvert\mathbf{q} \times \mathbf{p}_{had}\rvert/\lvert\mathbf{q}\rvert$	Transverse momentum of a hadron relative to the virtual-photon direction
$x_F = p_l^*/p_{l\ max}^*$ (in cms)	Feynman-x variable; p_l^* is the longitudinal momentum (relative to the virtual-photon direction) in the cms, $p_{l\ max}^*$ its maximum value for a given W.
$z_{had} = E_{had}/\nu$	Fractional energy of a hadron

Table 3. Estimated systematic errors for charged hadrons (positive + negative).

quantity	defined in formula	estimated systematic error
$\Delta D(x_F)\ /\ D(x_F)$	(1)	4%
$\Delta D(p_t^2, x_F)\ /\ D(p_t^2, x_F)$	(3)	4%
$\Delta\langle n_F\rangle/\langle n_F\rangle$	(2)	1%
$\Delta\langle p_t^2\rangle/\langle p_t^2\rangle$		2%

Table 2. Number of reconstructed events after the selections (4), (5) and (6) and after removing the events defined by (8). For each bin in W and Q^2 also the average values of W, Q^2 and x_{Bj} are given.

W (GeV)	Q^2 (GeV^2)	no. of reconstr. events	$\langle W \rangle$ (GeV)	$\langle Q^2 \rangle$ (GeV^2)	$\langle x_{Bj} \rangle$
all W	all Q^2	191445	15.6	2.51	0.0131
	$0.15 < Q^2 < 0.4$	43761	16.5	0.283	0.0015
	$0.4 < Q^2 < 0.7$	42208	15.0	0.536	0.0034
	$0.7 < Q^2 < 1.45$	44159	15.1	1.00	0.0062
	$1.45 < Q^2 < 3.2$	28814	15.8	2.14	0.0118
	$3.2 < Q^2 < 7$	17324	15.8	4.69	0.0258
	$7 < Q^2 < 20$	11584	15.4	11.3	0.0612
	$20 < Q^2 < 100$	3595	16.0	35.5	0.1464
$7.5 < W < 10.0$	all Q^2	33972	8.79	2.26	0.0264
	$0.15 < Q^2 < 0.4$	6414	8.81	0.297	0.0039
	$0.4 < Q^2 < 0.7$	8796	8.79	0.540	0.0072
	$0.7 < Q^2 < 1.45$	8878	8.79	0.991	0.0131
	$1.45 < Q^2 < 3.2$	4560	8.79	2.12	0.0274
	$3.2 < Q^2 < 7$	2788	8.80	4.69	0.0585
	$7 < Q^2 < 20$	2051	8.75	11.19	0.1292
	$20 < Q^2 < 100$	485	8.83	31.90	0.2864
$10.0 < W < 12.5$	all Q^2	31874	11.2	2.489	0.0182
	$0.15 < Q^2 < 0.4$	6209	11.2	0.296	0.0024
	$0.4 < Q^2 < 0.7$	7757	11.2	0.539	0.0044
	$0.7 < Q^2 < 1.45$	8035	11.2	0.988	0.0079
	$1.45 < Q^2 < 3.2$	4478	11.3	2.13	0.0168
	$3.2 < Q^2 < 7$	2813	11.2	4.74	0.0368
	$7 < Q^2 < 20$	2005	11.2	11.4	0.0838
	$20 < Q^2 < 100$	577	11.2	34.1	0.2096
$12.5 < W < 15.0$	all Q^2	29251	13.7	2.64	0.0131
	$0.15 < Q^2 < 0.4$	6110	13.8	0.293	0.0016
	$0.4 < Q^2 < 0.7$	6630	13.7	0.535	0.0029
	$0.7 < Q^2 < 1.45$	6935	13.7	1.00	0.0053
	$1.45 < Q^2 < 3.2$	4440	13.8	2.15	0.0113
	$3.2 < Q^2 < 7$	2641	13.7	4.73	0.0248
	$7 < Q^2 < 20$	1876	13.7	11.2	0.0567
	$20 < Q^2 < 100$	619	13.7	35.3	0.1550
$15.0 < W < 17.5$	all Q^2	17525	16.2	2.62	0.0095
	$0.15 < Q^2 < 0.4$	6052	16.2	0.284	0.0011
	$0.4 < Q^2 < 0.7$	5841	16.2	0.535	0.0021
	$0.7 < Q^2 < 1.45$	6206	16.2	1.01	0.0038
	$1.45 < Q^2 < 3.2$	4537	16.3	2.15	0.0081
	$3.2 < Q^2 < 7$	2666	16.3	4.68	0.0176
	$7 < Q^2 < 20$	1691	16.2	11.1	0.0408
	$20 < Q^2 < 100$	532	16.2	37.5	0.1222
$17.5 < W < 20.0$	all Q^2	24163	18.7	2.62	0.0072
	$0.15 < Q^2 < 0.4$	5960	18.7	0.276	0.0008
	$0.4 < Q^2 < 0.7$	4768	18.7	0.533	0.0015
	$0.7 < Q^2 < 1.45$	5124	18.7	1.01	0.0029
	$1.45 < Q^2 < 3.2$	3998	18.7	2.15	0.0062
	$3.2 < Q^2 < 7$	2372	18.7	4.65	0.0132
	$7 < Q^2 < 20$	1454	18.7	11.3	0.0313
	$20 < Q^2 < 100$	487	18.7	36.5	0.0931
$20.0 < W < 25.0$	all Q^2	36594	22.3	2.58	0.0051
	$0.15 < Q^2 < 0.4$	10566	22.4	0.268	0.0005
	$0.4 < Q^2 < 0.7$	6900	22.3	0.533	0.0011
	$0.7 < Q^2 < 1.45$	7348	22.3	1.01	0.0021
	$1.45 < Q^2 < 3.2$	5583	22.3	2.14	0.0044
	$3.2 < Q^2 < 7$	3343	22.3	4.65	0.0094
	$7 < Q^2 < 20$	2074	22.3	11.5	0.0229
	$20 < Q^2 < 100$	780	22.2	37.3	0.0701
$25.0 < W < 30.0$	all Q^2	8066	26.1	2.21	0.0032
	$0.15 < Q^2 < 0.4$	2450	26.1	0.264	0.0004
	$0.4 < Q^2 < 0.7$	1516	26.2	0.535	0.0008
	$0.7 < Q^2 < 1.45$	1633	26.1	1.00	0.0015
	$1.45 < Q^2 < 3.2$	1218	26.1	2.13	0.0031
	$3.2 < Q^2 < 7$	701	26.2	4.71	0.0069
	$7 < Q^2 < 20$	433	26.1	11.2	0.0162
	$20 < Q^2 < 100$	115	26.0	34.3	0.0481

Table 4. Fitted parameters b_W and b_Q from fits of the expressions (13) and (14) to the data points on $D(x_F)$ in Fig. 7. In the fits a systematic error of 4% for the data points $\langle n_F \rangle$ has been assumed, which was added quadratically to the statistical error.

	slope b_Q					
W range (GeV)	$0 < x_F < 0.1$	$0.1 < x_F < 0.2$	$0.2 < x_F < 0.3$	$0.3 < x_F < 0.4$	$0.4 < x_F < 0.6$	$0.6 < x_F < 1$
all W	0.029 ± 0.024	0.034 ± 0.017	0.026 ± 0.012	0.005 ± 0.009	-0.059 ± 0.007	-0.200 ± 0.015
$7.5 < W < 10$	0.034 ± 0.024	-0.004 ± 0.019	0.009 ± 0.017	-0.009 ± 0.017	-0.048 ± 0.016	-0.147 ± 0.024
$10 < W < 12$	0.014 ± 0.024	0.016 ± 0.019	0.022 ± 0.017	-0.017 ± 0.019	-0.050 ± 0.017	-0.184 ± 0.028
$12 < W < 14$	0.020 ± 0.025	0.015 ± 0.019	0.027 ± 0.017	-0.022 ± 0.019	-0.079 ± 0.018	-0.216 ± 0.031
$14 < W < 16$	0.031 ± 0.025	0.045 ± 0.019	0.019 ± 0.017	-0.010 ± 0.019	-0.099 ± 0.019	-0.233 ± 0.032
$16 < W < 18$	0.027 ± 0.025	0.028 ± 0.019	0.030 ± 0.018	0.004 ± 0.020	-0.095 ± 0.020	-0.194 ± 0.032
$18 < W < 20$	0.031 ± 0.026	0.033 ± 0.020	0.022 ± 0.018	0.016 ± 0.021	-0.068 ± 0.021	-0.219 ± 0.034
$20 < W < 22$	0.046 ± 0.027	0.062 ± 0.020	0.017 ± 0.019	0.014 ± 0.022	-0.030 ± 0.023	-0.260 ± 0.037
$22 < W < 25$	0.051 ± 0.027	0.063 ± 0.020	0.057 ± 0.019	0.040 ± 0.021	-0.047 ± 0.022	-0.325 ± 0.035
$25 < W < 30$	0.069 ± 0.029	0.091 ± 0.026	0.060 ± 0.027	0.035 ± 0.036	-0.026 ± 0.036	-0.271 ± 0.052
	slope b_W					
Q^2 range (GeV^2)	$0 < x_F < 0.1$	$0.1 < x_F < 0.2$	$0.2 < x_F < 0.3$	$0.3 < x_F < 0.4$	$0.4 < x_F < 0.6$	$0.6 < x_F < 1$
all Q^2	0.297 ± 0.058	0.073 ± 0.040	0.005 ± 0.027	-0.010 ± 0.019	-0.048 ± 0.011	-0.044 ± 0.027
$0.15 < Q^2 < 0.25$	0.334 ± 0.060	0.064 ± 0.044	-0.020 ± 0.038	0.011 ± 0.040	-0.083 ± 0.037	-0.069 ± 0.048
$0.25 < Q^2 < 0.40$	0.302 ± 0.059	0.054 ± 0.042	0.013 ± 0.033	-0.103 ± 0.031	-0.034 ± 0.027	-0.014 ± 0.039
$0.40 < Q^2 < 0.60$	0.267 ± 0.059	0.041 ± 0.042	-0.012 ± 0.034	-0.039 ± 0.031	-0.059 ± 0.027	0.001 ± 0.040
$0.60 < Q^2 < 0.80$	0.274 ± 0.060	0.047 ± 0.044	-0.023 ± 0.036	-0.020 ± 0.036	-0.037 ± 0.033	-0.032 ± 0.047
$0.80 < Q^2 < 1$	0.288 ± 0.060	0.072 ± 0.046	-0.024 ± 0.040	-0.019 ± 0.041	-0.019 ± 0.040	0.009 ± 0.058
$1 < Q^2 < 2$	0.287 ± 0.060	0.070 ± 0.043	0.021 ± 0.033	0.061 ± 0.031	-0.028 ± 0.027	-0.078 ± 0.045
$2 < Q^2 < 5$	0.297 ± 0.061	0.096 ± 0.045	0.053 ± 0.036	0.041 ± 0.034	-0.064 ± 0.032	-0.144 ± 0.055
$5 < Q^2 < 10$	0.350 ± 0.063	0.136 ± 0.048	0.033 ± 0.043	0.029 ± 0.049	-0.075 ± 0.050	-0.244 ± 0.083
$10 < Q^2 < 20$	0.340 ± 0.065	0.178 ± 0.053	0.073 ± 0.053	-0.024 ± 0.067	-0.050 ± 0.069	-0.327 ± 0.113
$20 < Q^2 < 100$	0.400 ± 0.070	0.268 ± 0.062	0.039 ± 0.071	0.017 ± 0.088	-0.065 ± 0.093	-0.684 ± 0.168

Table 5. Normalized inclusive single-particle distributions $D(x_F)$ of charged hadrons for all events in different intervals of W (GeV) and Q^2 (GeV^2) (Fig. 5) and x_{Bj} (Fig. 6).

$\langle W \rangle$ (GeV)	$0.0 < x_F < 0.1$	$0.1 < x_F < 0.2$	$0.2 < x_F < 0.3$	$0.3 < x_F < 0.4$	$0.4 < x_F < 0.6$	$0.6 < x_F < 1.0$
8.79	14.58 ± 0.14	7.02 ± 0.07	3.80 ± 0.05	2.26 ± 0.04	1.20 ± 0.02	0.35 ± 0.01
11.0	16.67 ± 0.15	7.46 ± 0.08	3.71 ± 0.05	2.16 ± 0.04	1.13 ± 0.02	0.32 ± 0.01
13.0	18.43 ± 0.16	7.73 ± 0.08	3.71 ± 0.05	2.21 ± 0.04	1.09 ± 0.02	0.30 ± 0.01
15.0	20.46 ± 0.17	7.61 ± 0.08	3.78 ± 0.06	2.18 ± 0.04	1.07 ± 0.02	0.29 ± 0.01
17.0	21.67 ± 0.17	7.86 ± 0.08	3.91 ± 0.06	2.21 ± 0.05	1.12 ± 0.03	0.30 ± 0.01
19.0	23.08 ± 0.19	8.09 ± 0.09	4.06 ± 0.07	2.22 ± 0.05	1.08 ± 0.03	0.30 ± 0.01
21.0	24.79 ± 0.21	8.20 ± 0.10	3.86 ± 0.07	2.20 ± 0.06	1.06 ± 0.03	0.31 ± 0.01
23.4	26.34 ± 0.20	8.26 ± 0.10	3.86 ± 0.07	2.23 ± 0.05	1.09 ± 0.03	0.30 ± 0.01
26.1	27.47 ± 0.32	8.22 ± 0.15	3.58 ± 0.10	2.10 ± 0.08	1.10 ± 0.05	0.32 ± 0.02
$\langle Q^2 \rangle$ (GeV^2)	$0.0 < x_F < 0.1$	$0.1 < x_F < 0.2$	$0.2 < x_F < 0.3$	$0.3 < x_F < 0.4$	$0.4 < x_F < 0.6$	$0.6 < x_F < 1.0$
0.20	18.93 ± 0.19	7.02 ± 0.09	3.68 ± 0.07	2.12 ± 0.05	1.18 ± 0.03	0.40 ± 0.01
0.32	18.73 ± 0.15	7.27 ± 0.07	3.58 ± 0.05	2.20 ± 0.04	1.18 ± 0.02	0.38 ± 0.01
0.49	18.98 ± 0.15	7.46 ± 0.07	3.77 ± 0.05	2.18 ± 0.04	1.15 ± 0.02	0.34 ± 0.01
0.69	19.17 ± 0.19	7.50 ± 0.09	3.68 ± 0.06	2.19 ± 0.05	1.15 ± 0.02	0.33 ± 0.01
0.89	19.10 ± 0.22	7.75 ± 0.11	3.93 ± 0.07	2.20 ± 0.05	1.11 ± 0.03	0.31 ± 0.01
1.40	20.04 ± 0.15	7.90 ± 0.07	3.84 ± 0.05	2.25 ± 0.04	1.06 ± 0.02	0.28 ± 0.01
3.14	20.76 ± 0.17	8.09 ± 0.08	3.98 ± 0.06	2.18 ± 0.04	0.99 ± 0.02	0.23 ± 0.01
7.02	21.04 ± 0.26	8.11 ± 0.12	3.99 ± 0.08	2.10 ± 0.06	1.02 ± 0.03	0.19 ± 0.01
13.8	20.88 ± 0.34	8.01 ± 0.17	4.06 ± 0.12	2.29 ± 0.09	0.95 ± 0.04	0.18 ± 0.01
35.4	21.33 ± 0.43	8.59 ± 0.23	4.11 ± 0.16	2.26 ± 0.12	0.92 ± 0.06	0.15 ± 0.01
$\langle x_{Bj} \rangle$	$0.0 < x_F < 0.1$	$0.1 < x_F < 0.2$	$0.2 < x_F < 0.3$	$0.3 < x_F < 0.4$	$0.4 < x_F < 0.6$	$0.6 < x_F < 1.0$
0.00039	25.55 ± 0.32	7.85 ± 0.15	3.69 ± 0.10	2.11 ± 0.08	1.07 ± 0.05	0.38 ± 0.02
0.00098	21.34 ± 0.14	7.38 ± 0.06	3.65 ± 0.05	2.10 ± 0.04	1.17 ± 0.02	0.38 ± 0.01
0.00198	18.78 ± 0.15	7.36 ± 0.08	3.69 ± 0.05	2.18 ± 0.04	1.17 ± 0.02	0.35 ± 0.01
0.00320	17.89 ± 0.15	7.34 ± 0.07	3.67 ± 0.05	2.27 ± 0.04	1.15 ± 0.02	0.35 ± 0.01
0.00514	18.47 ± 0.16	7.65 ± 0.08	3.79 ± 0.05	2.26 ± 0.04	1.11 ± 0.02	0.31 ± 0.01
0.00805	18.22 ± 0.18	7.73 ± 0.09	3.84 ± 0.06	2.19 ± 0.04	1.09 ± 0.02	0.30 ± 0.01
0.01220	18.57 ± 0.22	7.70 ± 0.10	3.96 ± 0.07	2.19 ± 0.05	1.06 ± 0.03	0.27 ± 0.01
0.02403	18.33 ± 0.18	7.79 ± 0.09	3.85 ± 0.06	2.18 ± 0.05	1.01 ± 0.02	0.24 ± 0.01
0.08827	17.62 ± 0.22	7.66 ± 0.11	3.93 ± 0.08	2.18 ± 0.06	1.03 ± 0.03	0.21 ± 0.01
0.33246	14.83 ± 0.79	7.18 ± 0.45	4.57 ± 0.41	2.29 ± 0.26	1.05 ± 0.12	0.32 ± 0.05

Table 6. Normalized inclusive single-particle distributions $D(x_F)$ of charged hadrons in different intervals of W (GeV) and Q^2 (GeV^2) (Fig. 7). Corresponding average values of x_{Bj} are given as well.

$< W >$	$< Q^2 >$	$< x_{Bj} >$	$0 < x_F < 0.1$	$0.1 < x_F < 0.2$	$0.2 < x_F < 0.3$	$0.3 < x_F < 0.4$	$0.4 < x_F < 0.6$	$0.6 < x_F < 1$
8.81	0.21	$2.78E-3$	12.83 ± 0.58	6.81 ± 0.28	4.03 ± 0.20	2.30 ± 0.16	1.23 ± 0.08	0.43 ± 0.03
8.80	0.33	$4.35E-3$	13.81 ± 0.36	6.71 ± 0.17	3.55 ± 0.12	2.38 ± 0.10	1.22 ± 0.05	0.41 ± 0.02
8.79	0.50	$6.58E-3$	14.57 ± 0.34	7.12 ± 0.15	3.83 ± 0.11	2.20 ± 0.08	1.24 ± 0.04	0.36 ± 0.02
8.79	0.69	$9.16E-3$	14.43 ± 0.40	7.11 ± 0.19	3.78 ± 0.13	2.22 ± 0.10	1.23 ± 0.05	0.36 ± 0.02
8.78	0.89	$1.18E-2$	14.55 ± 0.47	7.20 ± 0.23	4.03 ± 0.16	2.28 ± 0.11	1.11 ± 0.06	0.29 ± 0.02
8.79	1.38	$1.81E-2$	15.04 ± 0.34	7.26 ± 0.16	3.80 ± 0.11	2.13 ± 0.08	1.11 ± 0.04	0.31 ± 0.02
8.79	3.15	$4.02E-2$	15.98 ± 0.44	7.63 ± 0.20	3.78 ± 0.14	2.16 ± 0.10	1.12 ± 0.06	0.27 ± 0.02
8.77	7.06	$8.61E-2$	15.63 ± 0.62	7.25 ± 0.28	3.95 ± 0.21	2.17 ± 0.15	1.09 ± 0.08	0.25 ± 0.03
8.77	13.72	$1.54E-1$	14.96 ± 0.76	6.89 ± 0.36	3.82 ± 0.27	2.33 ± 0.23	1.01 ± 0.11	0.25 ± 0.04
8.83	32.08	$2.88E-1$	15.90 ± 1.10	6.09 ± 0.50	4.18 ± 0.49	2.47 ± 0.35	1.03 ± 0.16	0.27 ± 0.07
11.01	0.21	$1.76E-3$	16.60 ± 0.65	7.08 ± 0.32	3.59 ± 0.21	1.94 ± 0.15	1.21 ± 0.09	0.42 ± 0.04
10.99	0.33	$2.75E-3$	16.20 ± 0.40	7.42 ± 0.20	3.50 ± 0.12	2.24 ± 0.10	1.22 ± 0.06	0.37 ± 0.02
10.97	0.50	$4.17E-3$	16.63 ± 0.36	7.24 ± 0.18	3.76 ± 0.12	2.34 ± 0.10	1.14 ± 0.05	0.35 ± 0.02
10.99	0.69	$5.80E-3$	17.40 ± 0.46	7.43 ± 0.22	3.58 ± 0.14	2.24 ± 0.11	1.11 ± 0.06	0.32 ± 0.02
10.98	0.89	$7.46E-3$	16.54 ± 0.51	7.48 ± 0.26	3.80 ± 0.17	2.24 ± 0.13	1.20 ± 0.08	0.32 ± 0.03
10.97	1.39	$1.16E-2$	17.12 ± 0.38	7.92 ± 0.19	3.79 ± 0.13	2.18 ± 0.09	1.05 ± 0.05	0.27 ± 0.02
11.00	3.15	$2.57E-2$	18.12 ± 0.46	7.55 ± 0.23	4.03 ± 0.16	2.07 ± 0.11	1.02 ± 0.06	0.23 ± 0.02
10.97	7.01	$5.58E-2$	17.15 ± 0.61	7.60 ± 0.32	3.90 ± 0.22	1.92 ± 0.15	1.09 ± 0.09	0.21 ± 0.03
10.99	13.75	$1.03E-1$	18.74 ± 0.87	7.58 ± 0.44	3.90 ± 0.30	2.26 ± 0.24	0.92 ± 0.10	0.19 ± 0.04
10.97	33.92	$2.16E-1$	16.55 ± 1.03	7.99 ± 0.63	3.66 ± 0.42	2.22 ± 0.43	1.09 ± 0.17	0.20 ± 0.05
12.99	0.21	$1.26E-3$	17.97 ± 0.66	6.98 ± 0.31	3.74 ± 0.21	1.97 ± 0.16	1.36 ± 0.10	0.41 ± 0.04
13.01	0.33	$1.95E-3$	17.87 ± 0.41	7.63 ± 0.21	3.59 ± 0.13	2.48 ± 0.11	1.13 ± 0.06	0.35 ± 0.02
12.99	0.50	$2.96E-3$	18.06 ± 0.39	7.76 ± 0.20	3.65 ± 0.12	2.22 ± 0.10	1.15 ± 0.06	0.32 ± 0.02
12.98	0.70	$4.16E-3$	18.72 ± 0.48	7.70 ± 0.24	3.57 ± 0.15	2.26 ± 0.12	1.08 ± 0.07	0.31 ± 0.02
12.95	0.89	$5.36E-3$	18.39 ± 0.57	8.01 ± 0.31	3.87 ± 0.19	2.21 ± 0.15	1.07 ± 0.07	0.33 ± 0.03
12.98	1.40	$8.33E-3$	19.19 ± 0.38	7.64 ± 0.20	3.87 ± 0.13	2.18 ± 0.10	1.07 ± 0.05	0.26 ± 0.02
12.99	3.15	$1.85E-2$	19.25 ± 0.45	8.11 ± 0.23	4.01 ± 0.15	2.04 ± 0.11	0.93 ± 0.05	0.22 ± 0.02
12.99	7.06	$4.05E-2$	19.29 ± 0.62	8.27 ± 0.35	4.01 ± 0.23	2.14 ± 0.17	0.96 ± 0.08	0.17 ± 0.02
12.98	13.78	$7.61E-2$	20.60 ± 0.93	7.34 ± 0.42	4.10 ± 0.34	2.35 ± 0.26	1.01 ± 0.12	0.13 ± 0.03
13.00	35.65	$1.71E-1$	18.85 ± 1.07	8.11 ± 0.60	3.87 ± 0.41	1.86 ± 0.27	0.77 ± 0.14	0.19 ± 0.06
15.01	0.21	$9.21E-4$	18.99 ± 0.61	6.88 ± 0.28	3.86 ± 0.21	2.17 ± 0.15	1.18 ± 0.09	0.36 ± 0.03
14.98	0.32	$1.45E-3$	19.59 ± 0.43	7.67 ± 0.21	3.67 ± 0.14	2.15 ± 0.11	1.18 ± 0.06	0.35 ± 0.02
14.98	0.49	$2.22E-3$	20.50 ± 0.42	7.29 ± 0.19	3.83 ± 0.14	2.16 ± 0.10	1.14 ± 0.06	0.31 ± 0.02
14.98	0.69	$3.10E-3$	20.12 ± 0.52	7.44 ± 0.24	3.83 ± 0.17	2.11 ± 0.13	1.09 ± 0.07	0.31 ± 0.03
14.98	0.89	$3.99E-3$	20.43 ± 0.60	7.42 ± 0.29	4.03 ± 0.20	2.12 ± 0.16	0.91 ± 0.07	0.29 ± 0.03
14.99	1.41	$6.28E-3$	21.15 ± 0.41	8.18 ± 0.20	3.66 ± 0.13	2.24 ± 0.11	1.03 ± 0.05	0.26 ± 0.02
14.99	3.13	$1.38E-2$	21.90 ± 0.46	8.12 ± 0.23	3.73 ± 0.15	2.35 ± 0.12	0.90 ± 0.06	0.20 ± 0.02
15.02	7.05	$3.05E-2$	21.87 ± 0.71	8.48 ± 0.35	3.91 ± 0.23	1.98 ± 0.16	0.92 ± 0.09	0.14 ± 0.02
15.05	13.78	$5.77E-2$	22.33 ± 0.96	8.74 ± 0.55	4.41 ± 0.35	1.96 ± 0.24	0.82 ± 0.10	0.15 ± 0.03
14.95	35.53	$1.35E-1$	22.19 ± 1.22	8.66 ± 0.61	4.19 ± 0.43	1.91 ± 0.28	0.66 ± 0.13	0.11 ± 0.03
17.02	0.21	$7.15E-4$	20.37 ± 0.59	6.99 ± 0.27	3.33 ± 0.18	2.07 ± 0.14	1.28 ± 0.10	0.35 ± 0.03
16.98	0.32	$1.13E-3$	20.96 ± 0.46	7.41 ± 0.21	4.01 ± 0.15	2.15 ± 0.12	1.22 ± 0.07	0.37 ± 0.02
16.97	0.49	$1.72E-3$	21.28 ± 0.45	7.94 ± 0.22	3.71 ± 0.15	2.21 ± 0.12	1.12 ± 0.06	0.31 ± 0.02
16.96	0.70	$2.43E-3$	20.85 ± 0.53	8.13 ± 0.27	3.97 ± 0.19	2.08 ± 0.14	1.13 ± 0.08	0.33 ± 0.03
17.00	0.90	$3.12E-3$	21.67 ± 0.64	8.28 ± 0.32	3.62 ± 0.23	2.21 ± 0.17	1.11 ± 0.10	0.32 ± 0.03
17.00	1.42	$4.92E-3$	22.51 ± 0.42	8.18 ± 0.21	4.09 ± 0.15	2.21 ± 0.12	1.04 ± 0.06	0.25 ± 0.02
16.99	3.11	$1.07E-2$	23.09 ± 0.48	8.50 ± 0.24	3.98 ± 0.16	2.26 ± 0.13	0.91 ± 0.06	0.23 ± 0.02
16.96	6.96	$2.38E-2$	24.48 ± 0.76	8.43 ± 0.36	4.24 ± 0.27	2.30 ± 0.21	1.00 ± 0.09	0.17 ± 0.03
17.02	13.71	$4.54E-2$	24.19 ± 1.02	8.42 ± 0.53	3.79 ± 0.35	2.19 ± 0.27	0.81 ± 0.14	0.17 ± 0.04
16.96	38.85	$1.17E-1$	21.89 ± 1.15	8.09 ± 0.62	4.24 ± 0.44	1.74 ± 0.29	0.76 ± 0.15	0.14 ± 0.04

Table 6. (continued) Normalized inclusive single-particle distributions $D(x_F)$ of charged hadrons in different intervals of W (GeV) and Q^2 (GeV^2) (Fig. 7). Corresponding average values of x_{Bj} are given as well.

$< W >$	$< Q^2 >$	$< x_{Bj} >$	$0 < x_F < 0.1$	$0.1 < x_F < 0.2$	$0.2 < x_F < 0.3$	$0.3 < x_F < 0.4$	$0.4 < x_F < 0.6$	$0.6 < x_F < 1$
19.01	0.20	$5.64E-4$	22.04 ± 0.58	7.49 ± 0.28	4.12 ± 0.21	2.13 ± 0.15	1.19 ± 0.09	0.36 ± 0.03
18.97	0.32	$9.03E-4$	22.52 ± 0.49	7.73 ± 0.23	3.69 ± 0.16	2.08 ± 0.12	1.15 ± 0.07	0.39 ± 0.03
18.96	0.49	$1.37E-3$	22.70 ± 0.49	7.86 ± 0.24	3.99 ± 0.17	2.08 ± 0.13	1.07 ± 0.07	0.32 ± 0.03
18.97	0.70	$1.94E-3$	22.84 ± 0.60	7.75 ± 0.29	3.91 ± 0.21	2.21 ± 0.16	1.08 ± 0.08	0.33 ± 0.03
18.96	0.90	$2.50E-3$	23.10 ± 0.75	8.64 ± 0.38	4.16 ± 0.26	2.07 ± 0.19	0.99 ± 0.10	0.27 ± 0.03
18.98	1.43	$3.96E-3$	23.86 ± 0.48	8.30 ± 0.24	4.10 ± 0.16	2.52 ± 0.13	1.05 ± 0.06	0.26 ± 0.02
18.96	3.14	$8.70E-3$	24.96 ± 0.52	8.72 ± 0.26	4.33 ± 0.19	2.07 ± 0.13	1.01 ± 0.07	0.21 ± 0.02
18.97	6.96	$1.91E-2$	25.36 ± 0.83	8.61 ± 0.41	3.93 ± 0.27	2.16 ± 0.21	0.90 ± 0.10	0.16 ± 0.03
18.97	13.75	$3.69E-2$	25.78 ± 1.11	8.87 ± 0.54	4.22 ± 0.38	2.17 ± 0.32	0.89 ± 0.13	0.13 ± 0.04
18.99	35.80	$8.92E-2$	24.88 ± 1.30	8.61 ± 0.73	4.53 ± 0.51	2.42 ± 0.40	0.75 ± 0.16	0.17 ± 0.05
21.02	0.20	$4.59E-4$	24.60 ± 0.59	7.54 ± 0.26	3.59 ± 0.18	2.27 ± 0.16	1.02 ± 0.08	0.39 ± 0.04
21.00	0.32	$7.30E-4$	24.42 ± 0.53	7.60 ± 0.24	3.59 ± 0.16	2.07 ± 0.13	1.09 ± 0.07	0.35 ± 0.03
20.97	0.49	$1.13E-3$	23.39 ± 0.54	8.12 ± 0.27	3.92 ± 0.19	2.16 ± 0.14	1.06 ± 0.07	0.36 ± 0.03
20.95	0.70	$1.59E-3$	23.17 ± 0.69	7.75 ± 0.32	3.82 ± 0.23	2.10 ± 0.17	1.16 ± 0.11	0.32 ± 0.03
20.97	0.89	$2.04E-3$	24.38 ± 0.82	7.89 ± 0.41	3.93 ± 0.27	2.37 ± 0.23	1.10 ± 0.12	0.28 ± 0.04
20.98	1.42	$3.23E-3$	25.36 ± 0.52	8.52 ± 0.26	4.08 ± 0.18	2.22 ± 0.14	1.04 ± 0.07	0.26 ± 0.02
20.97	3.13	$7.09E-3$	26.73 ± 0.60	8.99 ± 0.30	4.12 ± 0.21	2.32 ± 0.15	0.93 ± 0.07	0.20 ± 0.02
21.01	6.97	$1.56E-2$	28.72 ± 0.97	9.16 ± 0.48	3.90 ± 0.30	2.23 ± 0.25	0.91 ± 0.11	0.19 ± 0.03
20.99	13.94	$3.08E-2$	27.29 ± 1.25	9.52 ± 0.67	4.41 ± 0.47	2.29 ± 0.34	1.13 ± 0.17	0.13 ± 0.03
20.95	37.33	$7.75E-2$	30.08 ± 1.62	10.50 ± 0.87	3.18 ± 0.41	2.24 ± 0.41	0.92 ± 0.19	0.03 ± 0.02
23.44	0.20	$3.68E-4$	26.25 ± 0.52	7.99 ± 0.24	3.86 ± 0.17	2.25 ± 0.14	1.10 ± 0.07	0.37 ± 0.03
23.43	0.32	$5.88E-4$	24.48 ± 0.46	7.65 ± 0.22	3.57 ± 0.15	1.92 ± 0.11	1.13 ± 0.07	0.42 ± 0.03
23.38	0.49	$9.06E-4$	25.39 ± 0.54	7.65 ± 0.24	3.66 ± 0.17	2.11 ± 0.14	1.18 ± 0.08	0.38 ± 0.03
23.45	0.69	$1.27E-3$	26.33 ± 0.66	8.18 ± 0.31	3.57 ± 0.20	2.23 ± 0.18	1.15 ± 0.10	0.30 ± 0.03
23.43	0.89	$1.63E-3$	26.15 ± 0.80	8.24 ± 0.38	3.68 ± 0.26	2.25 ± 0.21	1.20 ± 0.13	0.31 ± 0.04
23.39	1.41	$2.59E-3$	26.33 ± 0.50	8.41 ± 0.24	3.90 ± 0.17	2.38 ± 0.14	1.06 ± 0.07	0.26 ± 0.02
23.42	3.11	$5.67E-3$	28.63 ± 0.58	9.03 ± 0.29	4.30 ± 0.20	2.49 ± 0.16	1.02 ± 0.07	0.17 ± 0.02
23.43	6.95	$1.26E-2$	30.56 ± 0.95	9.37 ± 0.49	4.39 ± 0.32	2.10 ± 0.22	1.02 ± 0.12	0.13 ± 0.03
23.41	13.96	$2.50E-2$	30.01 ± 1.23	9.38 ± 0.63	4.60 ± 0.44	2.25 ± 0.32	0.79 ± 0.13	0.13 ± 0.03
23.35	37.51	$6.39E-2$	32.68 ± 1.64	11.31 ± 0.93	4.89 ± 0.62	2.74 ± 0.42	0.92 ± 0.18	0.04 ± 0.02
26.07	0.20	$2.95E-4$	27.15 ± 0.83	7.61 ± 0.37	3.57 ± 0.26	2.01 ± 0.20	1.00 ± 0.11	0.40 ± 0.05
26.11	0.32	$4.72E-4$	26.85 ± 0.76	7.92 ± 0.36	3.53 ± 0.24	1.88 ± 0.18	1.23 ± 0.13	0.37 ± 0.05
26.17	0.49	$7.22E-4$	25.31 ± 0.80	7.53 ± 0.37	3.42 ± 0.26	1.97 ± 0.21	1.06 ± 0.13	0.36 ± 0.05
26.17	0.70	$1.02E-3$	26.59 ± 1.06	7.67 ± 0.48	2.93 ± 0.28	2.18 ± 0.28	1.16 ± 0.17	0.38 ± 0.06
26.12	0.89	$1.31E-3$	26.35 ± 1.30	8.50 ± 0.63	3.56 ± 0.40	2.04 ± 0.33	1.19 ± 0.18	0.38 ± 0.08
26.16	1.41	$2.07E-3$	27.75 ± 0.78	8.53 ± 0.39	3.68 ± 0.27	2.52 ± 0.25	1.05 ± 0.12	0.26 ± 0.03
26.12	3.13	$4.58E-3$	30.05 ± 0.94	9.08 ± 0.47	4.23 ± 0.31	2.00 ± 0.22	0.91 ± 0.11	0.21 ± 0.03
26.17	6.96	$1.01E-2$	31.98 ± 1.37	10.19 ± 0.80	4.26 ± 0.49	2.36 ± 0.44	1.03 ± 0.21	0.16 ± 0.04
26.14	13.68	$1.97E-2$	33.12 ± 2.22	10.63 ± 1.22	4.33 ± 0.72	2.31 ± 0.67	0.92 ± 0.24	0.12 ± 0.05
26.05	34.79	$4.86E-2$	38.15 ± 3.28	12.87 ± 2.14	4.24 ± 1.01	1.67 ± 0.62	1.36 ± 0.45	0.07 ± 0.04

Table 7. Normalized inclusive single-particle distributions $D(p_t^2, x_F)$ of charged hadrons in different intervals of W (GeV) (Fig. 10, left). $\langle p_t^2 \rangle$ is given in GeV^2.

$\langle p_t^2 \rangle$	$0.0 < x_F < 0.1$	$0.1 < x_F < 0.2$	$0.2 < x_F < 0.3$	$0.3 < x_F < 0.4$	$0.4 < x_F < 0.6$	$0.6 < x_F < 1.0$
$7.5 < W < 10.0$ GeV						
$1.74E-3$	$(2.01 \pm 0.21)E+2$	$(3.37 \pm 0.48)E+1$	$(1.75 \pm 0.35)E+1$		$(5.39 \pm 1.35)E+0$	
$2.34E-3$	$(1.94 \pm 0.15)E+2$	$(4.69 \pm 0.45)E+1$	$(2.05 \pm 0.33)E+1$	$(7.71 \pm 1.66)E+0$	$(3.10 \pm 0.80)E+0$	$(1.47 \pm 0.40)E+0$
$4.49E-3$	$(1.73 \pm 0.11)E+2$	$(4.57 \pm 0.33)E+1$	$(1.67 \pm 0.19)E+1$	$(9.67 \pm 1.34)E+0$	$(3.65 \pm 0.59)E+0$	$(1.27 \pm 0.28)E+0$
$1.03E-2$	$(1.57 \pm 0.07)E+2$	$(4.53 \pm 0.25)E+1$	$(1.54 \pm 0.13)E+1$	$(7.59 \pm 0.84)E+0$	$(4.20 \pm 0.50)E+0$	$(1.56 \pm 0.22)E+0$
$1.75E-2$	$(1.34 \pm 0.05)E+2$	$(4.41 \pm 0.19)E+1$	$(1.57 \pm 0.10)E+1$	$(6.90 \pm 0.59)E+0$	$(4.10 \pm 0.38)E+0$	$(1.57 \pm 0.17)E+0$
$3.33E-2$	$(1.15 \pm 0.03)E+2$	$(3.94 \pm 0.13)E+1$	$(1.55 \pm 0.07)E+1$	$(7.35 \pm 0.49)E+0$	$(3.70 \pm 0.24)E+0$	$(1.34 \pm 0.12)E+0$
$5.63E-2$	$(7.71 \pm 0.19)E+1$	$(3.46 \pm 0.09)E+1$	$(1.38 \pm 0.05)E+1$	$(6.98 \pm 0.34)E+0$	$(3.40 \pm 0.17)E+0$	$(1.13 \pm 0.08)E+0$
$1.06E-1$	$(4.21 \pm 0.10)E+1$	$(2.27 \pm 0.05)E+1$	$(1.16 \pm 0.03)E+1$	$(5.83 \pm 0.24)E+0$	$(2.93 \pm 0.12)E+0$	$(8.40 \pm 0.48)E-1$
$2.01E-1$	$(1.85 \pm 0.04)E+1$	$(1.15 \pm 0.03)E+1$	$(7.14 \pm 0.20)E+0$	$(4.41 \pm 0.15)E+0$	$(2.16 \pm 0.08)E+0$	$(5.55 \pm 0.27)E-1$
$3.88E-1$	$(5.40 \pm 0.16)E+0$	$(4.19 \pm 0.11)E+0$	$(3.19 \pm 0.10)E+0$	$(2.23 \pm 0.08)E+0$	$(1.16 \pm 0.04)E+0$	$(2.84 \pm 0.14)E-1$
$5.94E-1$	$(1.07 \pm 0.05)E+0$	$(1.02 \pm 0.04)E+0$	$(8.56 \pm 0.37)E-1$	$(6.79 \pm 0.35)E-1$	$(4.11 \pm 0.20)E-1$	$(1.09 \pm 0.07)E-1$
$9.53E-1$	$(1.35 \pm 0.13)E-1$	$(1.44 \pm 0.12)E-1$	$(1.47 \pm 0.11)E-1$	$(1.12 \pm 0.09)E-1$	$(8.31 \pm 0.67)E-2$	$(2.98 \pm 0.31)E-2$
$2.82E+0$	$(1.29 \pm 0.30)E-2$	$(1.52 \pm 0.38)E-2$	$(1.23 \pm 0.22)E-2$	$(1.20 \pm 0.26)E-2$	$(9.32 \pm 1.49)E-3$	
$2.99E+0$						$(2.78 \pm 0.72)E-4$
$10.0 < W < 12.5$ GeV						
$1.42E-3$	$(1.95 \pm 0.18)E+2$	$(3.54 \pm 0.51)E+1$	$(1.35 \pm 0.33)E+1$			
$2.63E-3$	$(2.21 \pm 0.14)E+2$	$(3.77 \pm 0.41)E+1$	$(1.72 \pm 0.23)E+1$	$(6.46 \pm 1.40)E+0$	$(2.95 \pm 0.76)E+0$	
$4.94E-3$	$(1.95 \pm 0.10)E+2$	$(4.15 \pm 0.34)E+1$	$(1.32 \pm 0.15)E+1$	$(8.23 \pm 1.26)E+0$	$(4.04 \pm 0.67)E+0$	$(1.29 \pm 0.27)E+0$
$9.62E-3$	$(1.98 \pm 0.07)E+2$	$(4.06 \pm 0.23)E+1$	$(1.55 \pm 0.13)E+1$	$(7.58 \pm 0.94)E+0$	$(3.54 \pm 0.46)E+0$	$(1.43 \pm 0.24)E+0$
$1.27E-2$	$(1.62 \pm 0.05)E+2$	$(4.06 \pm 0.18)E+1$	$(1.49 \pm 0.10)E+1$	$(8.20 \pm 0.70)E+0$	$(3.19 \pm 0.30)E+0$	$(1.30 \pm 0.15)E+0$
$3.28E-2$	$(1.32 \pm 0.03)E+2$	$(3.80 \pm 0.12)E+1$	$(1.54 \pm 0.07)E+1$	$(7.30 \pm 0.49)E+0$	$(3.38 \pm 0.24)E+0$	$(1.17 \pm 0.11)E+0$
$5.01E-2$	$(8.73 \pm 0.18)E+1$	$(3.42 \pm 0.09)E+1$	$(1.31 \pm 0.05)E+1$	$(6.64 \pm 0.34)E+0$	$(3.15 \pm 0.17)E+0$	$(1.01 \pm 0.07)E+0$
$1.07E-1$	$(4.90 \pm 0.09)E+1$	$(2.40 \pm 0.05)E+1$	$(1.05 \pm 0.03)E+1$	$(5.67 \pm 0.23)E+0$	$(2.79 \pm 0.12)E+0$	$(7.71 \pm 0.46)E-1$
$1.87E-1$	$(2.03 \pm 0.04)E+1$	$(1.29 \pm 0.03)E+1$	$(6.75 \pm 0.19)E+0$	$(3.91 \pm 0.14)E+0$	$(1.99 \pm 0.08)E+0$	$(4.79 \pm 0.26)E-1$
$3.38E-1$	$(6.39 \pm 0.16)E+0$	$(5.10 \pm 0.13)E+0$	$(3.00 \pm 0.09)E+0$	$(2.07 \pm 0.08)E+0$	$(1.06 \pm 0.04)E+0$	$(2.63 \pm 0.15)E-1$
$4.68E-1$	$(1.42 \pm 0.05)E+0$	$(1.35 \pm 0.05)E+0$	$(9.80 \pm 0.40)E-1$	$(6.37 \pm 0.31)E-1$	$(4.06 \pm 0.19)E-1$	$(1.01 \pm 0.07)E-1$
$1.20E+0$	$(2.07 \pm 0.14)E-1$	$(2.10 \pm 0.14)E-1$	$(1.96 \pm 0.15)E-1$	$(1.45 \pm 0.13)E-1$	$(9.19 \pm 0.76)E-2$	$(2.57 \pm 0.27)E-2$
$2.26E+0$	$(2.90 \pm 0.56)E-2$	$(2.13 \pm 0.32)E-2$	$(2.39 \pm 0.41)E-2$	$(1.88 \pm 0.38)E-2$	$(1.24 \pm 0.22)E-2$	
$12.5 < W < 15.0$ GeV						
$1.42E-3$	$(2.43 \pm 0.20)E+2$	$(4.04 \pm 0.56)E+1$	$(1.73 \pm 0.40)E+1$			
$2.63E-3$	$(2.57 \pm 0.16)E+2$	$(4.07 \pm 0.41)E+1$	$(1.57 \pm 0.24)E+1$	$(4.84 \pm 1.25)E+0$	$(2.42 \pm 0.64)E+0$	
$4.53E-3$	$(2.33 \pm 0.11)E+2$	$(3.91 \pm 0.30)E+1$	$(1.52 \pm 0.19)E+1$	$(6.87 \pm 1.17)E+0$	$(2.69 \pm 0.60)E+0$	$(1.20 \pm 0.28)E+0$
$8.98E-3$	$(2.17 \pm 0.08)E+2$	$(4.15 \pm 0.24)E+1$	$(1.49 \pm 0.14)E+1$	$(7.68 \pm 0.98)E+0$	$(3.15 \pm 0.44)E+0$	$(9.69 \pm 1.83)E-1$
$1.66E-2$	$(1.78 \pm 0.05)E+2$	$(3.73 \pm 0.17)E+1$	$(1.51 \pm 0.10)E+1$	$(7.17 \pm 0.72)E+0$	$(3.61 \pm 0.36)E+0$	$(1.25 \pm 0.16)E+0$
$3.87E-2$	$(1.37 \pm 0.03)E+2$	$(3.85 \pm 0.13)E+1$	$(1.34 \pm 0.07)E+1$	$(7.76 \pm 0.56)E+0$	$(3.02 \pm 0.26)E+0$	$(1.13 \pm 0.12)E+0$
$5.82E-2$	$(1.00 \pm 0.02)E+2$	$(3.28 \pm 0.08)E+1$	$(1.30 \pm 0.05)E+1$	$(6.39 \pm 0.37)E+0$	$(3.05 \pm 0.18)E+0$	$(8.88 \pm 0.70)E-1$
$8.67E-2$	$(5.44 \pm 0.10)E+1$	$(2.37 \pm 0.05)E+1$	$(1.06 \pm 0.03)E+1$	$(5.57 \pm 0.25)E+0$	$(2.46 \pm 0.12)E+0$	$(7.64 \pm 0.49)E-1$
$1.81E-1$	$(2.36 \pm 0.04)E+1$	$(1.33 \pm 0.03)E+1$	$(6.87 \pm 0.19)E+0$	$(3.93 \pm 0.16)E+0$	$(1.84 \pm 0.08)E+0$	$(4.41 \pm 0.26)E-1$
$3.04E-1$	$(7.61 \pm 0.17)E+0$	$(5.41 \pm 0.14)E+0$	$(3.11 \pm 0.10)E+0$	$(2.04 \pm 0.08)E+0$	$(1.01 \pm 0.04)E+0$	$(2.47 \pm 0.15)E-1$
$6.05E-1$	$(1.71 \pm 0.06)E+0$	$(1.47 \pm 0.05)E+0$	$(1.00 \pm 0.04)E+0$	$(6.82 \pm 0.36)E-1$	$(4.15 \pm 0.21)E-1$	$(9.93 \pm 0.73)E-2$
$1.09E+0$	$(2.57 \pm 0.16)E-1$	$(2.72 \pm 0.18)E-1$	$(1.97 \pm 0.14)E-1$	$(1.44 \pm 0.12)E-1$	$(1.04 \pm 0.08)E-1$	$(2.94 \pm 0.35)E-2$
$2.02E+0$	$(3.26 \pm 0.45)E-2$	$(2.91 \pm 0.39)E-2$	$(2.43 \pm 0.41)E-2$	$(2.15 \pm 0.40)E-2$	$(1.47 \pm 0.26)E-2$	
$4.17E+0$		$(2.36 \pm 0.61)E-3$	$(1.98 \pm 0.59)E-3$			

Table 7. (continued) Normalized inclusive single-particle distributions $D(p_t^2, x_F)$ of charged hadrons in different intervals of W (GeV) (Fig. 10, left). $\langle p_t^2 \rangle$ is given in GeV^2.

$\langle p_t^2 \rangle$	$0 < x_F < 0.1$	$0.1 < x_F < 0.2$	$0.2 < x_F < 0.3$	$0.3 < x_F < 0.4$	$0.4 < x_F < 0.6$	$0.6 < x_F < 1$
$15.0 < W < 17.5$ GeV						
$1.42E-3$	$(2.83 \pm 0.22)E+2$	$(4.09 \pm 0.59)E+1$	$(1.68 \pm 0.35)E+1$			
$2.63E-3$	$(2.82 \pm 0.16)E+2$	$(4.42 \pm 0.44)E+1$	$(1.55 \pm 0.28)E+1$	$(6.94 \pm 1.67)E+0$	$(4.21 \pm 1.12)E+0$	$(1.36 \pm 0.38)E+0$
$4.47E-3$	$(2.53 \pm 0.11)E+2$	$(3.73 \pm 0.32)E+1$	$(1.50 \pm 0.19)E+1$	$(8.53 \pm 1.61)E+0$	$(2.83 \pm 0.55)E+0$	$(1.29 \pm 0.38)E+0$
$8.98E-3$	$(2.29 \pm 0.08)E+2$	$(3.83 \pm 0.23)E+1$	$(1.24 \pm 0.12)E+1$	$(6.91 \pm 0.94)E+0$	$(2.63 \pm 0.46)E+0$	$(1.18 \pm 0.22)E+0$
$1.43E-2$	$(1.93 \pm 0.05)E+2$	$(3.87 \pm 0.17)E+1$	$(1.34 \pm 0.09)E+1$	$(6.40 \pm 0.68)E+0$	$(3.13 \pm 0.35)E+0$	$(1.09 \pm 0.16)E+0$
$3.67E-2$	$(1.57 \pm 0.03)E+2$	$(3.64 \pm 0.12)E+1$	$(1.39 \pm 0.08)E+1$	$(6.75 \pm 0.55)E+0$	$(3.23 \pm 0.28)E+0$	$(9.28 \pm 1.01)E-1$
$4.77E-2$	$(1.09 \pm 0.02)E+2$	$(3.13 \pm 0.08)E+1$	$(1.26 \pm 0.05)E+1$	$(6.24 \pm 0.37)E+0$	$(2.96 \pm 0.19)E+0$	$(8.49 \pm 0.71)E-1$
$9.88E-2$	$(6.04 \pm 0.10)E+1$	$(2.41 \pm 0.05)E+1$	$(1.05 \pm 0.03)E+1$	$(5.63 \pm 0.27)E+0$	$(2.29 \pm 0.13)E+0$	$(6.96 \pm 0.49)E-1$
$1.88E-1$	$(2.63 \pm 0.05)E+1$	$(1.35 \pm 0.03)E+1$	$(6.86 \pm 0.21)E+0$	$(3.76 \pm 0.16)E+0$	$(1.77 \pm 0.08)E+0$	$(5.10 \pm 0.31)E-1$
$3.60E-1$	$(8.86 \pm 0.18)E+0$	$(5.62 \pm 0.14)E+0$	$(3.33 \pm 0.11)E+0$	$(1.85 \pm 0.08)E+0$	$(9.49 \pm 0.44)E-1$	$(2.51 \pm 0.16)E-1$
$4.75E-1$	$(2.12 \pm 0.07)E+0$	$(1.58 \pm 0.05)E+0$	$(1.11 \pm 0.05)E+0$	$(8.18 \pm 0.43)E-1$	$(4.17 \pm 0.22)E-1$	$(1.10 \pm 0.09)E-1$
$9.81E-1$	$(3.34 \pm 0.20)E-1$	$(2.87 \pm 0.18)E-1$	$(2.59 \pm 0.17)E-1$	$(1.77 \pm 0.15)E-1$	$(1.06 \pm 0.09)E-1$	$(2.67 \pm 0.30)E-2$
$2.26E+0$	$(4.50 \pm 0.57)E-2$	$(4.53 \pm 0.55)E-2$	$(3.67 \pm 0.61)E-2$	$(2.52 \pm 0.45)E-2$	$(1.72 \pm 0.42)E-2$	$(3.41 \pm 0.88)E-3$
$4.17E+0$	$(2.69 \pm 0.63)E-3$	$(2.55 \pm 0.76)E-3$				
$17.5 < W < 20.0$ GeV						
$1.46E-3$	$(2.70 \pm 0.21)E+2$	$(3.40 \pm 0.55)E+1$	$(1.44 \pm 0.39)E+1$			
$2.22E-3$	$(3.13 \pm 0.18)E+2$	$(3.57 \pm 0.41)E+1$	$(1.59 \pm 0.32)E+1$			
$4.86E-3$	$(2.77 \pm 0.12)E+2$	$(3.91 \pm 0.34)E+1$	$(1.37 \pm 0.22)E+1$	$(9.42 \pm 1.74)E+0$	$(3.23 \pm 0.77)E+0$	$(7.39 \pm 1.94)E-1$
$8.67E-3$	$(2.58 \pm 0.09)E+2$	$(4.05 \pm 0.26)E+1$	$(1.48 \pm 0.15)E+1$	$(7.82 \pm 1.22)E+0$	$(3.80 \pm 0.59)E+0$	$(8.40 \pm 1.88)E-1$
$1.71E-2$	$(2.03 \pm 0.06)E+2$	$(3.82 \pm 0.19)E+1$	$(1.42 \pm 0.11)E+1$	$(7.39 \pm 0.90)E+0$	$(3.46 \pm 0.40)E+0$	$(7.83 \pm 1.26)E-1$
$2.58E-2$	$(1.62 \pm 0.04)E+2$	$(3.61 \pm 0.13)E+1$	$(1.49 \pm 0.09)E+1$	$(7.51 \pm 0.65)E+0$	$(2.84 \pm 0.27)E+0$	$(1.12 \pm 0.13)E+0$
$5.32E-2$	$(1.12 \pm 0.02)E+2$	$(3.24 \pm 0.09)E+1$	$(1.25 \pm 0.06)E+1$	$(6.32 \pm 0.43)E+0$	$(2.68 \pm 0.20)E+0$	$(9.16 \pm 0.87)E-1$
$1.04E-1$	$(6.22 \pm 0.11)E+1$	$(2.40 \pm 0.06)E+1$	$(1.04 \pm 0.04)E+1$	$(5.22 \pm 0.28)E+0$	$(2.51 \pm 0.15)E+0$	$(6.74 \pm 0.51)E-1$
$1.63E-1$	$(2.81 \pm 0.05)E+1$	$(1.38 \pm 0.03)E+1$	$(7.08 \pm 0.23)E+0$	$(3.56 \pm 0.17)E+0$	$(1.79 \pm 0.09)E+0$	$(4.63 \pm 0.34)E-1$
$4.14E-1$	$(1.00 \pm 0.02)E+1$	$(6.09 \pm 0.16)E+0$	$(3.55 \pm 0.12)E+0$	$(2.00 \pm 0.09)E+0$	$(1.06 \pm 0.05)E+0$	$(2.71 \pm 0.19)E-1$
$6.05E-1$	$(2.48 \pm 0.08)E+0$	$(1.62 \pm 0.06)E+0$	$(1.24 \pm 0.06)E+0$	$(7.62 \pm 0.45)E-1$	$(4.07 \pm 0.25)E-1$	$(9.88 \pm 0.80)E-2$
$1.22E+0$	$(4.52 \pm 0.26)E-1$	$(3.28 \pm 0.20)E-1$	$(2.77 \pm 0.21)E-1$	$(2.03 \pm 0.17)E-1$	$(1.03 \pm 0.10)E-1$	$(3.57 \pm 0.46)E-2$
$2.26E+0$	$(4.94 \pm 0.63)E-2$	$(4.93 \pm 0.68)E-2$	$(4.62 \pm 0.61)E-2$	$(2.97 \pm 0.67)E-2$	$(1.96 \pm 0.27)E-2$	
$4.17E+0$		$(3.97 \pm 1.12)E-3$				
$20.0 < W < 25.0$ GeV						
$1.17E-3$	$(3.13 \pm 0.19)E+2$	$(3.68 \pm 0.53)E+1$	$(1.13 \pm 0.28)E+1$			
$2.74E-3$	$(2.92 \pm 0.13)E+2$	$(3.86 \pm 0.39)E+1$	$(1.08 \pm 0.18)E+1$	$(4.30 \pm 1.09)E+0$	$(3.34 \pm 0.93)E+0$	$(1.38 \pm 0.40)E+0$
$4.77E-3$	$(2.98 \pm 0.10)E+2$	$(3.50 \pm 0.26)E+1$	$(1.23 \pm 0.16)E+1$	$(5.52 \pm 1.07)E+0$	$(2.65 \pm 0.48)E+0$	$(1.15 \pm 0.23)E+0$
$8.03E-3$	$(2.63 \pm 0.07)E+2$	$(3.70 \pm 0.20)E+1$	$(1.27 \pm 0.13)E+1$	$(6.60 \pm 0.90)E+0$	$(2.63 \pm 0.42)E+0$	$(1.33 \pm 0.21)E+0$
$1.58E-2$	$(2.15 \pm 0.05)E+2$	$(3.59 \pm 0.15)E+1$	$(1.28 \pm 0.09)E+1$	$(7.48 \pm 0.78)E+0$	$(2.63 \pm 0.31)E+0$	$(1.10 \pm 0.15)E+0$
$3.04E-2$	$(1.76 \pm 0.03)E+2$	$(3.58 \pm 0.11)E+1$	$(1.29 \pm 0.07)E+1$	$(6.43 \pm 0.51)E+0$	$(2.67 \pm 0.23)E+0$	$(1.14 \pm 0.11)E+0$
$5.09E-2$	$(1.25 \pm 0.02)E+2$	$(3.23 \pm 0.08)E+1$	$(1.26 \pm 0.05)E+1$	$(5.46 \pm 0.33)E+0$	$(2.31 \pm 0.16)E+0$	$(9.39 \pm 0.75)E-1$
$1.03E-1$	$(7.14 \pm 0.09)E+1$	$(2.46 \pm 0.05)E+1$	$(1.00 \pm 0.03)E+1$	$(5.06 \pm 0.23)E+0$	$(2.45 \pm 0.13)E+0$	$(6.35 \pm 0.45)E-1$
$1.71E-1$	$(3.21 \pm 0.04)E+1$	$(1.42 \pm 0.03)E+1$	$(6.61 \pm 0.18)E+0$	$(3.83 \pm 0.15)E+0$	$(1.67 \pm 0.07)E+0$	$(4.70 \pm 0.27)E-1$
$3.54E-1$	$(1.17 \pm 0.02)E+1$	$(6.18 \pm 0.13)E+0$	$(3.30 \pm 0.10)E+0$	$(1.99 \pm 0.08)E+0$	$(1.04 \pm 0.04)E+0$	$(2.47 \pm 0.14)E-1$
$5.32E-1$	$(3.08 \pm 0.07)E+0$	$(1.85 \pm 0.05)E+0$	$(1.15 \pm 0.04)E+0$	$(8.02 \pm 0.38)E-1$	$(4.04 \pm 0.21)E-1$	$(9.79 \pm 0.67)E-2$
$1.06E+0$	$(5.66 \pm 0.24)E-1$	$(3.80 \pm 0.18)E-1$	$(2.91 \pm 0.16)E-1$	$(2.05 \pm 0.15)E-1$	$(1.10 \pm 0.08)E-1$	$(2.95 \pm 0.31)E-2$
$2.10E+0$	$(7.03 \pm 0.74)E-2$	$(6.03 \pm 0.59)E-2$	$(5.04 \pm 0.78)E-2$	$(3.71 \pm 0.70)E-2$	$(2.22 \pm 0.32)E-2$	$(3.95 \pm 0.77)E-3$
$4.17E+0$	$(8.14 \pm 1.54)E-3$	$(6.47 \pm 1.24)E-3$	$(5.97 \pm 1.71)E-3$	$(7.15 \pm 1.90)E-3$		

Table 8. Normalized inclusive single-particle distributions $D(p_t^2, x_F)$ of charged hadrons in different intervals of Q^2 (GeV^2) (Fig. 10, right). $\langle p_t^2 \rangle$ is given in GeV^2.

$\langle p_t^2 \rangle$	$0.0 < x_F < 0.1$	$0.1 < x_F < 0.2$	$0.2 < x_F < 0.3$	$0.3 < x_F < 0.4$	$0.4 < x_F < 0.6$	$0.6 < x_F < 1.0$
$0.15 < Q^2 < 0.40\ \mathrm{GeV}^2$						
$1.46E-3$	$(2.27 \pm 0.14)E+2$	$(3.46 \pm 0.41)E+1$	$(1.41 \pm 0.31)E+1$	$(9.73 \pm 2.54)E+0$	$(3.17 \pm 0.84)E+0$	$(3.71 \pm 1.02)E+0$
$2.51E-3$	$(2.45 \pm 0.12)E+2$	$(4.16 \pm 0.35)E+1$	$(1.55 \pm 0.20)E+1$	$(6.21 \pm 1.24)E+0$	$(2.77 \pm 0.65)E+0$	$(2.67 \pm 0.58)E+0$
$4.69E-3$	$(2.27 \pm 0.08)E+2$	$(3.65 \pm 0.24)E+1$	$(1.51 \pm 0.15)E+1$	$(8.62 \pm 1.18)E+0$	$(3.20 \pm 0.49)E+0$	$(1.77 \pm 0.26)E+0$
$8.23E-3$	$(2.11 \pm 0.06)E+2$	$(3.69 \pm 0.18)E+1$	$(1.45 \pm 0.12)E+1$	$(7.77 \pm 0.83)E+0$	$(3.93 \pm 0.42)E+0$	$(1.94 \pm 0.25)E+0$
$1.58E-2$	$(1.71 \pm 0.04)E+2$	$(3.80 \pm 0.14)E+1$	$(1.45 \pm 0.08)E+1$	$(6.96 \pm 0.59)E+0$	$(4.29 \pm 0.34)E+0$	$(1.68 \pm 0.15)E+0$
$2.96E-2$	$(1.33 \pm 0.02)E+2$	$(3.51 \pm 0.09)E+1$	$(1.35 \pm 0.06)E+1$	$(6.84 \pm 0.42)E+0$	$(3.65 \pm 0.23)E+0$	$(1.65 \pm 0.12)E+0$
$5.50E-2$	$(9.42 \pm 0.14)E+1$	$(3.09 \pm 0.06)E+1$	$(1.26 \pm 0.04)E+1$	$(6.11 \pm 0.29)E+0$	$(3.27 \pm 0.16)E+0$	$(1.40 \pm 0.08)E+0$
$1.02E-1$	$(5.24 \pm 0.07)E+1$	$(2.26 \pm 0.04)E+1$	$(1.02 \pm 0.03)E+1$	$(5.65 \pm 0.21)E+0$	$(3.12 \pm 0.12)E+0$	$(9.90 \pm 0.47)E-1$
$1.86E-1$	$(2.30 \pm 0.03)E+1$	$(1.18 \pm 0.02)E+1$	$(6.61 \pm 0.16)E+0$	$(4.11 \pm 0.13)E+0$	$(2.09 \pm 0.07)E+0$	$(6.05 \pm 0.26)E-1$
$3.12E-1$	$(7.72 \pm 0.13)E+0$	$(5.01 \pm 0.10)E+0$	$(2.95 \pm 0.08)E+0$	$(2.00 \pm 0.07)E+0$	$(1.05 \pm 0.03)E+0$	$(2.96 \pm 0.13)E-1$
$6.18E-1$	$(1.89 \pm 0.05)E+0$	$(1.34 \pm 0.04)E+0$	$(9.44 \pm 0.32)E-1$	$(6.60 \pm 0.28)E-1$	$(4.00 \pm 0.17)E-1$	$(1.06 \pm 0.06)E-1$
$1.03E+0$	$(3.26 \pm 0.15)E-1$	$(2.43 \pm 0.12)E-1$	$(1.94 \pm 0.12)E-1$	$(1.42 \pm 0.10)E-1$	$(9.44 \pm 0.62)E-2$	$(2.80 \pm 0.26)E-2$
$2.26E+0$	$(3.85 \pm 0.49)E-2$	$(3.27 \pm 0.41)E-2$	$(2.67 \pm 0.36)E-2$	$(1.80 \pm 0.30)E-2$	$(1.54 \pm 0.30)E-2$	$(3.29 \pm 0.68)E-3$
$3.80E+0$	$(3.19 \pm 0.78)E-3$	$(2.72 \pm 0.56)E-3$				
$0.40 < Q^2 < 0.70\ \mathrm{GeV}^2$						
$1.42E-3$	$(2.48 \pm 0.17)E+2$	$(3.39 \pm 0.45)E+1$	$(1.46 \pm 0.27)E+1$	$(5.90 \pm 1.71)E+0$	$(5.19 \pm 1.31)E+0$	
$2.71E-3$	$(2.39 \pm 0.12)E+2$	$(3.93 \pm 0.34)E+1$	$(1.58 \pm 0.21)E+1$	$(6.39 \pm 1.24)E+0$	$(4.11 \pm 0.89)E+0$	$(1.87 \pm 0.42)E+0$
$3.59E-3$	$(2.34 \pm 0.09)E+2$	$(3.87 \pm 0.27)E+1$	$(1.42 \pm 0.15)E+1$	$(8.38 \pm 1.18)E+0$	$(4.21 \pm 0.61)E+0$	$(1.66 \pm 0.31)E+0$
$9.42E-3$	$(2.11 \pm 0.06)E+2$	$(3.88 \pm 0.20)E+1$	$(1.41 \pm 0.11)E+1$	$(7.22 \pm 0.81)E+0$	$(4.31 \pm 0.49)E+0$	$(1.73 \pm 0.22)E+0$
$1.70E-2$	$(1.74 \pm 0.04)E+2$	$(3.73 \pm 0.14)E+1$	$(1.53 \pm 0.09)E+1$	$(6.85 \pm 0.59)E+0$	$(3.88 \pm 0.32)E+0$	$(1.60 \pm 0.15)E+0$
$3.82E-2$	$(1.42 \pm 0.03)E+2$	$(3.78 \pm 0.11)E+1$	$(1.43 \pm 0.06)E+1$	$(7.74 \pm 0.46)E+0$	$(3.53 \pm 0.22)E+0$	$(1.36 \pm 0.10)E+0$
$5.00E-2$	$(9.58 \pm 0.15)E+1$	$(3.27 \pm 0.07)E+1$	$(1.31 \pm 0.04)E+1$	$(6.61 \pm 0.31)E+0$	$(3.15 \pm 0.15)E+0$	$(1.12 \pm 0.07)E+0$
$9.77E-2$	$(5.28 \pm 0.08)E+1$	$(2.27 \pm 0.04)E+1$	$(1.08 \pm 0.03)E+1$	$(5.46 \pm 0.21)E+0$	$(2.63 \pm 0.10)E+0$	$(8.42 \pm 0.42)E-1$
$2.02E-1$	$(2.36 \pm 0.04)E+1$	$(1.25 \pm 0.02)E+1$	$(6.71 \pm 0.16)E+0$	$(3.89 \pm 0.13)E+0$	$(2.00 \pm 0.07)E+0$	$(5.06 \pm 0.23)E-1$
$3.61E-1$	$(7.79 \pm 0.14)E+0$	$(5.27 \pm 0.11)E+0$	$(2.97 \pm 0.08)E+0$	$(2.05 \pm 0.07)E+0$	$(1.07 \pm 0.04)E+0$	$(2.86 \pm 0.13)E-1$
$5.62E-1$	$(1.86 \pm 0.05)E+0$	$(1.41 \pm 0.04)E+0$	$(1.00 \pm 0.03)E+0$	$(6.91 \pm 0.30)E-1$	$(3.97 \pm 0.17)E-1$	$(1.02 \pm 0.06)E-1$
$9.52E-1$	$(3.17 \pm 0.16)E-1$	$(2.53 \pm 0.14)E-1$	$(2.14 \pm 0.12)E-1$	$(1.55 \pm 0.12)E-1$	$(9.56 \pm 0.66)E-2$	$(2.67 \pm 0.26)E-2$
$2.10E+0$	$(3.48 \pm 0.52)E-2$	$(3.47 \pm 0.57)E-2$	$(3.01 \pm 0.53)E-2$	$(2.23 \pm 0.52)E-2$	$(1.39 \pm 0.24)E-2$	$(3.85 \pm 1.05)E-3$
$4.17E+0$	$(2.63 \pm 0.66)E-3$			$(3.71 \pm 1.09)E-3$		
$0.70 < Q^2 < 1.45\ \mathrm{GeV}^2$						
$1.42E-3$	$(2.47 \pm 0.17)E+2$	$(4.88 \pm 0.56)E+1$	$(2.03 \pm 0.35)E+1$	$(6.63 \pm 1.76)E+0$	$(2.57 \pm 0.69)E+0$	
$2.63E-3$	$(2.57 \pm 0.12)E+2$	$(4.60 \pm 0.40)E+1$	$(2.02 \pm 0.25)E+1$	$(5.86 \pm 1.19)E+0$	$(3.29 \pm 0.76)E+0$	
$4.92E-3$	$(2.26 \pm 0.09)E+2$	$(4.11 \pm 0.28)E+1$	$(1.42 \pm 0.15)E+1$	$(8.08 \pm 1.06)E+0$	$(3.09 \pm 0.47)E+0$	$(9.83 \pm 2.07)E-1$
$8.98E-3$	$(2.15 \pm 0.06)E+2$	$(4.10 \pm 0.20)E+1$	$(1.53 \pm 0.12)E+1$	$(6.50 \pm 0.70)E+0$	$(2.98 \pm 0.36)E+0$	$(1.00 \pm 0.14)E+0$
$1.58E-2$	$(1.77 \pm 0.04)E+2$	$(4.04 \pm 0.15)E+1$	$(1.42 \pm 0.08)E+1$	$(7.20 \pm 0.55)E+0$	$(2.93 \pm 0.26)E+0$	$(1.07 \pm 0.12)E+0$
$3.26E-2$	$(1.42 \pm 0.03)E+2$	$(3.85 \pm 0.11)E+1$	$(1.44 \pm 0.06)E+1$	$(7.32 \pm 0.46)E+0$	$(2.90 \pm 0.20)E+0$	$(1.10 \pm 0.09)E+0$
$6.04E-2$	$(9.65 \pm 0.15)E+1$	$(3.40 \pm 0.07)E+1$	$(1.34 \pm 0.04)E+1$	$(6.44 \pm 0.30)E+0$	$(2.99 \pm 0.15)E+0$	$(8.75 \pm 0.58)E-1$
$1.07E-1$	$(5.50 \pm 0.08)E+1$	$(2.39 \pm 0.04)E+1$	$(1.05 \pm 0.03)E+1$	$(5.75 \pm 0.21)E+0$	$(2.62 \pm 0.11)E+0$	$(7.38 \pm 0.39)E-1$
$1.72E-1$	$(2.40 \pm 0.04)E+1$	$(1.33 \pm 0.02)E+1$	$(6.89 \pm 0.16)E+0$	$(3.98 \pm 0.13)E+0$	$(1.83 \pm 0.06)E+0$	$(4.98 \pm 0.23)E-1$
$3.47E-1$	$(8.10 \pm 0.14)E+0$	$(5.27 \pm 0.11)E+0$	$(3.30 \pm 0.09)E+0$	$(2.03 \pm 0.07)E+0$	$(1.01 \pm 0.04)E+0$	$(2.47 \pm 0.12)E-1$
$5.69E-1$	$(1.96 \pm 0.05)E+0$	$(1.47 \pm 0.04)E+0$	$(1.04 \pm 0.04)E+0$	$(7.50 \pm 0.32)E-1$	$(4.22 \pm 0.18)E-1$	$(1.05 \pm 0.06)E-1$
$1.17E+0$	$(3.16 \pm 0.16)E-1$	$(2.71 \pm 0.14)E-1$	$(2.24 \pm 0.13)E-1$	$(1.68 \pm 0.12)E-1$	$(1.08 \pm 0.07)E-1$	$(3.05 \pm 0.29)E-2$
$2.82E+0$	$(3.93 \pm 0.48)E-2$	$(3.58 \pm 0.44)E-2$	$(3.33 \pm 0.50)E-2$	$(2.32 \pm 0.44)E-2$	$(1.89 \pm 0.30)E-2$	$(4.77 \pm 1.27)E-3$
$4.17E+0$	$(6.92 \pm 1.89)E-3$	$(2.77 \pm 0.70)E-3$	$(3.28 \pm 0.94)E-3$		$(2.22 \pm 0.64)E-3$	

Table 8. (continued) Normalized inclusive single-particle distributions $D(p_t^2, x_F)$ of charged hadrons in different intervals of Q^2 (GeV^2) (Fig. 10, right). $\langle p_t^2 \rangle$ is given in GeV^2.

$\langle p_t^2 \rangle$	$0.0 < x_F < 0.1$	$0.1 < x_F < 0.2$	$0.2 < x_F < 0.3$	$0.3 < x_F < 0.4$	$0.4 < x_F < 0.6$	$0.6 < x_F < 1.0$
$1.45 < Q^2 < 3.20$ GeV^2						
$1.42E-3$	$(2.78 \pm 0.23)E+2$	$(3.13 \pm 0.49)E+1$	$(1.48 \pm 0.33)E+1$			
$2.63E-3$	$(2.46 \pm 0.15)E+2$	$(3.72 \pm 0.44)E+1$	$(1.35 \pm 0.25)E+1$	$(7.84 \pm 1.94)E+0$	$(3.24 \pm 0.88)E+0$	
$4.94E-3$	$(2.38 \pm 0.11)E+2$	$(3.80 \pm 0.31)E+1$	$(1.21 \pm 0.18)E+1$	$(7.26 \pm 1.36)E+0$	$(2.70 \pm 0.54)E+0$	$(7.50 \pm 2.12)E-1$
$1.04E-2$	$(2.16 \pm 0.08)E+2$	$(3.93 \pm 0.24)E+1$	$(1.33 \pm 0.13)E+1$	$(8.20 \pm 1.02)E+0$	$(2.65 \pm 0.45)E+0$	$(6.63 \pm 1.52)E-1$
$1.27E-2$	$(1.84 \pm 0.05)E+2$	$(3.92 \pm 0.18)E+1$	$(1.33 \pm 0.10)E+1$	$(8.11 \pm 0.82)E+0$	$(2.85 \pm 0.33)E+0$	$(6.91 \pm 1.20)E-1$
$3.17E-2$	$(1.52 \pm 0.03)E+2$	$(3.69 \pm 0.13)E+1$	$(1.41 \pm 0.08)E+1$	$(6.54 \pm 0.53)E+0$	$(3.04 \pm 0.27)E+0$	$(6.95 \pm 0.92)E-1$
$4.87E-2$	$(1.04 \pm 0.02)E+2$	$(3.31 \pm 0.09)E+1$	$(1.24 \pm 0.05)E+1$	$(6.08 \pm 0.37)E+0$	$(2.55 \pm 0.17)E+0$	$(6.02 \pm 0.57)E-1$
$1.09E-1$	$(5.72 \pm 0.10)E+1$	$(2.54 \pm 0.06)E+1$	$(1.08 \pm 0.04)E+1$	$(5.07 \pm 0.25)E+0$	$(2.06 \pm 0.11)E+0$	$(4.60 \pm 0.37)E-1$
$2.04E-1$	$(2.46 \pm 0.04)E+1$	$(1.38 \pm 0.03)E+1$	$(6.94 \pm 0.22)E+0$	$(3.68 \pm 0.16)E+0$	$(1.61 \pm 0.08)E+0$	$(3.65 \pm 0.24)E-1$
$3.68E-1$	$(8.49 \pm 0.18)E+0$	$(5.67 \pm 0.14)E+0$	$(3.43 \pm 0.11)E+0$	$(2.05 \pm 0.09)E+0$	$(1.05 \pm 0.05)E+0$	$(2.38 \pm 0.16)E-1$
$5.88E-1$	$(2.10 \pm 0.07)E+0$	$(1.59 \pm 0.05)E+0$	$(1.08 \pm 0.05)E+0$	$(8.17 \pm 0.44)E-1$	$(3.94 \pm 0.22)E-1$	$(9.96 \pm 0.76)E-2$
$1.22E+0$	$(3.44 \pm 0.21)E-1$	$(3.14 \pm 0.19)E-1$	$(2.65 \pm 0.18)E-1$	$(1.82 \pm 0.15)E-1$	$(1.05 \pm 0.09)E-1$	$(3.48 \pm 0.41)E-2$
$2.26E+0$	$(4.51 \pm 0.58)E-2$	$(4.42 \pm 0.60)E-2$	$(3.97 \pm 0.65)E-2$	$(2.97 \pm 0.75)E-2$	$(1.80 \pm 0.29)E-2$	$(5.51 \pm 1.39)E-3$
$3.2 < Q^2 < 7.0$ GeV^2						
$1.42E-3$	$(2.75 \pm 0.28)E+2$	$(3.82 \pm 0.80)E+1$				
$2.63E-3$	$(2.97 \pm 0.22)E+2$	$(4.21 \pm 0.58)E+1$	$(1.48 \pm 0.33)E+1$			
$4.86E-3$	$(2.63 \pm 0.16)E+2$	$(4.04 \pm 0.42)E+1$	$(1.65 \pm 0.27)E+1$	$(8.35 \pm 1.99)E+0$		
$8.98E-3$	$(2.28 \pm 0.11)E+2$	$(4.53 \pm 0.37)E+1$	$(1.46 \pm 0.18)E+1$	$(7.59 \pm 1.51)E+0$	$(1.61 \pm 0.40)E+0$	
$1.98E-2$	$(1.77 \pm 0.07)E+2$	$(4.12 \pm 0.24)E+1$	$(1.37 \pm 0.14)E+1$	$(6.92 \pm 0.92)E+0$	$(2.33 \pm 0.39)E+0$	$(4.24 \pm 1.21)E-1$
$3.07E-2$	$(1.49 \pm 0.04)E+2$	$(3.73 \pm 0.16)E+1$	$(1.55 \pm 0.10)E+1$	$(7.63 \pm 0.79)E+0$	$(2.14 \pm 0.26)E+0$	$(4.91 \pm 0.94)E-1$
$5.09E-2$	$(1.05 \pm 0.03)E+2$	$(3.28 \pm 0.11)E+1$	$(1.29 \pm 0.07)E+1$	$(5.87 \pm 0.47)E+0$	$(2.31 \pm 0.22)E+0$	$(4.64 \pm 0.68)E-1$
$9.44E-2$	$(5.88 \pm 0.13)E+1$	$(2.46 \pm 0.07)E+1$	$(1.05 \pm 0.05)E+1$	$(4.93 \pm 0.31)E+0$	$(2.06 \pm 0.15)E+0$	$(3.55 \pm 0.43)E-1$
$1.78E-1$	$(2.61 \pm 0.06)E+1$	$(1.46 \pm 0.04)E+1$	$(6.93 \pm 0.28)E+0$	$(3.37 \pm 0.19)E+0$	$(1.59 \pm 0.10)E+0$	$(3.11 \pm 0.30)E-1$
$3.47E-1$	$(9.02 \pm 0.25)E+0$	$(5.80 \pm 0.18)E+0$	$(3.47 \pm 0.15)E+0$	$(1.94 \pm 0.11)E+0$	$(9.31 \pm 0.56)E-1$	$(1.92 \pm 0.18)E-1$
$5.04E-1$	$(2.14 \pm 0.09)E+0$	$(1.61 \pm 0.07)E+0$	$(1.17 \pm 0.06)E+0$	$(7.33 \pm 0.52)E-1$	$(4.87 \pm 0.33)E-1$	$(9.49 \pm 1.00)E-2$
$9.82E-1$	$(3.50 \pm 0.26)E-1$	$(3.16 \pm 0.25)E-1$	$(2.77 \pm 0.24)E-1$	$(1.81 \pm 0.17)E-1$	$(1.10 \pm 0.12)E-1$	$(3.27 \pm 0.46)E-2$
$2.02E+0$	$(4.37 \pm 0.66)E-2$	$(4.49 \pm 0.60)E-2$	$(4.09 \pm 0.66)E-2$	$(3.05 \pm 0.91)E-2$	$(1.55 \pm 0.26)E-2$	$(6.02 \pm 1.68)E-3$
$7.0 < Q^2 < 20.0$ GeV^2						
$1.42E-3$	$(2.47 \pm 0.30)E+2$	$(3.18 \pm 0.72)E+1$				
$2.63E-3$	$(2.43 \pm 0.23)E+2$	$(3.82 \pm 0.67)E+1$	$(1.86 \pm 0.46)E+1$			
$4.86E-3$	$(2.32 \pm 0.17)E+2$	$(4.46 \pm 0.57)E+1$	$(1.52 \pm 0.32)E+1$			
$8.98E-3$	$(2.35 \pm 0.13)E+2$	$(4.19 \pm 0.38)E+1$	$(1.16 \pm 0.19)E+1$	$(7.32 \pm 1.63)E+0$	$(2.89 \pm 0.75)E+0$	
$1.66E-2$	$(1.86 \pm 0.08)E+2$	$(3.39 \pm 0.26)E+1$	$(1.30 \pm 0.15)E+1$	$(7.73 \pm 1.46)E+0$	$(2.20 \pm 0.46)E+0$	
$3.07E-2$	$(1.51 \pm 0.05)E+2$	$(3.61 \pm 0.19)E+1$	$(1.37 \pm 0.12)E+1$	$(5.78 \pm 0.81)E+0$	$(2.37 \pm 0.35)E+0$	$(3.06 \pm 0.88)E-1$
$6.59E-2$	$(1.06 \pm 0.03)E+2$	$(3.32 \pm 0.14)E+1$	$(1.28 \pm 0.08)E+1$	$(5.65 \pm 0.56)E+0$	$(1.81 \pm 0.24)E+0$	$(3.40 \pm 0.80)E-1$
$8.33E-2$	$(6.10 \pm 0.17)E+1$	$(2.46 \pm 0.09)E+1$	$(1.02 \pm 0.06)E+1$	$(5.28 \pm 0.44)E+0$	$(1.48 \pm 0.15)E+0$	$(2.04 \pm 0.38)E-1$
$1.52E-1$	$(2.70 \pm 0.08)E+1$	$(1.43 \pm 0.05)E+1$	$(6.99 \pm 0.34)E+0$	$(3.74 \pm 0.27)E+0$	$(1.41 \pm 0.11)E+0$	$(2.31 \pm 0.33)E-1$
$3.45E-1$	$(8.95 \pm 0.29)E+0$	$(5.78 \pm 0.23)E+0$	$(3.65 \pm 0.19)E+0$	$(2.01 \pm 0.13)E+0$	$(1.09 \pm 0.08)E+0$	$(1.43 \pm 0.18)E-1$
$6.50E-1$	$(1.92 \pm 0.10)E+0$	$(1.76 \pm 0.09)E+0$	$(1.27 \pm 0.08)E+0$	$(7.89 \pm 0.68)E-1$	$(4.00 \pm 0.34)E-1$	$(1.04 \pm 0.13)E-1$
$1.04E+0$	$(3.30 \pm 0.30)E-1$	$(2.90 \pm 0.27)E-1$	$(2.78 \pm 0.27)E-1$	$(1.85 \pm 0.23)E-1$	$(1.16 \pm 0.13)E-1$	$(3.28 \pm 0.54)E-2$
$2.26E+0$	$(4.85 \pm 0.77)E-2$	$(5.60 \pm 0.82)E-2$	$(5.12 \pm 0.89)E-2$	$(2.54 \pm 0.52)E-2$	$(1.97 \pm 0.44)E-2$	$(5.63 \pm 1.68)E-3$

Table 9. Results of fitting expression (15) to the normalized inclusive single-particle distributions $D(p_t^2, x_F)$ for charged hadrons in different intervals of x_F for different regions of W (GeV) and Q^2 (GeV^2) (Fig. 10). For a given interval in x_F the parameter m was fixed at the average value obtained in the respective fit of $D(p_t^2, x_F)$ in the different W or Q^2 regions. In the fits a systematic error of 4% for the data points has been assumed, which was added quadratically to the statistical error. The data refer to a W range 7.5 to 25 GeV and to a Q^2 range 0.15 to 20 GeV^2.

	$0.0 < x_F < 0.1$	$0.1 < x_F < 0.2$	$0.2 < x_F < 0.3$	$0.3 < x_F < 0.4$	$0.4 < x_F < 0.6$	$0.6 < x_F < 1.0$
m(GeV)	0.445 ± 0.007	0.915 ± 0.027	1.190 ± 0.058	1.535 ± 0.130	1.870 ± 0.243	0.770 ± 0.048
$\langle W \rangle$	α					
8.79	3.75 ± 0.03	7.12 ± 0.09	8.42 ± 0.12	11.01 ± 0.20	14.34 ± 0.30	3.75 ± 0.09
11.2	3.64 ± 0.03	6.44 ± 0.08	7.81 ± 0.13	10.67 ± 0.23	13.44 ± 0.31	3.68 ± 0.10
13.7	3.56 ± 0.03	6.15 ± 0.08	7.72 ± 0.13	10.42 ± 0.22	12.87 ± 0.31	3.52 ± 0.11
16.2	3.47 ± 0.03	6.01 ± 0.08	7.19 ± 0.13	9.59 ± 0.24	12.53 ± 0.34	3.46 ± 0.10
18.7	3.37 ± 0.03	5.88 ± 0.08	6.97 ± 0.14	9.67 ± 0.27	12.62 ± 0.37	3.22 ± 0.11
22.3	3.28 ± 0.03	5.59 ± 0.07	6.83 ± 0.12	9.02 ± 0.21	11.87 ± 0.30	3.48 ± 0.10
χ^2/NDF	87.5/60	91.2/60	69.3/60	65.2/53	36.1/54	27.8/51
$\langle Q^2 \rangle$	α					
0.28	3.45 ± 0.03	6.22 ± 0.07	7.73 ± 0.12	10.58 ± 0.17	13.84 ± 0.28	4.05 ± 0.09
0.54	3.48 ± 0.02	6.17 ± 0.07	7.64 ± 0.12	10.26 ± 0.21	13.94 ± 0.29	3.86 ± 0.09
1.00	3.46 ± 0.02	6.23 ± 0.07	7.57 ± 0.11	10.01 ± 0.19	12.50 ± 0.28	3.43 ± 0.09
2.14	3.44 ± 0.03	5.93 ± 0.08	7.16 ± 0.13	9.52 ± 0.23	12.06 ± 0.33	2.81 ± 0.11
4.70	3.43 ± 0.02	6.04 ± 0.09	7.14 ± 0.16	9.47 ± 0.30	10.80 ± 0.29	2.56 ± 0.14
11.3	3.44 ± 0.04	5.91 ± 0.10	6.82 ± 0.16	9.22 ± 0.33	10.46 ± 0.42	2.10 ± 0.18
χ^2/NDF	68.8/60	94.9/60	68.2/58	44.5/54	55.6/53	31.2/46

Table 10. Results of fitting expression (15) to the normalized inclusive single-particle distributions $1/N_\mu \cdot dN_h/dp_t^2$ from EMC [13] for charged hadrons in different bins of z_{had} and different W (GeV) regions. (combined μp and μd data). The data refer to the Q^2 range 2 to $\approx$ 100 GeV^2. It should be noted that the α values obtained differ by a factor of ~ 2 from those quoted in [13].

	$0.1 < z_{had} < 0.2$	$0.2 < z_{had} < 0.4$	$0.4 < z_{had} < 1.0$
m (GeV)	0.87 ± 0.02	1.08 ± 0.02	1.50 ± 0.04
$\langle W \rangle$	α		
7.7	5.81 ± 0.15	6.28 ± 0.18	7.87 ± 0.32
10.7	5.04 ± 0.14	5.44 ± 0.15	6.35 ± 0.23
13.2	4.90 ± 0.13	5.06 ± 0.14	5.67 ± 0.23
15.4	4.68 ± 0.11	4.90 ± 0.13	5.30 ± 0.22
17.6	4.56 ± 0.11	4.71 ± 0.12	5.06 ± 0.20
19.7	4.45 ± 0.11	4.53 ± 0.12	4.93 ± 0.20
χ^2/NDF	98.7/59	107.3/70	101.0/74

Table 11. $\langle p_t^2 \rangle$ of charged hadrons in different intervals of x_F in different regions of W^2 (GeV^2) and of Q^2 (GeV^2) (Fig. 13).

$< W^2 >$	$0 < x_F < 0.1$	$0.1 < x_F < 0.2$	$0.2 < x_F < 0.4$	$0.4 < x_F < 0.6$	$0.6 < x_F < 0.8$	$0.8 < x_F < 1$
77.3	0.115 ± 0.002	0.174 ± 0.002	0.249 ± 0.003	0.316 ± 0.007	0.343 ± 0.013	0.300 ± 0.022
126.0	0.124 ± 0.002	0.194 ± 0.003	0.278 ± 0.004	0.345 ± 0.008	0.379 ± 0.014	0.229 ± 0.014
188.9	0.130 ± 0.002	0.211 ± 0.003	0.288 ± 0.005	0.364 ± 0.009	0.393 ± 0.018	0.263 ± 0.017
263.4	0.136 ± 0.002	0.225 ± 0.003	0.313 ± 0.005	0.409 ± 0.013	0.404 ± 0.018	0.299 ± 0.022
350.1	0.143 ± 0.002	0.233 ± 0.003	0.326 ± 0.006	0.411 ± 0.013	0.418 ± 0.020	0.324 ± 0.026
497.6	0.154 ± 0.002	0.254 ± 0.003	0.362 ± 0.006	0.447 ± 0.014	0.471 ± 0.026	0.278 ± 0.028
$< Q^2 >$	$0 < x_F < 0.1$	$0.1 < x_F < 0.2$	$0.2 < x_F < 0.4$	$0.4 < x_F < 0.6$	$0.6 < x_F < 0.8$	$0.8 < x_F < 1$
0.283	0.139 ± 0.002	0.214 ± 0.002	0.285 ± 0.004	0.336 ± 0.007	0.327 ± 0.011	0.217 ± 0.011
0.536	0.134 ± 0.001	0.214 ± 0.002	0.292 ± 0.004	0.350 ± 0.007	0.348 ± 0.010	0.247 ± 0.017
1.00	0.139 ± 0.001	0.211 ± 0.002	0.297 ± 0.004	0.395 ± 0.010	0.398 ± 0.012	0.271 ± 0.013
2.14	0.139 ± 0.002	0.227 ± 0.003	0.329 ± 0.006	0.425 ± 0.012	0.488 ± 0.022	0.386 ± 0.040
4.70	0.138 ± 0.003	0.228 ± 0.004	0.328 ± 0.007	0.429 ± 0.016	0.574 ± 0.037	0.423 ± 0.055
11.3	0.139 ± 0.003	0.236 ± 0.006	0.354 ± 0.010	0.519 ± 0.027	0.740 ± 0.090	0.573 ± 0.072
35.3	0.141 ± 0.005	0.250 ± 0.011	0.344 ± 0.018	0.522 ± 0.056	0.818 ± 0.128	

Table 12. $\langle p_t^2 \rangle$ of charged hadrons in different intervals of W^2 (GeV^2) and Q^2 (GeV^2) (Fig. 14). Corresponding values of x_{Bj} are given as well.

			$\langle p_t^2 \rangle$ (GeV^2)					
$\langle W^2 \rangle$	$\langle Q^2 \rangle$	$\langle x_{Bj} \rangle$	$0.0 < x_F < 0.1$	$0.1 < x_F < 0.2$	$0.2 < x_F < 0.4$	$0.4 < x_F < 0.6$	$0.6 < x_F < 0.8$	$0.8 < x_F < 1.0$
78.0	0.297	$3.94E-3$	0.114 ± 0.004	0.173 ± 0.005	0.239 ± 0.007	0.294 ± 0.012	0.285 ± 0.018	0.233 ± 0.029
77.7	0.540	$7.15E-3$	0.117 ± 0.003	0.169 ± 0.004	0.251 ± 0.006	0.301 ± 0.012	0.322 ± 0.019	0.213 ± 0.028
77.7	0.991	$1.31E-2$	0.115 ± 0.003	0.173 ± 0.004	0.251 ± 0.006	0.316 ± 0.013	0.345 ± 0.021	0.284 ± 0.026
77.8	2.116	$2.74E-2$	0.118 ± 0.004	0.185 ± 0.006	0.255 ± 0.009	0.367 ± 0.021	0.427 ± 0.063	0.430 ± 0.066
77.9	4.690	$5.85E-2$	0.124 ± 0.006	0.176 ± 0.008	0.269 ± 0.012	0.330 ± 0.026	0.410 ± 0.049	0.373 ± 0.093
77.2	11.19	$1.29E-1$	0.103 ± 0.005	0.205 ± 0.010	0.253 ± 0.014	0.364 ± 0.037	0.529 ± 0.109	0.516 ± 0.117
78.5	31.90	$2.86E-1$	0.102 ± 0.010	0.211 ± 0.024	0.244 ± 0.029	0.554 ± 0.095	0.514 ± 0.125	
126.7	0.296	$2.39E-3$	0.125 ± 0.003	0.185 ± 0.005	0.260 ± 0.008	0.302 ± 0.014	0.321 ± 0.021	0.178 ± 0.018
126.0	0.539	$4.36E-3$	0.118 ± 0.003	0.197 ± 0.005	0.274 ± 0.007	0.329 ± 0.014	0.334 ± 0.021	0.228 ± 0.030
126.5	0.988	$7.94E-3$	0.125 ± 0.003	0.196 ± 0.005	0.281 ± 0.007	0.341 ± 0.015	0.351 ± 0.025	0.228 ± 0.026
127.3	2.132	$1.68E-2$	0.124 ± 0.004	0.200 ± 0.008	0.291 ± 0.012	0.380 ± 0.025	0.521 ± 0.050	0.370 ± 0.057
126.8	4.738	$3.68E-2$	0.123 ± 0.005	0.196 ± 0.009	0.284 ± 0.012	0.404 ± 0.029	0.472 ± 0.057	0.267 ± 0.062
126.1	11.38	$8.38E-2$	0.143 ± 0.007	0.195 ± 0.011	0.330 ± 0.022	0.503 ± 0.052	0.642 ± 0.143	
126.4	34.15	$2.10E-1$	0.154 ± 0.024	0.249 ± 0.029	0.341 ± 0.043	0.464 ± 0.094	0.558 ± 0.116	
190.0	0.293	$1.57E-3$	0.131 ± 0.003	0.203 ± 0.006	0.274 ± 0.010	0.322 ± 0.014	0.323 ± 0.041	0.232 ± 0.032
189.2	0.535	$2.87E-3$	0.126 ± 0.004	0.217 ± 0.006	0.283 ± 0.008	0.337 ± 0.017	0.334 ± 0.026	0.195 ± 0.025
189.3	1.001	$5.34E-3$	0.135 ± 0.003	0.210 ± 0.006	0.283 ± 0.008	0.363 ± 0.019	0.429 ± 0.032	0.272 ± 0.033
190.0	2.146	$1.13E-2$	0.133 ± 0.004	0.222 ± 0.008	0.316 ± 0.013	0.405 ± 0.026	0.393 ± 0.037	0.428 ± 0.070
189.1	4.734	$2.48E-2$	0.129 ± 0.006	0.219 ± 0.010	0.311 ± 0.016	0.426 ± 0.036	0.674 ± 0.090	0.479 ± 0.103
187.8	11.18	$5.67E-2$	0.122 ± 0.006	0.222 ± 0.014	0.348 ± 0.025	0.588 ± 0.072	0.748 ± 0.164	0.337 ± 0.084
189.4	35.27	$1.55E-1$	0.141 ± 0.012	0.207 ± 0.023	0.323 ± 0.036	0.592 ± 0.123		
264.2	0.284	$1.09E-3$	0.136 ± 0.003	0.213 ± 0.006	0.283 ± 0.008	0.343 ± 0.027	0.335 ± 0.031	0.267 ± 0.033
263.0	0.535	$2.05E-3$	0.132 ± 0.003	0.224 ± 0.006	0.295 ± 0.012	0.359 ± 0.021	0.357 ± 0.031	0.267 ± 0.043
263.7	1.005	$3.84E-3$	0.136 ± 0.003	0.212 ± 0.007	0.316 ± 0.010	0.521 ± 0.035	0.363 ± 0.030	0.318 ± 0.046
264.8	2.149	$8.14E-3$	0.140 ± 0.004	0.237 ± 0.008	0.354 ± 0.017	0.471 ± 0.033	0.527 ± 0.055	0.323 ± 0.067
264.8	4.684	$1.76E-2$	0.143 ± 0.005	0.253 ± 0.012	0.353 ± 0.018	0.410 ± 0.034	0.662 ± 0.115	
262.5	11.07	$4.08E-2$	0.140 ± 0.007	0.255 ± 0.016	0.368 ± 0.026	0.424 ± 0.066	0.582 ± 0.121	0.370 ± 0.103
264.2	37.47	$1.22E-1$	0.147 ± 0.014	0.307 ± 0.041	0.386 ± 0.055	0.579 ± 0.130		
351.5	0.276	$7.93E-4$	0.140 ± 0.004	0.227 ± 0.007	0.312 ± 0.010	0.371 ± 0.018	0.342 ± 0.027	0.239 ± 0.034
350.3	0.533	$1.53E-3$	0.148 ± 0.004	0.233 ± 0.007	0.315 ± 0.015	0.383 ± 0.025	0.367 ± 0.033	0.307 ± 0.063
350.2	1.010	$2.90E-3$	0.141 ± 0.003	0.225 ± 0.007	0.313 ± 0.011	0.412 ± 0.027	0.392 ± 0.042	0.299 ± 0.041
350.0	2.151	$6.16E-3$	0.148 ± 0.004	0.248 ± 0.010	0.370 ± 0.015	0.475 ± 0.036	0.552 ± 0.070	0.333 ± 0.061
350.1	4.645	$1.32E-2$	0.147 ± 0.005	0.240 ± 0.012	0.365 ± 0.023	0.488 ± 0.052	0.553 ± 0.111	0.523 ± 0.127
351.3	11.31	$3.13E-2$	0.143 ± 0.006	0.267 ± 0.018	0.391 ± 0.035	0.627 ± 0.109	0.796 ± 0.182	1.437 ± 0.363
351.7	36.45	$9.31E-2$	0.146 ± 0.012	0.215 ± 0.022	0.388 ± 0.058			
502.8	0.268	$5.42E-4$	0.156 ± 0.006	0.248 ± 0.006	0.326 ± 0.010	0.381 ± 0.017	0.354 ± 0.024	0.197 ± 0.023
499.6	0.533	$1.08E-3$	0.152 ± 0.003	0.255 ± 0.008	0.350 ± 0.013	0.432 ± 0.023	0.401 ± 0.033	0.314 ± 0.063
498.0	1.012	$2.06E-3$	0.162 ± 0.003	0.249 ± 0.008	0.367 ± 0.012	0.478 ± 0.044	0.525 ± 0.056	0.258 ± 0.033
498.3	2.139	$4.35E-3$	0.155 ± 0.003	0.260 ± 0.009	0.387 ± 0.019	0.471 ± 0.030	0.553 ± 0.061	
498.6	4.653	$9.40E-3$	0.143 ± 0.008	0.267 ± 0.012	0.413 ± 0.022	0.576 ± 0.064	0.729 ± 0.134	
497.0	11.47	$2.29E-2$	0.162 ± 0.006	0.287 ± 0.016	0.490 ± 0.037	0.704 ± 0.103		
495.2	37.29	$7.01E-2$	0.147 ± 0.009	0.298 ± 0.026	0.426 ± 0.051			

Table 13. Results for the slope parameters d_W and d_Q from fits of expression (16) and (17) to the $\langle p_t^2 \rangle$ in Fig. 14. The fits were performed for the W region $7.5 < W < 25$ GeV and the Q^2 region $0.15 < Q^2 < 100$ GeV^2 respectively. In the fits a systematic error of 2% for the $\langle p_t^2 \rangle$ data points has been assumed, which was added quadratically to the statistical error. The slope values are shown in Fig. 15.

	slope d_Q (GeV^2)					
W range (GeV)	$0 < x_F < 0.1$	$0.1 < x_F < 0.2$	$0.2 < x_F < 0.4$	$0.4 < x_F < 0.6$	$0.6 < x_F < 0.8$	$0.8 < x_F < 1$
all W	0.001 ± 0.005	0.008 ± 0.008	0.015 ± 0.011	0.042 ± 0.016	0.099 ± 0.023	0.082 ± 0.020
$7.5 < W < 10.0$	-0.003 ± 0.004	0.008 ± 0.007	0.002 ± 0.010	0.028 ± 0.016	0.054 ± 0.021	0.076 ± 0.027
$10.0 < W < 12.5$	0.005 ± 0.005	0.006 ± 0.008	0.015 ± 0.012	0.042 ± 0.017	0.065 ± 0.023	0.047 ± 0.024
$12.5 < W < 15.0$	0.000 ± 0.005	0.002 ± 0.008	0.014 ± 0.012	0.055 ± 0.020	0.090 ± 0.033	0.059 ± 0.024
$15.0 < W < 17.5$	0.003 ± 0.005	0.016 ± 0.010	0.023 ± 0.013	0.031 ± 0.020	0.084 ± 0.032	0.031 ± 0.030
$17.5 < W < 20.0$	0.001 ± 0.005	0.001 ± 0.009	0.020 ± 0.014	0.055 ± 0.027	0.093 ± 0.035	0.080 ± 0.034
$20.0 < W < 25.0$	-0.001 ± 0.005	0.010 ± 0.010	0.028 ± 0.015	0.068 ± 0.028	0.115 ± 0.042	0.052 ± 0.045
	slope d_W (GeV^2)					
Q^2 range (GeV^2)	$0 < x_F < 0.1$	$0.1 < x_F < 0.2$	$0.2 < x_F < 0.4$	$0.4 < x_F < 0.6$	$0.6 < x_F < 0.8$	$0.8 < x_F < 1$
all Q^2	0.020 ± 0.012	0.042 ± 0.019	0.055 ± 0.028	0.069 ± 0.035	0.057 ± 0.038	0.019 ± 0.031
$0.15 < Q^2 < 0.40$	0.020 ± 0.012	0.039 ± 0.019	0.045 ± 0.026	0.050 ± 0.032	0.035 ± 0.033	0.005 ± 0.026
$0.40 < Q^2 < 0.70$	0.020 ± 0.012	0.044 ± 0.019	0.047 ± 0.028	0.061 ± 0.035	0.037 ± 0.037	0.046 ± 0.036
$0.70 < Q^2 < 1.45$	0.021 ± 0.012	0.036 ± 0.019	0.052 ± 0.028	0.088 ± 0.039	0.057 ± 0.043	0.009 ± 0.032
$1.45 < Q^2 < 3.20$	0.020 ± 0.013	0.042 ± 0.021	0.074 ± 0.030	0.068 ± 0.042	0.064 ± 0.061	-0.062 ± 0.070
$3.20 < Q^2 < 7.00$	0.014 ± 0.013	0.049 ± 0.021	0.074 ± 0.032	0.102 ± 0.047	0.159 ± 0.073	0.135 ± 0.114
$7.00 < Q^2 < 20.0$	0.026 ± 0.012	0.048 ± 0.024	0.104 ± 0.035	0.136 ± 0.061	0.109 ± 0.131	-0.043 ± 0.140
$20.0 < Q^2 < 100.$	0.024 ± 0.014	0.027 ± 0.028	0.095 ± 0.040	0.040 ± 0.150	0.092 ± 0.420	

Table 14. Results for the slope parameters d_W and d_Q from fits of the expression (16) and (17) to the $\langle p_t^2 \rangle$ from EMC [13] (combined μp and μd data). The fits were performed for the W region 6 to 20 GeV and the Q^2 region 2 to $\approx$ 100 GeV^2 respectively. The slope values are shown in Fig. 15.

	slope d_Q (GeV^2)		
W^2 range (GeV^2)	$0.1 < z_{had} < 0.2$	$0.2 < z_{had} < 0.4$	$0.4 < z_{had} < 1$
$30 < W^2 < 50$	0.006 ± 0.005	-0.004 ± 0.006	0.011 ± 0.012
$50 < W^2 < 90$	0.002 ± 0.002	-0.007 ± 0.003	0.024 ± 0.007
$90 < W^2 < 120$	0.000 ± 0.002	0.009 ± 0.004	0.047 ± 0.008
$120 < W^2 < 150$	0.000 ± 0.004	-0.006 ± 0.006	0.022 ± 0.018
$150 < W^2 < 200$	0.004 ± 0.004	-0.008 ± 0.007	0.043 ± 0.018
$200 < W^2 < 275$	0.000 ± 0.003	0.007 ± 0.006	0.013 ± 0.018
$275 < W^2 < 350$	0.005 ± 0.004	0.007 ± 0.009	-0.004 ± 0.027
$350 < W^2$	-0.009 ± 0.006	0.018 ± 0.013	0.018 ± 0.044
	slope d_W (GeV^2)		
Q^2 range (GeV^2)	$0.1 < z_{had} < 0.2$	$0.2 < z_{had} < 0.4$	$0.4 < z_{had} < 1$
$2 < Q^2 < 5$	0.060 ± 0.005	0.064 ± 0.008	0.086 ± 0.017
$5 < Q^2 < 10$	0.063 ± 0.003	0.094 ± 0.005	0.177 ± 0.013
$10 < Q^2 < 20$	0.068 ± 0.003	0.099 ± 0.005	0.180 ± 0.012
$20 < Q^2 < 40$	0.061 ± 0.003	0.103 ± 0.006	0.183 ± 0.015
$40 < Q^2$	0.071 ± 0.006	0.105 ± 0.009	0.185 ± 0.025

Table 15. Average forward multiplicities for positive ($\langle n_F^+ \rangle$), negative ($\langle n_F^- \rangle$) and charged ($\langle n_F \rangle$) hadrons as shown in Fig. 18 (left).

W(GeV)	8.79	11.2	13.7	16.2	18.7	22.3	26.1
$\langle n_F^+ \rangle$	1.72 ± 0.01	1.80 ± 0.01	1.87 ± 0.01	1.99 ± 0.01	2.06 ± 0.01	2.19 ± 0.01	2.25 ± 0.02
$\langle n_F^- \rangle$	1.40 ± 0.01	1.57 ± 0.01	1.72 ± 0.01	1.85 ± 0.01	1.99 ± 0.01	2.14 ± 0.01	2.23 ± 0.02
$\langle n_F \rangle$	3.12 ± 0.01	3.37 ± 0.01	3.59 ± 0.01	3.84 ± 0.02	4.05 ± 0.02	4.33 ± 0.02	4.48 ± 0.03
Q^2(GeV^2)	0.283	0.536	1.00	2.14	4.70	11.3	35.4
$\langle n_F^+ \rangle$	1.85 ± 0.01	1.86 ± 0.01	1.91 ± 0.01	1.97 ± 0.01	2.01 ± 0.01	2.06 ± 0.02	2.12 ± 0.03
$\langle n_F^- \rangle$	1.70 ± 0.01	1.73 ± 0.01	1.75 ± 0.01	1.78 ± 0.01	1.78 ± 0.01	1.74 ± 0.02	1.76 ± 0.03
$\langle n_F \rangle$	3.55 ± 0.01	3.59 ± 0.01	3.66 ± 0.01	3.75 ± 0.02	3.79 ± 0.02	3.80 ± 0.03	3.88 ± 0.05
x_{Bj}	0.00028	0.00070	0.00125	0.00200	0.00325		
$\langle n_F^+ \rangle$	2.23 ± 0.03	1.99 ± 0.01	1.92 ± 0.01	1.84 ± 0.01	1.82 ± 0.01		
$\langle n_F^- \rangle$	2.14 ± 0.03	1.95 ± 0.01	1.81 ± 0.01	1.72 ± 0.01	1.66 ± 0.01		
$\langle n_F \rangle$	4.36 ± 0.05	3.94 ± 0.02	3.73 ± 0.02	3.56 ± 0.02	3.47 ± 0.01		
x_{Bj}	0.00525	0.00825	0.01250	0.02750	0.14502		
$\langle n_F^+ \rangle$	1.86 ± 0.01	1.85 ± 0.01	1.87 ± 0.01	1.88 ± 0.01	1.91 ± 0.01		
$\langle n_F^- \rangle$	1.68 ± 0.01	1.67 ± 0.01	1.67 ± 0.01	1.61 ± 0.01	1.51 ± 0.02		
$\langle n_F \rangle$	3.54 ± 0.01	3.52 ± 0.02	3.54 ± 0.02	3.50 ± 0.02	3.42 ± 0.02		

Table 16. Results of fits of the expressions (18) and (19) to the data points in Fig. 18 (left). In the fits a systematic error of 1% for the data points $\langle n_F \rangle$ has been assumed, which was added quadratically to the statistical error. The fits were performed for the W region $7.5 < W < 30$ GeV and the Q^2 region $0.15 < Q^2 < 100$ GeV^2 respectively.

hadrons	e_W	f_W	e_Q	f_Q
positive	1.923 ± 0.008	0.253 ± 0.012	1.930 ± 0.009	0.061 ± 0.006
negative	1.748 ± 0.008	0.391 ± 0.011	1.742 ± 0.008	0.012 ± 0.006
charged	3.673 ± 0.015	0.639 ± 0.022	3.672 ± 0.016	0.072 ± 0.011